Aus der Klinik für Neurologie

(Prof. Dr. med. M. Bähr)

der Medizinischen Fakultät der Universität Göttingen

Poststroke lipid droplet accumulation in residing microglia and its influence on inflammation

INAUGURAL-DISSERTATION

zur Erlangung des Doktorgrades

der Medizinischen Fakultät der

Georg-August-Universität zu Göttingen

vorgelegt von

Wei Wei

aus

Sichuan, China

Göttingen 2023

Dekan:	Prof. Dr. med. W. Brück

Betreuungsausschuss

Betreuer/in:	Prof. Dr. med. T. R. Döppner
Ko-Betreuer/in:	Prof. Dr. med. M. Sereda

Prüfungskommission

Referent/in:	Prof. Dr. med. T. R. Döppner
Ko-Referent/in:	..……..
Drittreferent/in:	…..……..

Datum der mündlichen Prüfung: ……

Hiermit erkläre ich, die Dissertation mit dem Titel " Poststroke lipid droplet accumulation in residing microglia and its influence on inflammation" eigenständig angefertigt und keine anderen als die von mir angegebenen Quellen und Hilfsmittel verwendet zu haben.

Göttingen, den …… ……

(Unterschrift)

List of publications

Publication 1: Zhang L, **Wei W,** Ai X, Kilic E, Hermann DM, Venkataramani V, Bähr M, Döppner TR. (2021): Extracellular vesicles from hypoxia-preconditioned microglia promote angiogenesis and repress apoptosis in stroke mice via the TGF-β/Smad2/3 pathway. Cell Death Dis. 12(11):1068.

Publication 2: Xin WQ, **Wei W**, Pan YL, Cui BL, Yang XY, Bähr M, Döppner TR. (2021): Modulating poststroke inflammatory mechanisms: Novel aspects of mesenchymal stem cells, extracellular vesicles and microglia. World J Stem Cells. 13(8):1030-1048.

Publication 3: Janssen L, Ai X, Zheng X, **Wei W**, Caglayan AB, Kilic E, Wang YC, Hermann DM, Venkataramani V, Bähr M, Döppner TR. (2021): Inhibition of Fatty Acid Synthesis Aggravates Brain Injury, Reduces Blood-Brain Barrier Integrity and Impairs Neurological Recovery in a Murine Stroke Model. Front Cell Neurosci. 15:733973.

Contents

List of figures

List of Tables

Abbreviations

ABCA1	ATP-binding cassette transporter 1
ACA	anterior cerebral artery
ATP	adenosine triphosphate
AMPK	AMP-activated protein kinase
ADRP	adipose differentiation-related protein
AD	Alzheimer's disease
A-FABP	adipocyte fatty acid binding protein
ACSL	Acyl-CoA synthase
ACAT	Acyl-CoA cholesterol acyltransferase
BA	basal artery
BBB	blood-brain barrier
BrdU	5-bromo-2'-deoxyuridine
Bcl-2	B-cell Lymphoma-2
CNS	central nervous system
CCA	common carotid artery
CE	cholesteryl ester
DAG	diacylglycerol
ECA	external carotid artery
EV	extracellular vesicle
ER	endoplasmic reticulum
ELISA	enzyme-linked immunosorbent assay
FAS	fatty acid synthesis
FAO	fatty acid oxidation
FA	fatty acid
FACS	fluorescence-activated cell sorting analysis
HMGCR	HMG-CoA reductase

ICA	internal carotid artery
IL-1β	interleukin-1β
iNOS	inducible nitric oxide synthase
IGF1	insulin-like growth factor 1
IF	immunofluorescence
IFN-γ	interferon-γ
LD	Lipid droplet
LB	lipid body
LPS	lipopolysaccharide
LDH	lactate dehydrogenase
LSIS	laser speckle imaging system
LDRM	lipid droplets-rich microglia
LC-PUFA	long-chain polyunsaturated fatty acid
LDAM	lipid droplet accumulating microglia
mtPTP	mitochondrial permeability transition pore
MCA	middle cerebral artery
MLKL	mixed-lineage kinase domain-like protein
MCAO	middle cerebral artery occlusion
MFI	mean fluorescence intensity
NMDA	N-methyl-d-aspartat
NMDAR	N-methyl-d-aspartate receptor
NO	nitric oxide
nNOS	neuronal nitric oxide synthase
NK	natural killer cells
OGD	oxygen-glucose deprivation
PCA	posterior cerebral artery
PT	photothrombosis

PP2A	protein phosphatase 2A
PD	Parkinson's disease
PLIN2	perilipin 2 protein
rtPA	recombinant tissue plasminogen activator
ROS	reactive oxygen species
RNS	nitrogen species
RIPK1	receptor-interacting protein kinase 1
RXR	retinoid X receptor
RO	reoxygenation
SREBPs	sterol regulatory element-binding proteins
TNF-α	tumor necrosis factor alpha
TNFR	tumor necrosis factor receptor
TRAIL	TNF-related apoptosis-inducing ligand
TRADD	TNF receptor-associated death domain
TLRs	toll-like receptors
TGF-β	transforming growth factor β
TG	triglyceride
TIP47	tail-interacting protein of 47 kDa
TAG	triacylglycerol
Trc	triacsin C
TTC	2,3,5-Triphenyltetrazolium chloride
TLR4	toll-like receptor 4
TREM2	triggering receptor expressed on myeloid cells 2
TCA	tricarboxylic acid cycle
VEGF	vascular endothelial growth factor

1 Introduction

1.1 Epidemiology of stroke

Stroke is one of the most devastating and fatal diseases worldwide (Feigin et al. 2016; Feigin et al. 2021; Katan and Luft 2018; Kim et al. 2020; Owolabi et al. 2021). According to the Global Burden of Disease, stroke is currently the second leading cause of death (11.6% of total deaths) and the major cause of disability (5.7% of total disability-adjusted life expectancy) in the world (Feigin et al. 2016; Feigin et al. 2021). Globally, there are 12.2 million cases of stroke and 6.55 million stroke deaths each year (Feigin et al. 2016). Approximately 3 - 4% of total health care expenditures in western countries are spent on stroke (Struijs et al. 2006). Although the age-standardized mortality rate for stroke has declined sharply over the past decades, the age-standardized incidence rate has declined much less, suggesting that stroke prevention efforts still need to be improved (Kim et al. 2020; Owolabi et al. 2021).

Stroke is a condition in which patients experience symptoms and incapacity due to a lack of blood supply of a specific brain region. There are two major types of stroke: ischemic and hemorrhagic. Among them, ischemic stroke can be further divided into thrombotic, embolic, and systemic hypoperfusion; thrombotic and embolic together account for about 85% of all ischemic strokes (Hisham et al. 2013). The current optimal treatment for acute ischemic stroke includes intravenous recombinant tissue plasminogen activator (rtPA) and endovascular thrombectomy for large vessel occlusion to improve clinical outcomes (Catanese et al. 2017; Ciccone et al. 2013; Herpich and Rincon 2020). However, due to the limited therapeutic window following the ischemic stroke (4 to 6 hours after stroke) and the risk of hemorrhage in the long run, only a limited number of patients receive thrombolytic therapy or endovascular treatment (Catanese et al. 2017; Furie et al. 2011; Herpich and Rincon 2020; Starke et al. 2016). Nevertheless, with the development of translational medicine in recent years, new therapeutic approaches such as stem cell transplantation and extracellular vesicles (EVs) therapy have provided new perspectives for the treatment of ischemic stroke (Doeppner et al. 2017; Kuang et al. 2020; Zhang et al. 2021a; Zhang et al. 2021b).

1.2 Pathology of ischemic stroke

Extensive research has been conducted on the mechanisms of ischemic stroke and subsequent cell death (Datta et al. 2020; Fricker et al. 2018; Sekerdag et al. 2018). Brain tissue has relatively high oxygen and glucose consumption and is almost entirely dependent on oxidative

phosphorylation for energy production (Dirnagl et al. 1999). The hypoxic state induces ATP deprivation in the damaged tissue within minutes when the blood supply is interrupted and decreased to less than 20% (Michiels 2004). The area of ischemia becomes severely compromised when focal blockage of cerebral blood flow limits substrate delivery, particularly oxygen and glucose, and impairs the energetics required to maintain ionic gradients (Dirnagl et al. 1999). When neuronal blood supply is diminished due to an ischemic event, a considerable loss in oxygen supply induces oxidative phosphorylation and ATP synthesis to fail, leading to reduced ATP production in the core region of ischemia (Ide and Secher 2000; Lipton 1999; Michiels 2004). The decrease in ATP synthesis causes malfunction of the Na^+/K^+ pump and the plasma membrane Ca^{2+}/ATP pump, resulting in plasma membrane depolarization and glutamate release at the cellular level. Glutamate receptors, such as the N-methyl-d-aspartate receptor (NMDAR), are activated by increased glutamate levels in the extracellular environment (Bano and Nicotera 2007; Brustovetsky et al. 2010; Siesjö et al. 1989). Ca^{2+} can freely pass through the cell membrane upon NMDAR activation, resulting in an increase of intracellular Ca^{2+} levels (Newcomer et al. 2000). Furthermore, during ischemia, K^+ is released into the extracellular space due to ATP deficiency, whereas intracellular calcium efflux is blocked (impaired plasma membrane-associated Ca^{2+}/ATPase and Na^+/Ca^{2+} exchanger), culminating in a dramatic increase in intracellular calcium concentration (Caplan and Biller 2000). Additionally, excess Ca^{2+} activates calpain in postsynaptic neurons via NMDAR, inhibiting Na^+/Ca^{2+}X3 receptors in the process (Brustovetsky et al. 2010; Wendt et al. 2004). Finally, numerous calcium-dependent proteases, lipases, and DNases can be activated as a consequence of the Ca^{2+}-over-accumulation and calpain activation, leading to proteolytic hydrolysis of cytoplasmic substrates and ischemia core excitatory cell death (Bano and Nicotera 2007; Brustovetsky et al. 2010). Many cell death pathways are involved, such as apoptosis, necrosis, necroptosis, ferroptosis, autophagy, oncosis, and phagoptosis (Datta et al. 2020; Khoshnam et al. 2017; Sekerdag et al. 2018).

Ischemia causes significant cell death in the ischemic core after a stroke, although the cell death processes in the ischemic core and ischemic penumbra are different (Puig et al. 2018). The ischemic penumbra indicates regions where cells are metabolically active but not electrically active (Vandenabeele et al. 2010). Within a few hours, these neurons acquire noxious signals from dead cells surrounding the ischemic core, leading to cell death within a few days (Broughton et al. 2009). Cellular necrosis is one of the major causes of cell death, characterized by the tumescence and destruction of organelles, leading to cell death and the breakage of the plasma membrane (Fink et al. 2005). Necrosis is a non-programmed cell death pathway triggered primarily by a considerable reduction in ATP due to insufficient perfusion. ATP maintains the

neuronal membrane potential via Na^+/K^+ ATPase pump, but in ischemia, Na^+/K^+ pump function is disrupted, and Na^+ accumulates intracellularly, resulting in the formation of cellular edema. Ongoing edema formation eventually creates swelling within the cell, enclosing the organelles (Edinger and Thompson 2004). Ultimately, the cells rupture and the contents of the cells spread to the surrounding extracellular areas, triggering an inflammatory response (Edinger and Thompson 2004; Kroemer et al. 2009). On the other hand, necrosis was previously believed to be an uncontrolled and unprogrammed method of cell death, however, new research has demonstrated that necrosis occurs and processes exist within a highly regulated pathway (Golstein and Kroemer 2007). This regulated form of necrosis is referred to as necroptosis (Jun-Long et al. 2018; Liu et al. 2018; Vandenabeele et al. 2010).

Numerous studies have shown that inflammation plays a key role in the pathophysiology of ischemic stroke and affects the long-term prognosis of ischemia (Anrather and Iadecola 2016; Chamorro and Hallenbeck 2006; Jin et al. 2013; McColl et al. 2009; Shi et al. 2019). After cerebral ischemia, the inflammatory response is caused by multiple factors (Iadecola and Anrather 2011; Jayaraj et al. 2019; Levard et al. 2021). Brain injury after ischemic stroke leads to brain necrosis and apoptosis, which promotes ROS formation, exacerbates the release of multiple cytokines in damaged brain tissue and peripheral blood, and activates inflammatory cells to drive the inflammatory response (Amantea et al. 2009; Wu et al. 2020). Furthermore, the inflammatory process involves several different cell types (e.g., microglia, astrocytes, lymphocytes), inflammatory cytokines (e.g., TNF-α, IL-1β, IL-6, IFN-γ) and anti-inflammatory cytokines (e.g., TGF-β, IL-10, IL-4), as well as cell receptors (e.g., toll-like receptors (TLRs)) (Chamorro and Hallenbeck 2006; Iadecola and Anrather 2011; Jin et al. 2013; Maida et al. 2020). In addition, ROS and inflammatory factors in infarct lesions induce the expression of pro-inflammatory genes and upregulate inflammation-related cellular signaling pathways such as TLR4/NF-κB, MAPK and JAK/STAT (Dong et al. 2019; Nazarinia et al. 2021; Satriotomo et al. 2006; Yi et al. 2007).

After brain damage, microglia activation and recruitment mediate the early inflammatory response (Hu et al. 2012; Qin et al. 2019). Microglia are macrophages residing in the brain, which are highly activated after brain injury (Hoehn et al. 2005). Inhibition of microglia activation can reduce post-ischemic injury (Qin et al. 2019; Zhang et al. 2021). Ischemia activates microglia, transforming them into phagocytes that secrete numerous cytotoxic or cytoprotective components. In response to ischemia, activated microglia secrete pro-inflammatory cytokines such as TNF-α, IL-1β, IL-6, and cytotoxic factors such as upregulated prostaglandins, ROS and NO (Jin et al. 2010; Mrak and Griffin 2005). Although the initial

purpose of microglia activation is neuronal protection for the brain, excessive microglial activation can result in a detrimental inflammatory response and exacerbate neuronal death (Fernandes et al. 2014; Hu et al. 2012; Zhang et al. 2021).

1.3 Microglia and ischemic stroke

Microglia are resident immune cells in the brain that are activated after stroke and are involved in the acute, chronic and recovery phases of ischemic stroke, exerting multiple beneficial or harmful effects (Jiang et al. 2020; Li et al. 2017; Qin et al. 2019). After ischemic injury, microglia are rapidly activated and migrate towards the injured area. Interestingly, Microglia can display multiple phenotypes depending on stimulus, environment, and period, a phenomenon known as microglia polarization (Hu et al. 2012; Kanazawa et al. 2017). Microglia can either exacerbate cellular damage by secreting inflammatory cytokines and cytotoxic substances or promote tissue repair and regeneration by phagocytosing myelin and dead cell debris and producing anti-inflammatory cytokines and growth factors (Ma et al. 2017; Xiong et al. 2016). Microglia polarization is classified into classical activation pro-inflammatory phenotype and alternate activation anti-inflammatory phenotype according to the harmful pro-inflammatory signals or beneficial anti-inflammatory signals released by activated microglia (Hu et al. 2012; Kanazawa et al. 2017). However, the role and the dynamic changes of microglial phenotype after ischemic stroke remain controversial.

After stroke, disruption of homeostasis in the brain leads to activation of microglia, which is manifested by changes in cell morphology and upregulation of several cell surface markers (Ransohoff and Perry 2009). Post-ischemic inflammation is initiated along with reactive oxygen species (ROS), upregulation of autophagy, glycolysis, and several other factors that activate M1-like microglia (Amantea et al. 2009). Thereafter, this microglia produce pro-inflammatory mediators, including TNF-α, IL-1β, IFN-c, IL-6, inducible nitric oxide synthase (iNOS) and protein hydrolase (MMP9, MMP3), which further upregulate inflammation levels (Yenari et al. 2010). In contrast, M2-like microglia are characterized as pro-angiogenic and anti-inflammatory, producing IL-10, transforming growth factor β (TGF-β), and vascular endothelial growth factor (VEGF) (Ponomarev et al. 2013). In fact, this binary classification is a simplification, and there are multiple intermediate phenotypes of microglia such as M2a, M2b, and M2c (Chhor et al. 2013; Colton 2009).

In addition, it was shown that the polarization phenotype of microglia correlates with the time phase after infarction. In the MCAO model, expression levels of pro-inflammatory cytokines were observed to increase from 12 hour, reaching a peak on day 14, followed by a continuous

decrease until 28 days after MCAO (Huang et al. 2017; Zhu et al. 2019). Another previous study reached similar conclusions and found that CD16 expression levels were significantly increased from day 3 and remained elevated in the cortex and striatum at the inner border of the infarct until day 14 (Hu et al. 2012). These results were also verified in the bilateral common carotid artery ligation (BCCA) and the photothrombosis (PT) stroke model (Shang et al. 2020). In addition, many inflammatory factors, such as TNF-α, IL-1β, and IL-6, remain highly expressed in the ischemic region 2-3 weeks after stroke (Yang et al. 2018; Zong et al. 2020). Based on these studies, it seems that microglia in the acute phase of the ischemic stroke may be dominated by a proinflammatory state.

Activation of anti-inflammatory microglia can alter stroke prognosis and is advantageous in mice ischemic stroke model (Cherry et al. 2014; Li et al. 2021). In the MCAO model (Hu et al. 2012), mRNA expression levels of cytokines produced by M2-like microglia, including Arg1, Ym1/2, CCL22, IL-10, and TGF-β, were elevated at 1 - 3 days after MCAO, and with a at 3 - 5 days after ischemic injury. After 5-7 days of MCAO, the expression levels of most genes in microglia began to decrease and at 14 days, returned to pre-injury levels in the ischemic region (Hu et al. 2012). In addition, there was a similar trend in the number of CD206+ cells (Hu et al. 2012). Specific anti-inflammatory cytokines were also observed to be highly expressed on days 14 and 21 after stroke (Shang et al. 2020; Zong et al. 2020). These studies have shown that the anti-inflammatory phenotype is the predominant phenotype during the first seven days after an ischemic stroke, ultimately promoting neuronal survival after OGD (Hu et al. 2012). Based on these alterations in the expression levels of inflammatory-related markers, the following hypothesis can be drawn: microglia are activated after an ischemic stroke, and the phenotype expression pattern changes dynamically after injury, with a beneficial anti-inflammatory phenotype during the hyperacute phase, followed by a transition to a deleterious pro- inflammatory phenotype. Modulation of the phenotype conversion of microglia therefor may be an important approach for the treatment of ischemic stroke. Recent research indicated that microglial phenotype seems to coincide with the dynamic of the altered energy metabolism and lipid metabolism in microglia (Desale and Chinnathambi 2020; Holland et al. 2018; Nielsen et al. 2016), suggesting that lipid metabolism in microglia may also be one of the key factors regulating phenotypic and inflammatory expression.

1.4 Lipid droplets biogenesis

Lipid droplets (LDs), also known as lipid bodies (LBs), are intracellular storage organelles for lipids and energy present in the vast majority of cells in animals and plants, including

microorganisms (Beller et al. 2010; Bozza et al. 2007; Farese Jr and Walther 2009). In most mammalian cells, LDs are spherical organelles with a unique structure and consist of a core of neutral lipids, mainly triglycerides (TG) and cholesterol esters (Beckman 2006; Murphy and Vance 1999). Their cores are surrounded by a single layer of phospholipids and associated proteins and range in size from 0.1-2 μm, except adipocytes (up to 150 μm) (Ohsaki et al. 2009; Thiele and Spandl 2008; Walther et al. 2009). Historically, LDs were thought to be static aggregates of neutral lipids, largely associated with lipid storage. This view has changed dramatically in recent years, and LDs are now considered dynamic and functionally active organelles involved in various functions such as lipid metabolism, cell signaling, and inflammation (Martin and Parton 2006).

There are multiple sources of fatty acids required for LD formation: when fatty acids transported through the extracellular space for example by association to albumin and lipoproteins enter the cell, lipoprotein lipase releases them from triacylglycerols in lipoproteins and they enter the cell by passive diffusion facilitated via fatty acid transport proteins or fatty acid translocases (Ehehalt et al. 2006; Guo et al. 2009). Fatty acids can also be de novo synthesized from carbohydrates in various cell types (Walther et al. 2009). Fatty acids enter the bioactive pool by binding to coenzyme A and form fatty acid-coenzyme A. Lipoyl coenzyme A generates diacylglycerol from glycerolipid synthase within the endoplasmic reticulum (ER). Diacylglycerols are eventually converted to neutral lipids (triacylglycerols) by DGATase or enter the phospholipid synthesis pathway (Murphy and Vance 1999; Ohsaki et al. 2009; Thiele and Spandl 2008; Walther et al. 2009). Unlike fatty acids, sterols enter the cell mainly through endocytosis and lysosomal degradation of lipoproteins. Most cells can also synthesize sterols. In the ER, excess sterols are converted to sterol esters by binding to fatty acyl-coenzyme A. Then, neutral lipids are synthesized in the ER as LDs (Ohsaki et al. 2009). Thereafter cytoplasmic LDs can further increase in size by local lipid synthesis (Kuerschner et al. 2008) or by LDs fusion (Olofsson et al. 2009). Stored lipids are mobilized through the activity of specific lipases and other metabolic enzymes depending on the cellular demand for energy. Therefore, these studies suggest that both anabolism and catabolism of lipids occur in LDs; thus, LDs play a key role in lipid metabolism. (Beller et al. 2010; Farese Jr and Walther 2009; Martin and Parton 2006; Melo et al. 2011).

The proteins of LDs are also important components and play a dynamic functional role (Bersuker et al. 2017; Bickel et al. 2009; Melo et al. 2011; Robenek et al. 2009). However, how these proteins are synthesized and transferred to LDs is still controversial. First, one possible pathway is that the proteins may use long membrane-embedded domains that enter and exit the

membrane on the same side of the lipid monolayer (Robenek et al. 2009). The caveolin of the LDs plasma membrane (Martin and Parton 2006) and the lipid synthase DGAT2 are synthesized in this manner (Kuerschner et al. 2008). Second, proteins may bind to the surface of LDs as peripheral membrane proteins by embedding amphipathic helices. These proteins of LDs have been extensively studied and play multiple roles in immune responses, inflammation and tumors (Lin et al. 2019; Luis et al. 2021; Mardani et al. 2019; Marschallinger et al. 2020; Zheng et al. 2017). The biogenesis and structure of lipid droplets are shown in Figure 1.

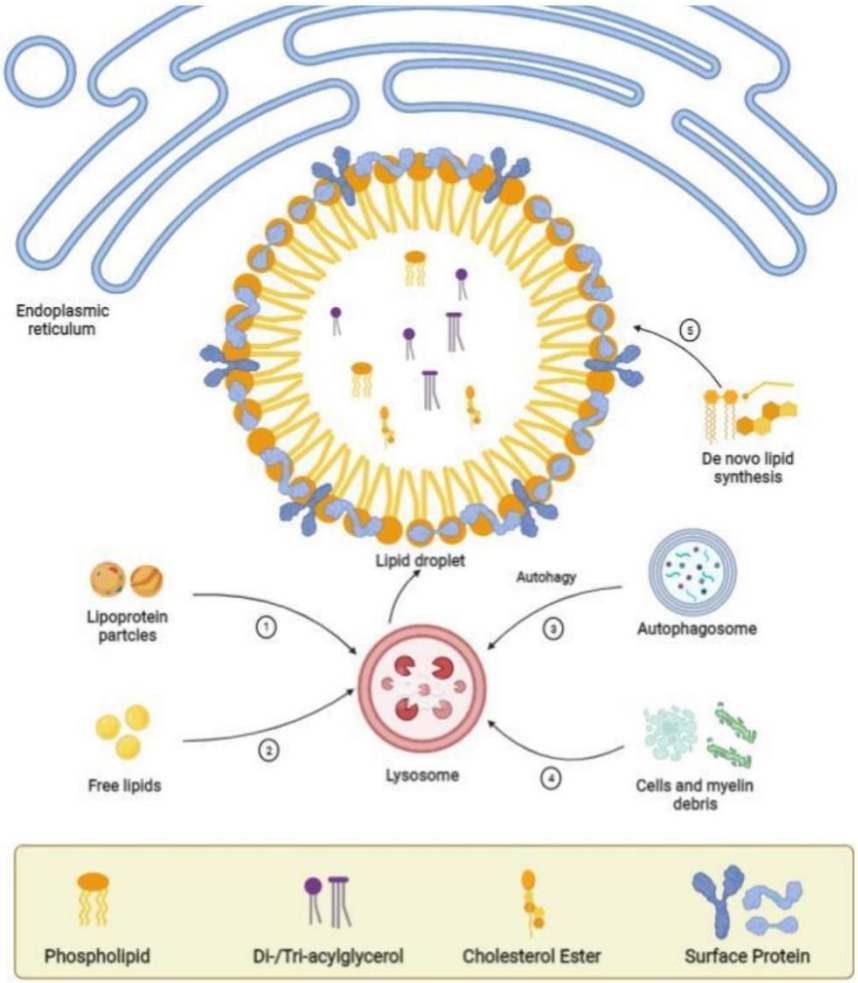

Figure 1. Lipid droplet biogenesis. Lipid droplets (LDs) are spherical organelles with a unique structure consisting of a core of neutral lipids, mainly triglycerides (TG) and cholesteryl esters. Their core is surrounded by a monolayer of phospholipids and associated proteins. LDs are dynamic and functionally active organelles involved in various functions such as lipid metabolism, cell signaling and inflammation.

1.5 Lipid metabolism in microglia

Under physiological conditions, microglia typically exhibit a resting morphology, but under the influence of different stimuli, microglia can polarize into various phenotypes, although there is controversy over how to delineate the microglia phenotype (Paolicelli et al. 2022; Ransohoff

2016). Microglia take an important role in regulating the inflammatory response and are responsible for the production of various cytokines and ROS (Hanisch and Kettenmann 2007; Kettenmann et al. 2011). On the other hand, microglia can also inhibit the neuroinflammatory response and promote tissue repair and immunosuppression, thus acting as neuroprotective agents (Bernier et al. 2020). However, although the mechanisms underlying microglia phenotype and function remain unclear, there is growing evidence that lipid metabolism and lipidomics of microglia may be relevant to their inflammatory and other functions. Microglia express a range of genes related to lipid metabolism, including fatty acid oxidase, lipoprotein lipase and lipid transport proteins (Brown and Neher 2014; Gao et al. 2017; Mecha et al. 2015). When microglia are exposed to external stimuli, such as starvation (Rambold et al. 2015), inflammation (Khatchadourian et al. 2012; Melo et al. 2011), and oxidative stress (Lee et al. 2013), lipids can act as signaling molecules that regulate microglial functions. This microglia lipidomic pattern regulates vital functions such as inflammation and phagocytosis (Bernier et al. 2020; Hickman et al. 2013).

Indeed, the morphology and function of microglia are in dynamic flux to adapt to different. As a result, the metabolic patterns of microglia are subsequently regulated so that they exhibit different phenotypes during physiological and pathological processes (Chausse et al. 2021). New evidence suggests that reprogramming of cellular metabolism mediates this phenotypic shift, and microglial lipid metabolism is particularly involved in controlling microglial activation and effector functions such as migration, phagocytosis and inflammatory signaling (Cheon and Cho 2021). Minor disturbances in microglial lipid processing are associated with altered brain function in diseases characterized by neuroinflammation (Cheon and Cho 2021). It has been suggested that glycolysis in microglia is upregulated when exposed to pro-inflammatory stimuli (Holland et al. 2018), and further upregulates fatty acid synthesis (Peruzzotti-Jametti and Pluchino 2018). First, mitochondrial citric acid is transported to the cytoplasm and converted to acetyl coenzyme A (Infantino et al. 2011), while transcription factor sterol regulatory element binding proteins (SREBPs) via mTOR activation and the production of NADPH may upregulate lipid synthesis (Gaber et al. 2017; Oishi et al. 2017). Ultimately, the increasing of ROS due to damaged mitochondria, the activation of SREBP, and the accumulation of triacylglycerols (TAGs) and cholesteryl esters (CEs) in microglia to form abundant LDs, transform microglia into "foam microglia" with impaired phagocytosis (Son et al. 2016), and upregulate the levels of inflammatory signals, ROS and NO via TLR4/NF-kB, JNK/ SREBP signaling pathway (Liu et al. 2015; Oishi et al. 2017; Rambold et al. 2015; Simpson and Oliver 2020; Wang et al. 2012). On the other hand, fatty acid oxidation (FAO) is essential for M2-like alternative activation in macrophages and microglia (Mehla and Singh 2019; Raas et al. 2019).

In addition, altered patterns of lipid synthesis and energy metabolism also regulate the dynamic phenotype of microglia (Cheon and Cho 2021). Long-chain fatty acid coenzyme A synthase in microglia, which catalyzes the formation of fatty acid coenzyme A and the subsequent β-oxidation of fatty acids to acetyl coenzyme A (Zhang et al. 2014), and is further involved in further metabolism in the TCA cycle, activates microglia (Doens and Fernández 2014; Khatchadourian et al. 2012). Multiple enzymes and biomarkers (e.g. PPAR-γ, IL-4) have been proposed to be involved in inducing microglia conversion to the anti-inflammatory phenotype through the regulation of fatty acid metabolism (Bruce et al. 2018; Li et al. 2021).

Taken together, microglia under pro-inflammatory stimuli may be more inclined to fatty acid synthesis, whereas microglia in the anti-inflammatory phenotype are more inclined to fatty acid oxidation. Modulation of lipid metabolism and composition within microglia may be a potential target for future treatments of neurological disorders (Arbaizar-Rovirosa et al. 2022; Farmer et al. 2020; Hu et al. 2017; Marschallinger et al. 2020).

1.6 Functions of lipid droplets in inflammation

Lipid droplets can affect the signaling pathway by actively removing biologically active signaling lipids into the storage pool or regulating their release and production from stored precursors (Coleman and Mashek 2011; Zechner et al. 2012). In addition to fatty acids (FAs), all other major intermediates of TAG synthesis and catabolism, such as acyl-coenzyme A, phosphatidic acid, diacylglycerol (DAG) (Coleman and Mashek 2011; Zechner et al. 2012), and sterols are involved in lipid droplet formation and affect various signaling pathways (Shmarakov et al. 2019; Stith et al. 2019). Regulation of lipid metabolism and prevention of lipotoxicity are essential to maintain intracellular homeostasis (Petan et al. 2018).

Lipid droplet biogenesis are involved by activating cellular stress and regulating inflammatory signaling pathways (Cantley et al. 2013; Jump 2004; Papackova and Cahova 2015; Zechner et al. 2012), including the PPAR signaling pathway and TLR/NF-kB inflammatory pathways which are activated by saturated FAs (Lu et al. 2015; Sun B et al. 2018), the conversion of PUFAs to dicarbonyl analogues; the regulation of SREBP signaling by cholesterol and FAs (Kim et al. 2002; Tai and Ding 2010); the activation of protein phosphatase 2A (PP2A) by ceramide (Choi et al. 2018; He Z et al. 2019); and the activation of membrane resident DAG by activation of protein kinase (Eichmann et al. 2015). Lipid droplet accumulation is accompanied by elevated levels of Perilipin-2 protein (Plin2) in macrophages (Huang et al. 2014; Maya-Monteiro et al. 2008). Increased Plin2 expression itself has been shown to directly associated with enhanced neutral lipid storage capacity, as Plin2 promotes triglyceride and cholesterol storage

and reduces cholesterol efflux (Larigauderie et al. 2004). Recently, mTOR-dependent mechanisms of lipid droplet biogenesis were identified (Cheon and Cho 2021; Maya-Monteiro and Bozza 2008) and the mTOR inhibitor rapamycin significantly reduced lipid droplets (Fazolini et al. 2015; Liao et al. 2021; Maya-Monteiro et al. 2008). Moreover, activation of PPAR transcription factors is involved in lipid droplet biogenesis and function. PPAR directly regulates the expression of fatty acid uptake, lipid storage and inflammatory responses involved in fatty acid uptake, including fatty acid synthase and Plin2, by binding to the retinoid X receptor (RXR) (Hellemans et al. 2007; Nagy et al. 1998; Suzuki et al. 2009).

As mentioned above, lipid droplets may serve as new treatment targets for inflammatory-related diseases. To date, the hypothesis that knockdown of perilipins, ADRP and TIP-47 proteins (Mardani et al. 2019; Szigeti et al. 2009; Zheng et al. 2017) and inhibitors of lipid droplets formation as anti-inflammatory therapeutics has been validated in various experimental model (Blakeman et al. 2012; Dechandt et al. 2017; Namatame et al. 1999; Prior et al. 2014; Zhang-Gandhi and Drew 2007).

1.7 The role of lipid droplets in ischemic stroke

LDs are associated with a variety of neurological diseases such as neurodegenerative diseases (Farmer et al. 2020; Hu et al. 2017; Marschallinger et al. 2020), stroke (Arbaizar-Rovirosa et al. 2022; Lin et al. 2019), multiple sclerosis (Haidar et al. 2022) and infectious diseases (Ogawa et al. 2009). Accumulation of LDs is primarily based on elevated lipid synthesis, abnormal lipid metabolism and impaired lipid clearance (Beller et al. 2010; Cantuti-Castelvetri et al. 2018; Melo et al. 2011). Several studies have shown that the accumulation of LDs and the dynamic alteration of lipid metabolism in Alzheimer's disease (AD) and Parkinson's disease (PD) (Liu et al. 2015; Marschallinger et al. 2020). However, the role of LDs in ischemic stroke is poorly understood.

Cerebral ischemia is a disease in which the brain suffers from a lack of energy and oxygen supply due to the interruption of the blood flood, which in turn causes massive neuronal death (Hisham et al. 2013; Lipton 1999; Michiels 2004). After glucose and oxygen supply of neurons are blocked, the ATP reserves are also depleted and lead to post-stroke excitotoxicity. The causes of cell death during this period include abnormal ion pump function, increased ROS production, inflammation, mitochondrial dysfunction, endoplasmic reticulum stress, excessive activation of autophagy and ferroptosis (Bano and Nicotera 2007; Forrester et al. 2018; Hou et al. 2016; Incalza et al. 2018; Jayaraj et al. 2019; Li et al. 2020; Radak et al. 2017; Sarmah et al. 2019; Xu et al. 2022). Most of these cellular damages can further induce LD formation. These studies found that neutral lipid signals were derived from triglycerides and cholesterol esters, which are

the main components of LDs. Similar to neurodegenerative pathology, lipid droplets formation during the stroke are mainly found in microglia and astrocytes (Gasparovic et al. 2001; Ioannou et al. 2019). Multiple mechanisms may contribute to the creation of LDs. One of these may be the rapid incidence of massive cell death, which may result in glial cell phagocytosis of dead cells and the subsequent formation of LDs (Lin et al. 2019). Another potential mechanism for LD formation during stroke may be the influx of peripheral lipoprotein particles due to disruption of the blood-brain barrier (Doll et al. 2015; Jackman et al. 2013). Other factors, such as direct exposure of glial cells to oxidative stress and inflammatory factors, can also result in enormous numbers of LDs-riched microglia (Khatchadourian et al. 2012; Rambold et al. 2015; Volobouеva et al. 2013). However, more research is required on the functions of such "foam microglia" in cerebral ischemia, especially in the non-acute and recovery phases.

1.8 Lipid metabolism and inflammation in microglia after stroke

After cerebral ischemia, it has been shown that the infarct core region of the brain and around the penumbra zone are colonized by a large number of activated microglia, which play a vital role in stroke prognosis for example through phagocytosis of dead cell debris and regulation of inflammatory factor levels (Kanazawa et al. 2017; Qin et al. 2019; Xiong et al. 2016). Furthermore, in models of ischemia *in vivo*, genes related to glycolysis and oxidative phosphorylation in CD11b+ microglia were found to increase during post-ischemia 24 hours, whereas the expression levels of genes related to glycolysis, such as lactate dehydrogenase A and pyruvate kinase M2, remained unchanged for 72 h (Lauro et al. 2019). Similarly, glycolytic reprogramming occurs together with microglia pro-inflammatory activation under hypoxia *in vitro* (Li et al. 2018). In summary, glycolysis in microglia is upregulated following ischemia, which is closely linked to its inflammation and phenotypic polarization (Yang et al. 2021).

Lipid metabolism is also involved in the phenotypic transformation of microglia after ischemia, particularly for polyunsaturated fatty acids. It has been shown that Omega-3, GPR120, and adipocyte fatty acid binding protein (A-FABP) are upregulated in microglia after ischemic injury and are protective against neurological damage (Liao et al. 2020). Briefly, microglia in the pro-inflammatory state preferentially produce energy through glycolysis, whereas cells in the anti-inflammatory state provide energy primarily through oxidative phosphorylation and fatty acid oxidation (Yang et al. 2021). Therefore, we speculate that during the acute phase of infarction (the first 3 days after stroke), when neurons have not yet died in large numbers, microglial cells in the core of the ischemic area can be mainly found in an M2-like phenotype that provides energy through oxidative phosphorylation and fatty acid oxidation, and upregulate anti-

inflammatory factors that might help to neuronal survival. Later (3 - 7 days after stroke), the internal environmental homeostasis is disrupted and the anti-inflammatory effect of microglia is not sufficient to rescue these neurons, and a large number of neurons begin to undergo massive necrosis and apoptosis. At this time, most microglia begin to transform into pro-inflammatory, M1-type microglia that preferentially produce energy through glycolysis. The rise of glycolysis is accompanied by a lipid metabolism disorder and the accumulation of harmful lipid components (e.g., triglycerides and cholesterol esters), impairment of mitochondrial function, upregulation of ROS, upregulation of inflammatory factors and phagocytosis of cellular debris, resulting in a large accumulation of lipid components in microglia and the formation of "foam microglia" overloaded with lipid droplets. Similar to the "foam microglia" in other neurological diseases, these special microglia no longer "protect" neurons, but instead swallow or release inflammatory factors that damage neurons through the "eat-me" signaling pathway (Jia et al. 2022; Lemke 2019). This is also in line with previous results in animal models where microglia changed from the initial M2 anti-inflammatory type to the M1 pro-inflammatory type overtime after stroke (Hu et al. 2014).

1.9 Aim of the study

Lipid metabolism and LD biogenesis have recently been described to regulate inflammation, immunomodulation, and microglial phagocytosis under neurodegenerative disorders, but their roles in post-stroke injury remain unclear. Therefore, the present thesis aims to certify the histological characterization of microglial phenotypes in the context of LD accumulation with MCAO model *in vivo* and OGD model *in vitro*, followed by correlating the data obtained with the expression of inflammation-related genes at the protein level and mRNA level. The lipid composition of brain regions that have undergone ischemic damage will be analyzed from the core of the ischemic lesion and the marginal zone and contralateral hemisphere. We aim to elucidate and differentiate lipid profiles resulting in LD formation, which in turn modulates microglial phenotypes and activity in ischemic conditions of the CNS, ultimately correlating with the extent of neurological impairment.

2 Materials and methods

2.1 Equipment

Table 1. Equipment

Instrument	Manufacturer, City, Country
Accu-jet Pro pipetting aid	Brand GmbH, Wertheim, Germany
Autoclave Systec VX-65	Systec GmbH, Linden, Germany
Centrifuge 5810R	Eppendorf, Hamburg, Germany
Fisherbrand Shaking device	Fisher Scientific GmbH, Schwerte, Germany
Freezer -20 °C	Liebherr, Bulle, Switzerland
Freezer -80 °C Heraeus	Fisher Scientific GmbH, Schwerte, Germany
Microbiological Safety Cabinet Class II	Fisher Scientific GmbH, Schwerte, Germany
Hypoxic Glovebox IBT-HGB16	Toepffer Lab Systems, Göppingen, Germany
KL 1500 LCD	Schott AG, Mainz, Germany
Multipette Plus	Eppendorf, Hamburg, Germany
Neubauer cell counting chamber	Carl Roth, Karlsruhe, Germany
Pipettes (2.5/10/100/1000/5000 µL)	Eppendorf, Hamburg, Germany
Pipetus pipetting aid	Hirschmann Laboratory, Germany
Refrigerator +4 °C	Liebherr, Bulle, Switzerland
VF Ultrapure Water System	Sartorius AG, Göttingen, Germany
Tecan Sunrise Microplate Reader	Tecan Group AG, Männedorf, Switzerland
Clean air workbench	Fisher Scientific GmbH, Schwerte, Germany
CO_2-Incubator	Fisher Scientific GmbH, Schwerte, Germany
Transferpette Pipettes (10/ 100/1000 µL)	Brand GmbH, Wertheim, Germany
Water Bath WNB 45	Memmert GmbH, Schwabach, Germany
Zeiss Axiovert 25 inverse microscope	Zeiss, Oberkochen, Germany
Zeiss Stemi 2000 ZOOM stereomicroscope	Zeiss, Oberkochen, Germany

2.2 Consumables

Table 2. Consumables

Consumables	Manufacturer, City, Country
0.45 µm filter Filterpur S0.45	Sarstedt, Nümbrecht, Germany
6-well plates for cell culture	Sarstedt, Nümbrecht, Germany
12-well plates for cell culture	Sarstedt, Nümbrecht, Germany
24-well plates for cell culture	Sarstedt, Nümbrecht, Germany
96-well plates, flat bottom	Sarstedt, Nümbrecht, Germany
Bottle-Top-Filter, 0.2 µm, 500 mL	Carl Roth GmbH, Karlsruhe, Germany
Cell culture flasks for adherent cells (25cm^2, 75 cm^2)	Sarstedt, Nümbrecht, Germany
Centrifugation tubes (15 mL)	Sarstedt, Nümbrecht, Germany
Centrifugation tubes (50 mL)	Sarstedt, Nümbrecht, Germany
Glass Pasteur pipettes (150 mm, 230 mm)	Th. Geyer Ingredients GmbH & Co. KG, Renningen, Germany
Petri dishes, 100 mm	Greiner Bio-One, Frickenhausen, Germany
Pipette tips filters, sterile (10 µL, 100 µL, 1000 µL)	Starlab, Hamburg, Germany
Pipette tips w/o filters (10 µL)	Starlab, Hamburg, Germany
Pipette tips w/o filters (200 µL, 1000 µL, 5000 µL)	Sarstedt, Nümbrecht, Germany
Reaction tubes (1.5 mL, 2.0 mL)	Sarstedt, Nümbrecht, Germany
Serological pipettes (2 mL, 5 mL, 10 mL, 25 mL, 50 mL)	Sarstedt, Nümbrecht, Germany
CryoPure® pipes	Sarstedt, Nümbrecht, Germany
Parafilm	Bemis NA, Neenah, USA

2.3 Chemicals

Table 3. Chemicals

Chemicals	Manufacturer,City, Country
B27™ Supplement (50X)	Fisher Scientific GmbH, Schwerte, Germany
Boric acid	Sigma-Aldrich, Taufkirchen, Germany
Dimethyl Sulfoxide	Th. Geyer GmbH, Renningen, Germany
DNase I	Sigma-Aldrich, Taufkirchen, Germany
Dulbecco's Phosphate Buffered Saline	Sigma-Aldrich, Taufkirchen, Germany
Ethanol 99%	Th. Geyer GmbH, Renningen, Germany
Ethanol 100%	Merck KGaA, Darmstadt, Germany
FBS Superior	Sigma-Aldrich, Taufkirchen, Germany
GlutaMAX™-I (100X)	Fisher Scientific GmbH, Schwerte, Germany
HEPES 1M	Sigma-Aldrich, Taufkirchen, Germany
holo-Transferrin (human)	Sigma-Aldrich, Taufkirchen, Germany
HyClone Characterized Fetal Bovine Serum	Cytiva, Freiburg in Breisgau, Germany
L-Glutamine 200mM (100X)	PAN-Biotech GmbH, Aidenbach, Germany
Neurobasalä Medium (1X)	Fisher Scientific GmbH, Schwerte, Germany
Penicillin-Streptomycin	Fisher Scientific GmbH, Schwerte, Germany
Poly-L-omithine hydrobromide	Sigma-Aldrich, Taufkirchen, Germany
Primocin®	InvivoGen, Toulouse, France
Thiazolyl Blue Tetrazolium Bromide	Sigma-Aldrich, Taufkirchen, Germany
Trypan Blue Solution 0.4%	Fisher Scientific GmbH, Schwerte, Germany

0.5% Trypsin-EDTA (10x)	Fisher Scientific GmbH, Schwerte, Germany
DMEM/F12 (1:1) Medium (1X)	PAN-Biotech, Aidenbach, Germany
Recombinant Murine M-CSF	Peprotech, Hamburg, Germany

Table 4. Components of cell culture media and OGD buffer

Primary neuron	**Primary microglia**	**BSS0 for OGD**
Neurobasalä Medium (1X)	DMEM/F12 (1:1) Medium	NaCl (116 mM)
B27 Supplement (2% in medium)	Fetal bovine serum (10% in medium)	KCl (5.4 mM)
Transferrin (5 μg/ml)	1x Pen-Strep (1% in medium)	$MgSO_4$ (0.8 mM)
L-glutamine (0.5 mM)	L-glutamine (0.5 mM)	$NaH_2PO_4H_2O$ (1 mM)
1x Pen-Strep (1% in medium)		$NaHCO_3$ (26.2 mM)
		HEPES (10 mM)
		Glycine (0.01 mM)
		$CaCl_2$ (1.8 mM)

2.4 Antibodies

2.4.1 Primary antibodies

Table 5. Primary antibodies

Antibodies	**Manufacturer**	**Identifier**	**Application**
GFAP	Invitrogen	13-0300	2 μg/ml (for IF)
CD11b	Abcam	Ab75476	2 μg/ml (for IF)

iNOS	Abcam	ab15323	2 μg/ml (for IF)
Iba1	WAKO	011-27991	2 μg/ml (for IF)
P2Y12	Alomone Labs	APR-012	2 μg/ml (for IF)
CD68	Bio-Rad	MCA1957GA	2 μg/ml (for IF)
TMEM119	Abcam	ab209064	2 μg/ml (for IF)
PLIN3	Progen	G37	2 μg/ml (for IF), 0.5 μg/ml (for WB)
PLIN2	Progen	G42	2 μg/ml (for IF), 0.5 μg/ml (for WB)
CD206 (Mannose Receptor)	Abcam	ab64693	2 μg/ml (for IF)
NeuN	Millipore	MAB377	4 μg/ml (for IF)
CX3CR1	Thermo Fisher	PA5-19910	2 μg/ml (for IF)
Arginase I	Santa Cruz Biotechnology	sc-20150	4 μg/ml (for IF)
BODIPY 493/503	Thermo Fisher	D3922	1 μg/ml (for IF), 0.5 μg/ml (for FACS)
NF-κB p65	Abcam	ab16502	0.5 μg/ml (for WB)
α-tubulin	GeneTex	GTX628802	0.1 μg/ml (for WB)
GAPDH	GeneTex	GTX627408	0.1 μg/ml (for WB)

β-actin	Abcam	ab6276	0.2 μg/ml (for WB)
IκBα	Cell Signaling Technology	#9242	0.5 μg/ml (for WB)
IL-1ß	Abcam	ab9722	0.5 μg/ml (for WB)
TGF-ß1	Abcam	ab92486	0.5 μg/ml (for WB)
SREBP2	Thermo Fisher	PA5-88943	0.5 μg/ml (for WB)
CD45	BD Biosciences	563891	20 μg/ml (for FACS)
CD11b	BD Biosciences	552850	20 μg/ml (for FACS)

WB: Western Blot

IF: Immunofluorescence Staining

FACS: Fluorescence-activated Cell Sorting

2.4.2 Secondary antibodies

Table 6. Secondary antibodies

Antibodies	Manufacturer	Identifier	Application
Alexa Fluor 488 donkey anti-mouse	Jackson Immuno	715-547-003	0.5 μg/ml (for IF)
Alexa Fluor 488 donkey anti-guinea pig	Jackson Immuno	706-545-148	0.5 μg/ml (for IF)

Alexa Fluor 488 donkey anti-rat	Jackson Immuno	712-547-003	0.5 μg/ml (for IF)
Alexa Fluor 488 donkey anti-rabbit	Jackson Immuno	711-547-003	0.5 μg/ml (for IF)
Cy 3 donkey anti-rabbit	Jackson Immuno	711-165-152	0.5 μg/ml (for IF)
Cy 3 donkey anti-rat	Jackson Immuno	712-165-153	0.5 μg/ml (for IF)
Goat Anti-Mouse IgG H&L	Abcam	ab97023	0.1 μg/ml (for WB)
Goat Anti-Rabbit IgG H&L	Abcam	ab97051	0.1 μg/ml (for WB)
Goat Anti-Guinea pig IgG H&L	Abcam	ab6908	0.1 μg/ml (for WB)

WB: Western Blot

IF: Immunofluorescence Staining

2.5 The mRNA candidates and primer sequences

Table 7. Primer sequence

mRNA	**Sequence** (5'-3')
CD206	Forward Sequence: CTCTGTTCAGCTATTGGACGC
	Reverse Sequence: CGGAATTTCTGGGATTCAGCTTC
iNOS	Forward Sequence: AGGAACCTACCAGCTCACTCTG
	Reverse Sequence: TTTCCTGTGCTGTGCTACAGTT

IL-1β	Forward Sequence: GCAACTGTTCCTGAACTCAACT
	Reverse Sequence: ATCTTTTGGGGTCCGTCCAACT
IL-6	Forward Sequence: GAGGATACCACTCCCAACAGACC
	Reverse Sequence: AAGTGCATCATCGTTGTTCATACA
IL-10	Forward Sequence: AGAAAAGAGAGCTCCATCATGC
	Reverse Sequence: TTATTGTCTTCCCGGCTGTACT
TNF-α	Forward Sequence: AAGCCTGTAGCCCACGTCGTA
	Reverse Sequence: GGCACCACTAGTTGGTTGTCTTTG
TGF-β1	Forward Sequence: CCTGTCCAAACTAAGGC
	Reverse Sequence: GGTTTTCTCATAGATGGCG
PLIN3	Forward Sequence: ATGTCTAGCAATGGTACAGATGC
	Reverse Sequence: CGTGGAACTGATAAGAGGCAGG
PLIN2	Forward Sequence: ACACCCTCCTGTCCAACATC
	Reverse Sequence: AAGGGACCTACCAGCCAGTT
TREM2	Forward Sequence: CCCACCTGGCTGTTGTCCTT
	Reverse Sequence TCGCTACCGTGGAGGCTCTG
ABCA1	Forward Sequence: GCTTGTTGGCCTCAGTTAAGG
	Reverse Sequence: GTAGCTCAGGCGTACAGAGAT
ApoE	Forward Sequence: CTGACAGGATGCCTAGCCG
	Reverse Sequence: CGCAGGTAATCCCAGAAGC
Lipa	Forward Sequence: AGCGACGACTTGGTGTTCC
	Reverse Sequence: CGCAGGTAATCCCAGAAGC
Npc2	Forward Sequence: AGGACTGCGGCTCTAAGGT
	Reverse Sequence: AGGCTCAGGAATAGGGAAGGG
Soat1	Forward Sequence: GAAGGCTCACTCATTTGTCAGA
	Reverse Sequence: GTCTCGGTAAATAAGTGTAGGCG
Nceh1	Forward Sequence: TTGAATACAGGCTAGTCCCACA

	Reverse Sequence: CAACGTAGGTAAACTGTTGTCCC
β-actin	Forward Sequence: CGTGCGTGACATCAAAGAGA
	Reverse Sequence: CCCAAGAAGGAAGGCTGGA
GAPDH	Forward Sequence: TGGATTTGGACGCATTGGTC
	Reverse Sequence: TTTGCACTGGTACGTGTTGAT
PPIA	Forward Sequence: GAGCTGTTTGCAGACAAAGTTC
	Reverse Sequence: CCCTGGCACATGAATCCTGG

2.6 Legal issues, animal housing, randomization and blinding

All animal experiments were performed with local government authorization, in accordance with EU guidelines and regulations, and in accordance with ARRIVE and STAIR principles for the care and management of laboratory animals. Male C57BL/6J mice aged 10-12 weeks, (Janvier Labs, Le Genest-Saint-Isle, France) were maintained in groups of 5 animals per cage on a regular 12 hour light/12 hour dark cycle. Animal surgery and sample collection were always performed in the morning throughout the study. At all stage of the studies, the experiments were strictly random. The researchers with local animal experimental licenses performed animal surgery and sample collection and remained blinded during all phases of the study, and another investigator prepared the experimental solution and data collection. These solutions and groups were received and disclosed only after the study.

2.7 Culture of primary neurons and microglia

Primary cortical neurons were prepared following the protocol from Thomas et al (Fath et al. 2009) with some modification. Pregnant C57BL/6J mice at embryonic day 16.5 were sacrificed by CO_2 euthanasia. Embryos were dissected and decapitated, the brain was carefully dissociated from the skull, and meninges were carefully removed. The cerebral cortex and hippocampus were carefully isolated and moved into a 15-ml tube with 8 ml cooled PBS on ice. Thereafter, PBS was carefully removed, and the tissue at the bottom was gently mixed by a polished pasteurpipette and digested with 1 ml of 0.05% Trypsin-EDTA in 15-ml tubes with 15 min of incubation in a 37℃ water bath. Then 50 µl of DNAse (Sigma-Aldrich, Taufkirchen, Germany) was added and mixed carefully by pipetting and incubating for another 1 min at room temperature (RT). Primary neuron culture medium (Components are shown in Table 4.) was

added to stop the digestion. The medium containing primary neurons was carefully pipetted and centrifuged at 300x g for 5 min at room temperature (RT). The supernatant was discarded and the pellet was washed three times with 10 ml culture medium. All the medium from each washing was collected in a 50-ml tube, and centrifuged at 300x g for 5 min at RT. The primary neuron pellet was finally resuspended in 2 ml of culture medium, and the cells were seeded on poly-L-ornithine/laminin (Sigma-Aldrich, Taufkirchen, Germany) pre-coated 6-well or 24-well plates at a density of 200,000 cells/cm^2 containing neurobasal medium in an incubator at 5% CO2, 37℃. Primary neuron cells were cultured for another 5 days before being used for subsequent experiments.

Primary microglia cells were isolated from C57BL/6J newborn pups at postnatal 0-2 day, based on the protocol of Hong et al (Lian et al. 2016) with some modification. The whole brains of pups were removed and placed into a 6-cm dish with 5 ml cold HBSS. The cerebellum and olfactory bulbs were carefully removed. The cortex and hippocampus were carefully separated with forceps and scissors and moved in a 15-ml tube containing 8 ml cold PBS. The discrete tissues were centrifuged at 100x g for 2 min at RT. After centrifugation, PBS was carefully removed, and the tissue was digested with 1 ml of 0.25 % Trypsin-EDTA in a 15-ml tube. After 15 min incubation in the 37℃ water bath, 100 µl of DNAse (Sigma-Aldrich, Taufkirchen, Germany) was added and mixed carefully by pipetting and for another 1 min incubation at room temperature (RT). Digestion was then terminated with 5 ml of warm primary microglia medium (Components are shown in Table 4.). The cell suspension was centrifuged at 300x g for 5 min, and then the pellet was gently resuspended with 5 ml of warm medium and transferred to a T75 flask precoated with poly-L-ornithine (PLO), incubated under 37°C, 5% CO_2 conditions. After 5 days, astrocytes at the bottom of the flask formed a confluent cell layer, while microglia and a few oligodendrocytes grew on top. To stimulate microglial proliferation, the culture medium was changed to a new medium with 5 µM suitable murine macrophage colony-stimulating factor (M-CSF, Peprotech, Hamburg, Germany). After another 3-4 days, to collect microglia, the flask was shaken vigorously and floating microglia was collected in conditioned medium. The floating cell density was calculated with the hemocytometer and primary microglia was seeded at 40,000 cells/cm^2 in PLO-coated dishes or flasks for upcoming experiments.

2.8 Oxygen-glucose deprivation (OGD) model

Primary neurons or microglia were incubated for 5–7 days, and when the cell confluence reached 80-90%, the cells were exposed to oxygen-glucose deprivation (OGD). For OGD procedure, cells were washed twice with PBS and incubated with the same volume of BSS0 solution buffer

(Components are shown in Table 4) and transferred to a hypoxic incubator (Toepffer Lab Systems, Goeppingen, Germany) containing 0.2 % O_2, 5% CO_2 and 70% humidity. After OGD, the BSS0 solution was removed, washed once with PBS, incubated the cells with the original medium and specific treatment, then the cells were reoxygenated (RO) for 24 h in the 5% CO_2 incubator at 37 °C. The cells would then be used in the following experiments. Depending on the resistance of various cell types to hypoxic damage, primary microglia and cortical neurons were exposed to OGD for 4 h, 8 h, and 12 h, respectively, to determine the ideal time point, with a 50% survival rate after hypoxia. For all *in vitro* experiments, intervention treatments were performed during OGD and RO.

2.9 Drug treatment of primary microglia

After seeding, the medium of primary cortical neurons was half replaced on the next day and then cultured for additional five days before OGD treatment. Similarly, the primary microglia medium was replaced the day after seeding, drug treatment was added, and cultured for another 24 hours. For drug treatment, Lipopolysaccharide (LPS, Sigma-Aldrich Chemie, Taufkirchen, Germany), Interleukin 4 (IL-4, Sigma-Aldrich Chemie, Taufkirchen, Germany) and Triacsin C (Trc, Cayman Chemical, Michigan, USA) were added to the culture medium for extra 24 hours. The Control group was given an equal volume of vehicle PBS. Therefore, cells including primary microglia and microglia-neuron co-culture models were divided into the following seven groups: group 1 (microglia treated with drug solvent in normoxic condition); group 2 (OGD/RO treatment with drug solvent); group 3 (1000 ng/ml LPS treatment); group 4 (2 μM Trc inhibitor treatment in group 3); group 5 (incubation with conditioned medium from neurons after OGD/RO), group 6 (2 μM Trc inhibitor treatment in group 5) and group 7 (10 ng/ml recombinant IL-4 treatment).

2.10 Primary microglia–neuron co-culture system

The co-culture model used primary microglia and primary neurons to study the effect of microglia on neuron survival under hypoxia condition. The experiment was based on the protocol of Skaper et al with some optimizations (Skaper and Facci 2018). Primary microglia was seeded into 6-well (4×10^5 cells/insert) or 24-well (2×10^4 cells/insert) transwells (3 μm pore size; Costar, Maryland, USA). To certificate the effect of different phenotypes of microglia under specific treatments on neurons, different treatments of microglia were tested: Lipopolysaccharide (LPS); OGD; conditioned medium from post-OGD neurons (OGD-CM); Triacsin C (Trc); Interleukin-4 (IL-4) as a positive control. After 24 hours of incubation, these

primary microglia were added to plates pre-seeded with primary neurons, and this co-culture system then was incubated for another 24 hours. Microglia were co-cultured with primary neurons at the start of the reoxygenation of neurons after OGD.

2.11 Cell viability assay

Cell viability was measured via a colorimetric assay by using the MTT (Thiazolyl Blue Tetrazolium Bromide, Sigma-Aldrich, St. Louis, MO) viability assay according to the protocol from Riss et al with some modifications(Riss et al. 2016). After 24 hours of reoxygenation culture, 50 µl of MTT solution (5 mg/ml) was added to each well of the 24-well plate, and incubated for extra 4 hours in 5% CO_2, 37°C. Afterward, the medium in the wells was carefully aspirated, and 500 µl of DMSO was added to each well to dissolve the blue formazan crystals, shaken for 10 minutes to fully dissolve the crystals, avoiding the light. Absorbance was measured with the Tecan Sunrise colorimetric microplate reader (Tecan Group AG, Männedorf, Switzerland) at a wavelength of 570 nm. Data were calculated with Graphpad prism 8.0. Cell viability data were presented as percent relative change from untreated control groups. In addition, the release of lactate dehydrogenase (LDH) from cells was utilized to measure cytotoxicity levels. For each group, 50 µl of medium was transferred to a fresh 96-well plate. Each well received an equal amount of the test reagent supplied by the manufacturer in order to quantify the release of LDH from the cells. The optical density was measured at 490 nm using an enzyme marker.

The cell death rate was also determined via morphological assay with fluorescence microscopy by using a LIVE/DEAD Viability kit (Lonza, Basel, Switzerland) as directed by the instructions of manufacturer. Living cells were identified with calcein AM (4 µmol/L, green fluorescence), and dead cells were identified with ethidium homodimer 1 (2 µmol/L, red fluorescence). Three independent experiments were conducted and ≥200 cells were evaluated for each condition.

2.12 Middle cerebral artery occlusion (MCAO) model and experimental animal paradigm

Our *in vivo* model of ischemic stroke was the middle cerebral artery occlusion (MCAO) model Based on our previous study (Doeppner et al. 2015). After subcutaneous injection of buprenorphine for analgesia, mice were anesthetized with 3% isoflurane at the beginning of surgery and maintained with 2.5% during surgery. After the mice were fixed on the operating table, the neck was sterilized with 70% ethanol, and a 1 cm incision was carefully incised. The skin was bluntly dissected to expose the trachea, and muscle and adipose tissue were carefully

separated to expose the right common carotid artery (CCA). The vagus nerve was then carefully separated from the common carotid artery. Next, permanent ligation was performed on the proximal right CCA and the proximal right external carotid artery (ECA), respectively. The right internal carotid artery (ICA) was briefly constricted using an arterial clip, and the right carotid artery (CCA) was ligated using surgical suture. Using ophthalmic scissors, a tiny incision was cut in the right CCA, a silicon-coated microfilament (diameter 0.06-0.09 mm, Doccol Corporation., Sharon, MA, USA) was inserted into the right CCA, and then the microfilament was slowly forwarded to the right middle cerebral artery (MCA). The experimental paradigm and schematic diagram of MCAO surgery are shown in Figure 2.

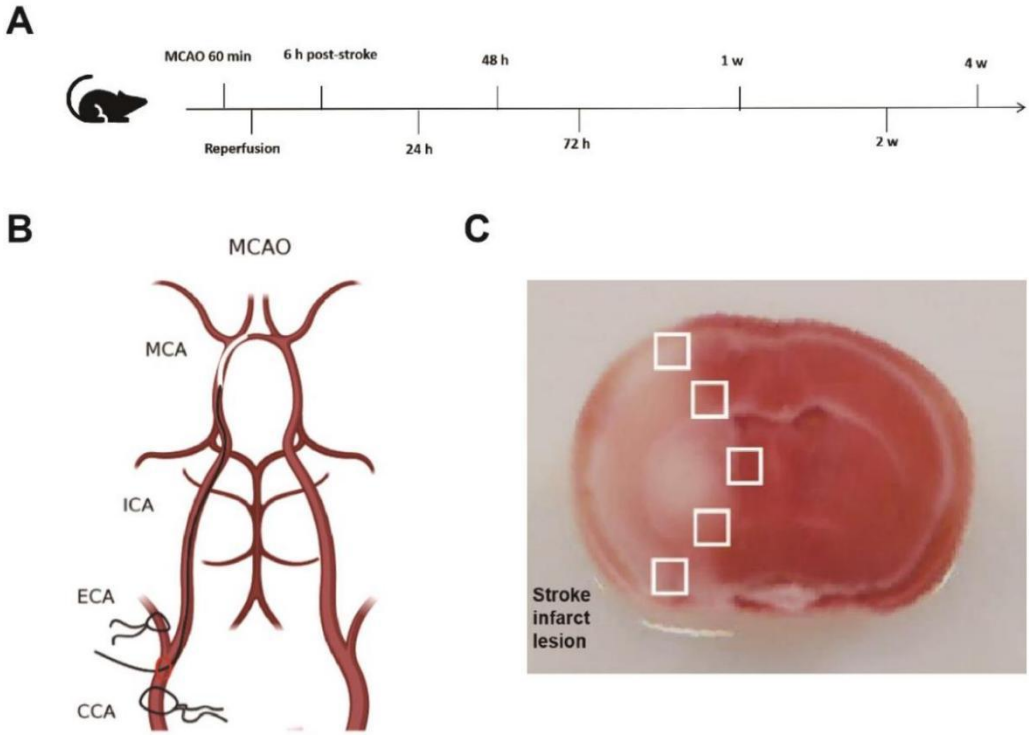

Figure 2. Experimental paradigm, middle cerebral artery occlusion (MCAO), and 2,3,5-Triphenyltetrazolium chloride (TTC) staining. (A) Mice were sacrificed 1 day, 2 days, 3 days, 1 week, 2 weeks and 4 weeks after MCAO to extract brain tissue samples for subsequent experiments, respectively. (B) The surgical experiment paradigm of MCAO. (C) The infarcted region was validated by TTC staining after MCAO surgery (24h). Abbreviations: ICA=internal carotid artery, ECA=external carotid artery, CCA=common carotid artery, MCA=middle cerebral artery.

Laser Speckle Imaging System (LSIS, RWD Life Science, Shenzhen, Guangdong, China) was applied to ensure successful blockage of blood flow and cerebral blood flow parameters were recorded. After sixty minutes, the microfilament was removed to initiate reperfusion, the cerebral blood flow parameters were recorded again with LSIS. The wound was carefully sutured,

and carprofen was injected subcutaneously for further analgesia. The cerebral blood flow parameters of LSIS are shown in Figure 3.

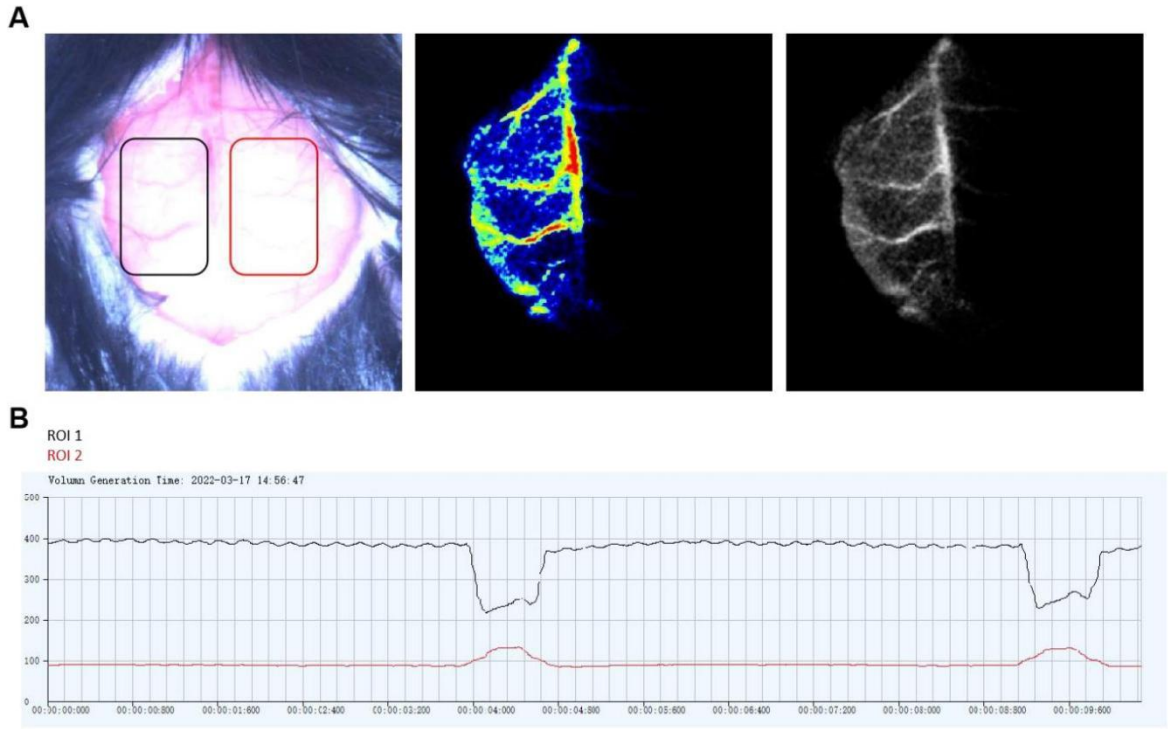

Figure 3. The laser speckle imaging system (LSIS) was applied to each experimental mouse before, during, and after the MCAO operation to record blood flow images and parameters, ensuring the successful blood flow block of the MCAO surgery. (A) The Real Pattern, Speckle Pattern and Pseudo-Colour Pattern images of the mouse skull indicated that the blood flow of the brain was blocked successfully. (B) The blood flow parameter map showed that the blood flow in the ROI 1 region (contralateral side, black) was significantly higher than that in the ROI 2 region (ipsilateral side, red).

2.13 Immunofluorescence and BODIPY staining in vivo

For *in vivo* tissue staining, post-perfusion brain samples from C57BL/6J mice were fixed in 4% paraformaldehyde for 24 hours, dehydrated with 30% sucrose, and prepared into 14 μm tissue sections with a cryostat. Cryosections were washed once in TBS, and incubated with citrate solution for antigen retrieval, followed by another wash in TBS. Brain sections were blocked with PBS-T based blocking buffer (PBS-T with 2% BSA (bovine serum albumin), 10% DS (donkey serum), 0.25% Triton X-100). Sections were incubated overnight with the following primary antibodies: NeuN, Iba1, iNOS, CD68, p2y12, TMEM119, PLIN2, PLIN3, CD206, Arginase I and GFAP. After primary antibody incubation, sections were washed three times in TBS, the respective secondary antibodies were added to PBS-T buffer containing 10% donkey

serum and incubated at room temperature for 2 h (RT): donkey anti-rabbit Alexa Fluor 488, donkey anti-mouse Alexa Fluor 488, donkey anti-rat Alexa Fluor 488, donkey anti-guinea pig Alexa Fluor 488; donkey anti-mouse Cy3, donkey anti-rabbit Cy3, donkey anti-goat Cy3, donkey anti-rat Cy3 (1:500, Jackson ImmunoResearch, Ely, UK). For BODIPY staining, the method was referred to Marschallinger et al with some modifications (Marschallinger et al. 2020). After primary antibody incubation, sections were washed once in TBS and then incubated with BODIPY 493/503 (1 μg/ml, Thermo Fisher) at a 1:1000 dilution in TBS for 30 min, then the sections were washed three times in TBS (antigen retrieval step and detergent must be avoided for BODIPY staining). Nuclei staining was then performed with 4',6-Diamidin-2-phenylindol (DAPI, 1:10,000; AppliChem, Darmstadt, Germany). Finally, Vectashield (Vector Laboratories, H-1000) was used for mounting. Specific antibody working dilutions are given in resources Table 5 and Table 6 of the Supplementary Material.

2.14 Immunocytochemistry and BODIPY staining in vitro

Primary microglia were seeded on poly-l-lysine-coated pre-coated chambers at a density of $4\times10^4/cm^2$, using DMEM/F12+10% fetal bovine serum as the medium. After specific treatments, cells were washed once with cold PBS and then fixed in 4% paraformaldehyde (PFA) for 20 min. The cells were washed three times with PBS, then permeabilized with 0.25% Triton X-100 for 15 min, and rewashed for three times. PBS with 10% DS, 1% BSA was used as blocking buffer for 1 hour blocking at room temperature. They were then followed by overnight incubation with primary antibodies (Iba1, iNOS, CD68, CD11b, p2y12, TMEM119, PLIN2, CD206 and CX3CR1). After three times washing with PBS, the slides were incubated with the corresponding secondary antibody for 2 hours or with BODIPY 493/503 for 30 minutes. The nuclei were stained with DAPI. Finally the slides were mounted with Vectashield 1000 (Vector Laboratories, H-1000). Specific antibody working concentrations are shown in Table 5 and Table 6.

2.15 Quantitative analysis of immunofluorescence data

The cortex and striatum were detected as regions of interest (ROI), five randomly selected fields of view per overlay were photographed, and three images were taken for each region to determine the average neuron or microglia density for all ROIs. For cells *in vitro*, photographs were taken in 3 fields of view (40x magnification), each overlay were randomly selected. For BODIPY+Iba1+ and BODIPY+iNOS+ microglia, images were analyzed blindly based on the number of BODIPY+ co-localized cells, and quantitative analysis of the number and size of

lipid droplets. Immunofluorescence slides were photographed on a Zeiss Axioplan 2 fluorescence microscope (Zeiss, Oberkochen, Germany) or confocal scanning laser microscope (Zeiss LSM 700, Germany). Images were processed with ZEN software version 3.20. Cell colocalization analysis and fluorescence intensity quantification were performed with ImageJ software version 1.60.

2.16 TUNEL assay

Terminal deoxynucleotidyl transferase dUTP nick end labeling (TUNEL, in situ cell death detection kit, Sigma-Aldrich) staining was used to detect cell death according to the manufacturer's instructions. After specific treatment, cells were fixed and permeabilized. Subsequently, working reaction mixture was prepared with 50 μl total volume of Enzyme solution into 450 μl Label solution to obtain 500 μl TUNEL reaction mixture. Then the cells were incubated with the TUNEL reaction mixture for 1 h at 37℃ in the dark. Afterward, 4', 6-diamidino-2-phenylindole (DAPI) staining was used to stain cell nuclei.

2.17 Analysis of phagocytosis

The analysis of microglial phagocytosis refers to the report of Hu et al with modification(Hu et al. 2012). Microglia were seeded on 96-well plates (1×10^4 cells/well) and incubated with respective treatments for 24 h. Nile red fluorescent microspheres (0.02 μm, Invitrogen, Germany) were dissolved in cell culture medium according to the instruction of the supplier. Cells were incubated with or without microspheres for 4 h. In order to extinguish the signal interference of the extracellular fluorescent microspheres, after removing the medium, cells were washed with 0.25 mg/ml trypan blue in PBS. After cells were subsequently lysed with 1% PBS-Triton, the samples were analyzed using a fluorescence plate reader (535 nm excitation wavelength and 575 nm emission wavelength). To acquire images of phagocytosis, microglia were seeded on 4-well chambers (4×10^4 cells/well, Sarstedt, Germany). Nile red fluorescent microspheres were added as described above. The cells were then washed twice with PBS before fixation and permeabilization, then incubated with specific primary and secondary antibodies. Nuclei were stained with DAPI. Immunofluorescence slides were photographed with Zeiss Axioplan 2 fluorescence microscope (Zeiss, Oberkochen, Germany) or confocal scanning laser microscope (Zeiss LSM 700, Germany)

2.18 ROS stress analysis

To measure reactive oxygen species (ROS) in microglia, cells were seeded on 4-well chambers at a density of 4×10^4 cells/well and treated with LPS, triacsin C, IL-4, conditioned medium or vehicle solution for 24 h. Then CellROX Orange (1:500; Invitrogen, Germany) was added to the cell culture medium and incubated at 37°C for 1 hour. Cells were washed twice with PBS, and nuclei were stained with Hoechst 33342 (1:5000; Thermo Fisher, Germany). CellROX Orange Intensity was detected with Zeiss Axioplan 2 fluorescence microscope (Zeiss, Oberkochen, Germany).

2.19 Lipid samples extraction

The method of lipid samples extraction was based on the protocol of Bligh and Dyer method with minor modifications (Breil et al. 2017). Small amounts of chloroform and methanol were used in the primary extraction step. After the tissue or cells were washed twice with cold PBS, samples were homogenized in ultrapure water with a homogenizer or sonicator (10 mg tissue or 1 x 10^6 cells). The homogenized samples were mixed with 1x volume of chloroform and 2x volumes of methanol. After vortexing thoroughly, the samples were incubated at room temperature for 20 minutes. Thereafter, another 1x volume of chloroform and 1x volume of ultrapure water was added. The suspension was then mixed and vortexed thoroughly and incubated for an additional 20 minutes. Then the samples were followed by ultracentrifugation at 15000 x g for 15 minutes and were completely separated into three layers. The upper aqueous layer was removed and the lower organic phase was transferred to a new tube. After air-drying at 50°C to remove chloroform, the samples were vacuumed for 30 minutes to remove trace organic solvent and finally stored at -20°C.

2.20 Total cholesterol/cholesteryl ester measurement

Total cholesterol and cholesteryl esters in tissue or cell samples were analyzed by commercially available cholesterol quantification kits (Abcam, ab65359, Germany). According to the manufacturer's instructions, the protocol of cholesteryl ester formation was quantified using a total cholesterol/cholesteryl ester quantification kit (colorimetric/fluorescence). For lipid samples previously collected from tissue or cells, the dried lipid samples were dissolved in 200 µL of assay buffer. To get a standard curve, diluting 25 µL of cholesterol standard solution in different proportions to prepare six sets of standard samples, added into a 96-well plate. Testing samples were divided into two reaction mixtures: with or without cholesterol esterase. Total cholesterol and free cholesterol were measured separately, and added to appropriate wells of a

96-well plate. Samples were mixed with reaction buffer and incubated at 37°C for 60 min in the dark. Measured the absorbance at 570 nm with a colorimetric microplate reader or the fluorescence value at Ex/Em = 535/587 nm with a fluorometric microplate reader, and normalizing with the standard curve to calculate the total cholesterol and free cholesterol concentrations in each well. The concentration of cholesteryl ester is equal to total cholesterol minus free cholesterol. Three independent assays were performed in replicates, using three independent organisms per experiment.

2.21 Free fatty acid quantification

The quantification of total free fatty acids (FFA) was measured by using a commercially available free fatty acid assay kit (ab65341, Abcam, Germany). Extraction, preparation and measurement of samples were performed according to the manufacturer's protocol. Briefly, the dried lipid samples for analysis were dissolved in 200 μL of assay buffer. In order to get the standard curve, 20 μL of palmitic acid standard solution was diluted in different proportions to prepare six sets of standard samples, which were added to 96-well plates. Fatty Acid Probe, Acyl-CoA Synthetase (ACS) Reagent and Enzyme Mix were mixed thoroughly as reaction buffer according to the commercial instruction. Samples were mixed with reaction buffer and incubated for 30 min at 37 °C in the dark. The absorbance at 570 nm was measured with a colorimetric microplate reader or the fluorescence value at Ex/Em = 535/587 nm with a fluorescence microplate reader, and normalized with the standard curve to calculate the free fatty acid concentration.

2.22 Tissue sample harvest

We used immunofluorescent analysis to investigate brain tissue samples at different time points after MCAO surgery. We found that LD-enriched microglia were mainly located in the ipsilateral hemisphere cortex region, in the lesion center. We defined the region as depicted in Figure 4. A-B, and then collected tissue samples of these regions from MCAO mice (Sham, 3 days, 7 days and 28 days post-ischemia). C57BL/6J mice with MCAO followed by different reperfusion time were anesthetized with isoflurane, then were killed by transcardial perfusion with cold PBS using a micropump. The mouse brains were sliced with a slicer matrix at a thickness of 2 mm, and brain specimens were collected at designated locations using a sample puncture needle (1 mm diameter, Kai medical, 0197, Germany). The collected brain samples were stored at -80°C for later analysis.

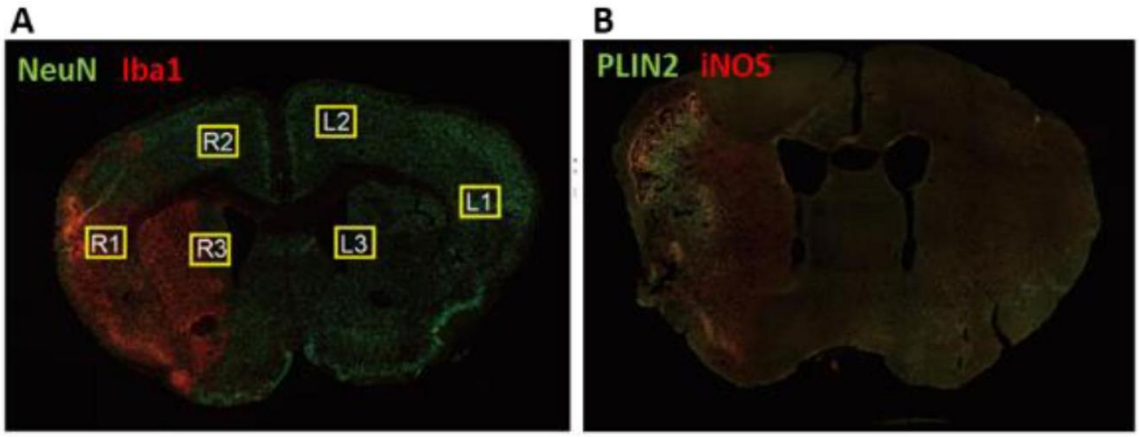

Figure 4. The tissue sample harvest in vivo. (A) Selected areas after MCAO: R1 (ipsilateral cortex lesion), R2 (ipsilateral cortex, out of lesion), R3 (white matter area of lesion margin). L1, L2, and L3 are the corresponding areas on the contralateral side. Most of LD-enriched iNOS and PLIN2 (B) as well as microglia (A, Iba1) was found in R1.

2.23 Western blot analysis

The brain tissue samples and the cell samples were lysed in a solution buffer containing RIPA Lysis and Extraction Buffer (Thermo Scientific, Waltham, USA), 1 mmol/L EDTA, 1% protease inhibitor, and 1% phosphatase inhibitor with a homogenisator or sonicator for 10 minutes and subsequently centrifuged at 4°C with 14000 rpm for 15 minutes. Supernatants containing protein were collected. Protein concentrations were quantified with the Pierce BCA protein assay kit (Thermo Fisher Scientific, USA). Reduced loading buffer (Carl Roth, Karlsruhe, Germany) was added, and the samples were heated at 95°C for 5 minutes. Equal amounts of protein were loaded on 8% to 12% SDS-PAGE gel and electrophoretically separated in sample buffer (dithiothreitol, final 0.1 M concentration, 0.1 % SDS, 0.1 M Tris HCl; pH 7.0). Then the electrophoresis gel was transferred to a polyvinylidene fluoride membrane (Merck Group, Darmstadt, Germany) by the tank transfer protocol. Membranes were pre-activated by incubating in methanol for 1 minute, and membranes and gels were arranged in the following order: foam (fiber) pad, filter paper, gel, membrane, second filter paper, second foam pad, and then the box rack (so-called "sandwich") was closed and placed in a transfer chamber filled with transfer buffer (25 mM Tris, 192 mM glycine, pH 8.3, 10%–20% methanol in 1 L ultrapure water). After transfer, membranes were incubated in blocking buffer (5 g milk powder or BSA in 100 ml TBS-T) for 1 hour at room temperature. Then followed by overnight incubation for optimal results with primary antibodies: PLIN2, SREBP2, NF-κB p65, IκBα, IL-1β, TGF-β1, β-actin, α-tubulin and GAPDH. After three times washes with tris-buffered saline supplemented

with 0.1% Tween 20 (TBS-T) detergent, the blots were incubated with horseradish peroxidase-conjugated secondary antibodies (1:10000) for 1 hour. Specific antibody working dilutions are given in the following resources Table 5. After washing another three times with TBS-T, the membrane was incubated in ECL reagent (Bio-Rad, Germany) for 1 minute and developed with the imaging system ChemiDoc XRS+ (Bio-Rad, Germany). Image J version 1.60 was used to measure the grey value of each blot. Western blot measurements were performed in triplicates.

2.24 RNA isolation and quantitative Real-Time polymerase chain reaction (qRT-PCR)

To extract total RNA, TRIzol (Invitrogen, Darmstadt, Germany) was used according to the manufacturer's instructions. Briefly, 800 µl of TRIzol was added to a cell or tissue homogenate sample, mixed well by inversion, and incubated at room temperature for 10 min. Then 200 µl of chloroform was added and shaken vigorously to mix well. The mixture was centrifuged at 12000 x g for 15 min. The upper layer (aqueous phase) was collected and transferred to a new Eppendorf tube. 500 µl of isopropanol was added to the collected aqueous phase. After gently mixing, RNA was precipitated at room temperature for another 10 min, followed by centrifugation at 12,000 x g for 10 min at 4 °C. The supernatant was discarded, and the pellet was washed with 75% ethanol, then followed by centrifugation again at 10,000 x g for 5 min. The supernatant was discarded and the pellet was left to dry naturally for 5 min. The pellet was dissolved in nuclease-free water pre-treated with diethylpyrocarbonate (DEPC). Total RNA concentration was determined with a NanoDrop ND1000 Spectrophotometer (NanoDrop, Wilmington, DE, USA). mRNA was reverse transcribed to cDNA with the RevertAid H Minus First Strand cDNA Synthesis Kit, followed by qRT-PCR with the SYBR Green I Master Kit for LightCycler® 480 (Merck Group) according to the manufacturer's instructions. All PCR primers were purchased from Eurofins Genomics (Luxembourg, Germany). (Table 7).

2.25 Enzyme linked immunosorbent assay (ELISA)

Concentrations of TNF-α, IL-1β and TGF-β1 were determined with commercial ELISA kits (Thermo Fisher Scientific, USA) according to the manufacturer's instructions. 96-well plate was coated with capture antibody at 100 µl/well, then the plate was sealed and incubated overnight at 4°C. 96-well plate was coated with capture antibody at 100 µl/well, then the plate was sealed and incubated overnight at 4°C. All the wells were aspirated and washed three times with 250 µl/well PBS-T. The wells were blocked with 200 µl ELISA/elispot diluent (1X) for 1 hour incubation at room temperature. Standard samples were prepared as instruction for a standard

curve. The standard and test samples were added into 96-well plate at 100 µl/well with another overnight incubation at 4°C (TGF-β1 needs to be pre-activated with acid-base neutralization). All the wells were aspirated and washed as in the previous steps, and 100 µl/well of diluted detection antibody was added to each well. The plate was sealed and incubated at room temperature for 1 hour. After aspirating and 3-5 times washing, 100 µl/well of diluted horseradish (Avidin-HRP) was added to each well and incubated at room temperature for 30 minutes. After 5-7 washes, 100 µl/well of 1x TMB solution was added with 15 minutes incubation at room temperature. Finally, 100 µL/well of stop solution was added to stop the reaction, the absorbance of the samples was detected at 450 nm by using a colorimetric plate reader.

2.26 Flow cytometry analysis in vivo

Microglia and LD-rich subpopulations of microglia in the cerebral hemisphere after MCAO were determined by flow cytometry with a fluorescence-activated cell sorter. Ischemic cerebral hemispheres were mechanically homogenized in lysis buffer (0.5% BSA, 5% glucose, 10 mg/ml DNase in PBS) and centrifuged at 2000 rpm for 10 min. Thereafter, the pellets were dissolved in 30% Percoll solution (GE Healthcare, USA) and loaded onto a gradient containing 45% and 70% Percoll. After centrifugation, the cells were aspirated between stages and dissolved in working solution (3% fetal bovine serum in PBS). Before antibody labeling, the cell suspension was incubated with anti-mouse Fc-Block (final concentration of 2.5 µg/ml) for 10 min at 4°C to prevent non-specific binding. After washing, cells were incubated with anti-CD45, anti-CD11b and BODIPY (BioLegend, San Diego, USA) overnight. Flow cytometry quantification was obtained using FlowJo v. 10.5.3 (BD FACSDiva™) software.

2.27 Statistical analyses

For comparison of two groups, the two-tailed independent Student's t-test was used. For comparison of three or more groups, a one-way analysis of variance (ANOVA) followed by Tukey's post-hoc-test and, if appropriate, a two-way ANOVA were used. Unless otherwise stated, data are presented as means with SD values. A p-value of <0.05 was considered statistically significant. Statistical software was Graphpad Prism version 8.0.

3 Results

3.1 Extraction and characterization of primary microglia and neurons

Characterization of primary microglia by phase-contrast microscopy and immunocytochemistry confirmed that the microglia phenotype was consistent with several known specific markers (i.e., Iba1, CD11b, CX3CR1, and TMEM119) (Figure 5. A). Primary microglia were exposed to different times of OGD then followed by 24 h reoxygenation (RO; Figure 5. B-C), and the OGD time of 4 h was accepted as the most suitable OGD time point (for 50% cell survival rate). Primary neurons were exposed to different times of OGD/RO, and the results of cell viability and cytotoxicity assays showed that the duration of OGD correlated with the degree of cell damage, and the cell survival rate of neuronal cells was 50% after 4 hours of OGD, similar to microglia (Figure 5. D-E). Therefore, 4 h was selected as the ideal OGD time point for primary microglia and neurons, and a co-culture model was constructed.

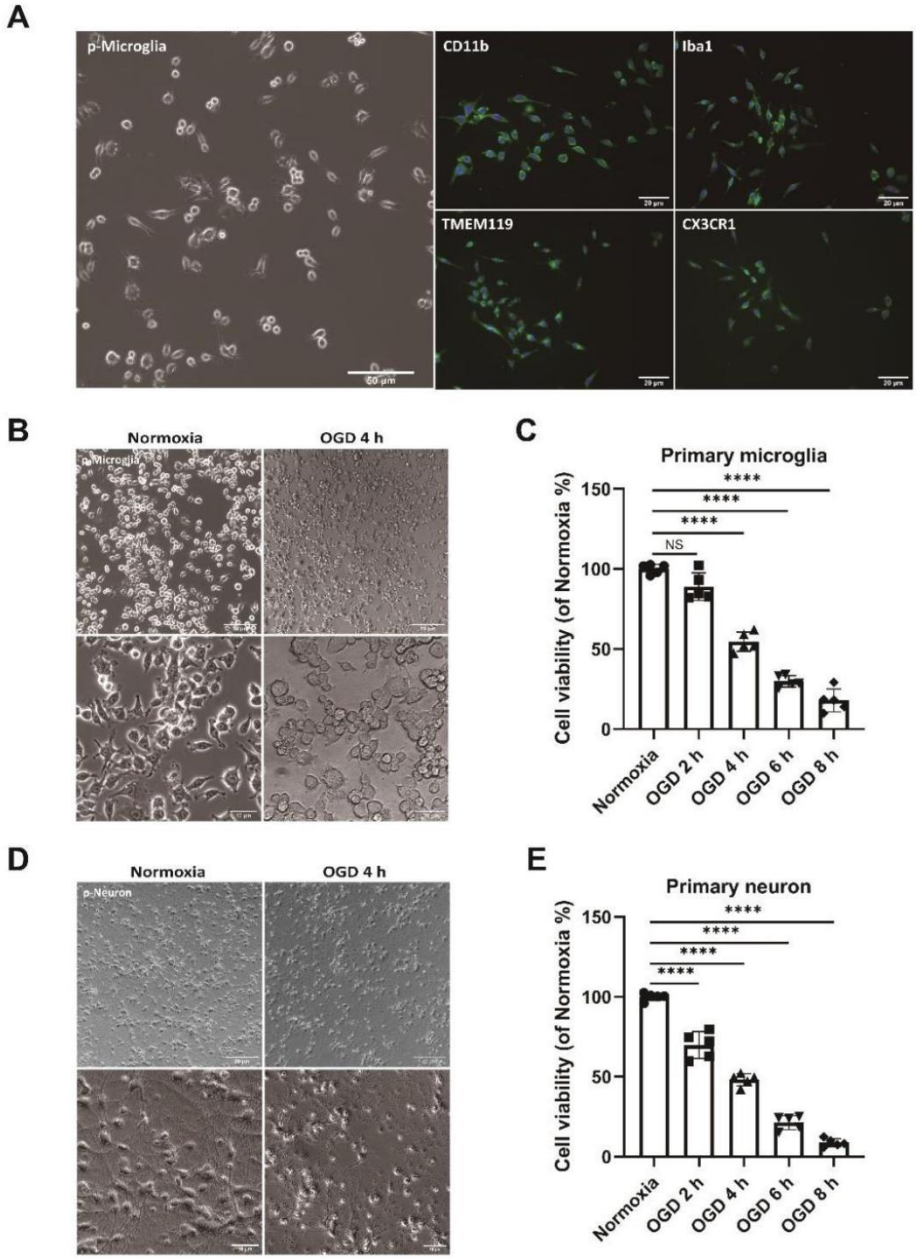

Figure 5. Extraction and characterization of primary microglia and neurons and cell survival rate after OGD/RO in vitro. A-C, Phase-contrast images of primary microglia under bright-field microscopy, as well as immunofluorescence stainings against the markers Iba1, CD11b, CX3CR1, and TMEM119, are shown (A). Quantitative measurement of cell survival rate by MTT assay: primary microglia exposed to different time points of OGD (2 h, 4 h, 6 h, and 8 h) followed by 24 h reoxygenation (RO). Microglia cultivated under standard cell culture conditions (Normoxia) served as control (n = 5) (B-C). **D-E**, Quantitative measurement of cell survival rate by MTT assay: primary neuron exposed to different time points of OGD (2 h, 4 h, 6 h, and 8 h) followed by 24 h RO. Neurons cultivated under standard cell culture conditions (Normoxia) served as control (n = 5). Data are expressed as mean ± SD, ****$p < 0.0001$. Scale bars, 50 µm and 20 µm (A), 50 µm and 10 µm (B, D). Abbreviations: OGD, oxygen glucose deprivation; RO, reoxygenation; MTT, 3-(4,5-dimethylthiazol-2-yl)-2,5-diphenyl tetrazolium bromide assay.

3.2 Oxygen-glucose deprivation (OGD) and inflammation induce accumulation of LDs in microglia in vitro.

We hypothesized that hypoxia and inflammation could induce LDs biogenesis in microglia. To investigate this, we characterized the LDs at different time points after reoxygenation. After 4 hours of OGD and following 24 hours of reoxygenation (RO), cells were stained with BODIPY, and a large number of LDs (BODIPY+) accumulated in microglia (Figure 6. A-C). Moreover, unlike the resting microglial morphology, this LDRM showed the amoeboid morphology possessed by immune-activated microglia: increased cell size and reduced branching. Interestingly, the increase in LDs depended on the duration of RO (2, 6, 12, 24, and 48 hours) and peaked after 24 hours RO (Figure 6. D-F). Furthermore, a significant accumulation of LDs was also found after stimulation of microglia with LPS and conditioned medium from primary neurons after OGD (OGD-CM). After inhibiting the long-chain fatty acid synthesis and cholesterol esterification by using triacsin C (Trc), an Acyl-CoA cholesterol acyltransferase inhibitor, the size and number of LDs were significantly reduced (Figure 6. G-I). Fluorescence images were quantified using ImageJ software: normalized by the mean fluorescence intensity (MFI) of control group (mean ± SD): 21.5 ± 5.8 and 13.5 ± 3.1 for the LPS and OGD-CM groups, respectively, which decreased to 5.1 ± 1.8 and 3.7 ± 2.3 after co-incubation with Trc. In addition, the percentage of BODIPY+Iba1+ microglial to total microglia in control group was 4.7±2.1%, while the percentage increased to 64.1±14.1% and 53.2±10.7% in the LPS and OGD-CM groups, and decreased to 9.5±5.9% and 13.6±4.5% with Trc treatment. It was confirmed that inhibition of long-chain fatty acid and cholesterol synthesis could reduce the biogenesis of LDs.

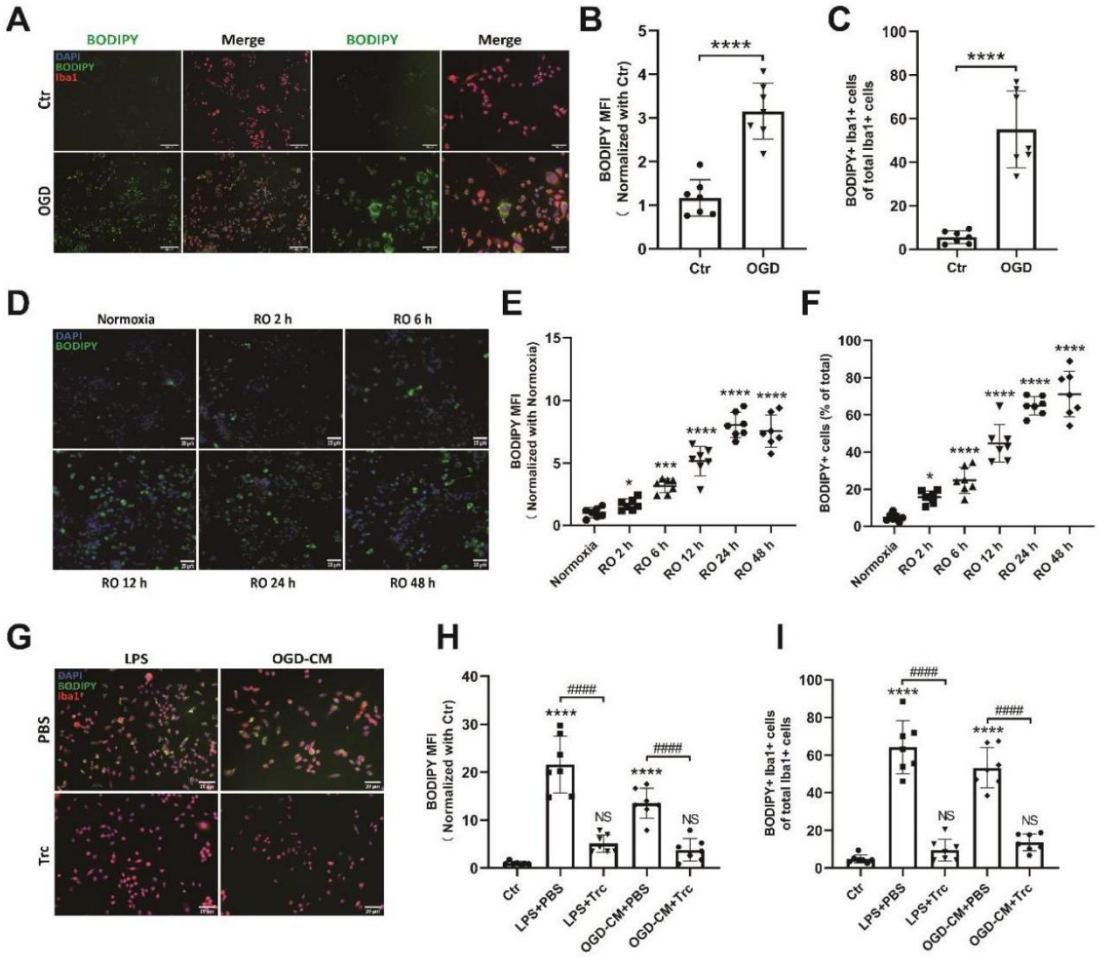

Figure 6. Oxygen-glucose deprivation (OGD), LPS and conditioned medium induce accumulation of lipid droplets (LDs) in primary microglia in vitro. A-C, LDs (BODIPY+ green) significantly increased in microglia after exposed to OGD under immunofluorescence staining (A), Quantification of BODIPY mean fluorescence intensity (MFI) of LDs (B), and percentage of BODIPY+ (green) Iba1+ (red) cells (C). (n = 7). **D-F**, LDs were accumulated in microglia within 48 h of reoxygenation (D), Quantification of MFI of BODIPY+ cells (E), percentage of BODIPY+ (green) cells (F). (n = 7). **G-I**, LPS and OGD-CM can also stimulate LD formation in microglia, and co-treated with triacsin C (Trc, 1 μM), an ACAT inhibitor, can inhibit this process (G), Quantification of MFI of BODIPY+ cells with LPS and OGD-CM treatment (H), and percentage of BODIPY+ Iba1+ cells (I). (n = 7). Statistical tests: Data are expressed as mean ± SD, NS: no significance, *$p < 0.05$, **$p < 0.01$, ***$p < 0.001$, ****$p < 0.0001$, and ####$P<0.0001$. Scale bars, 50 μm and 20 μm (A), 20 μm (D, G). Abbreviation: OGD, oxygen-glucose deprivation; RO, reoxygenation; OGD-CM, conditioned medium from primary neuron after OGD; LDs, lipid droplets; MFI, mean fluorescence intensity; Trc, triacsin C; ACAT, Acyl-CoA cholesterol acyltransferase.

We also verified the expression of PLIN2 and IL-1β at the protein level in microglia under different conditions by Western blotting. We found that PLIN2 expression was significantly elevated under both hypoxic and inflammatory conditions compared to controls, whereas it was

decreased under IL-4 condition treatment (Figure 7. A). In addition, IL-1β, the major inflammatory factor produced by microglia, was also elevated under hypoxic and inflammatory conditions, especially in the LPS and OGD-CM group, whereas no significant changes were observed between IL-4 and control group (Figure 7. B). These results support our hypothesis that lipid metabolism patterns and liposome formation in inflamed microglia may be related to inflammatory expression.

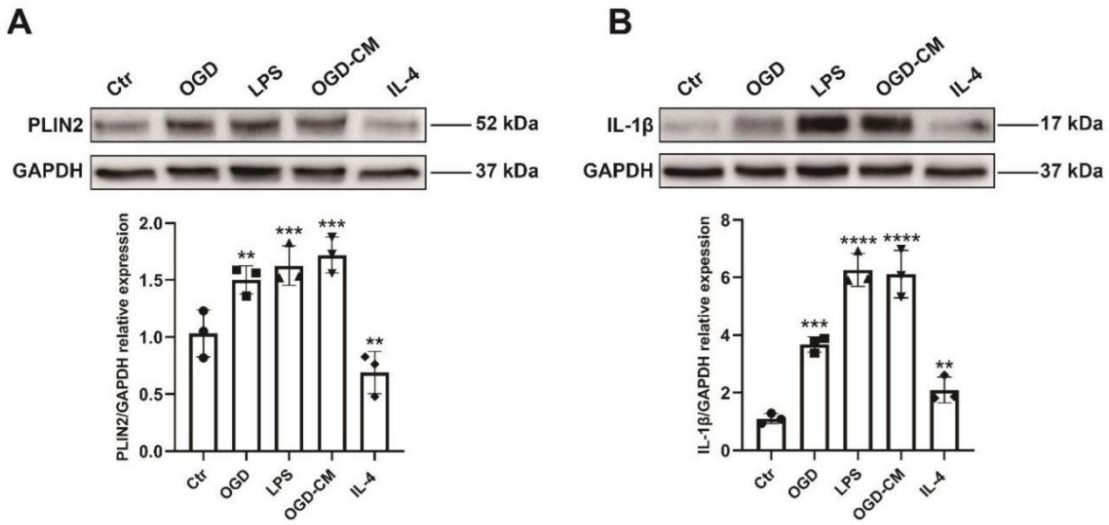

Figure 7. Upregulation of PLIN2 (Perilipin 2 protein) and IL-1β in lipid droplet-rich microglia (LDRM) under oxygen glucose deprivation (OGD) and inflammatory conditions. A, Quantitative analysis of PLIN2 expression in five group: normoxia as control group, OGD group, conditioned medium from primary neurons after OGD (OGD-CM) group, LPS group and IL-4 group using Western blot analysis normalized with the housekeeping protein GAPDH (n = 3). **B**, Quantitative analysis of IL-1β expression in these five group using Western blot analysis normalized with the housekeeping protein GAPDH (n = 3). Statistical tests: Data are expressed as mean ± SD, **p < 0.01, ***p < 0.001, ****p < 0.0001. Abbreviation: PLIN2, perilipin 2 protein; LDRM, lipid droplet-rich microglia; OGD, oxygen-glucose deprivation; OGD-CM, conditioned medium from primary neurons after OGD.

3.3 Middle cerebral artery occlusion (MCAO) induces the formation of LDs in microglia in vivo

We used the middle cerebral artery occlusion (MCAO) mouse model to analyze LD formation and microglia migration in the mouse brain after cerebral ischemia *in vivo*. Interestingly, using immunofluorescence (IF) staining labeling LDs with BODIPY and microglia with Iba1, we found that LDs do not accumulate immediately after ischemia, but gradually after the acute phase of stroke, peaking about one week after infarction. Moreover, most of the LDs were

found in microglia and macrophages, co-localized with Iba1+ (Figure 8. A). In addition, in the post-stroke brain (sham, 3, 7, 28 days), we found that the number of microglia in the sham group was limited and LDs were hardly observed. Then 3 days after ischemia, microglia aggregated in the cortical and white matter infarct areas on the ipsilateral side and the number of LDs in the microglia increased significantly. On post-ischemia day 7, large amount of LDs-rich microglia (LDRM) aggregates were found in the ipsilateral cortical infarct core. After that, there was a gradual decline until 28 days; where only a tiny amount of LDRM was observed in the brain (Figure 8. B-D).

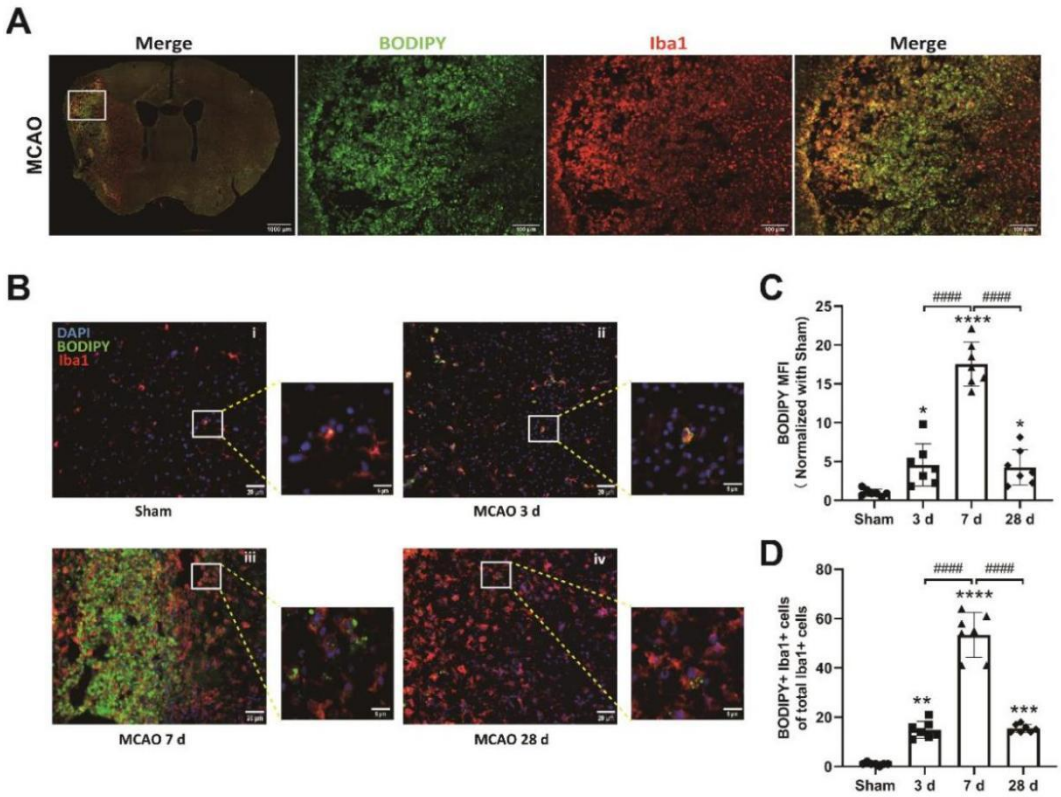

Figure 8. The formation of LDs in microglia in the mouse middle cerebral artery occlusion (MCAO) stroke model. A, Immunofluorescence of whole brain staining after MCAO with 1 week reperfusion. **B-D**, Immunofluorescence of cortical infarct core stainings at different reperfusion times (Sham, 3, 7, 28 d) after MCAO indicated that LDs mainly accumulated in microglia (B), Quantification of mean fluorescence intensity (MFI) of BODIPY(C), percentage of BODIPY+ Iba1+ cells (D). (n = 7). Statistical tests: Data are expressed as mean ± SD, $^{**}p < 0.01$, $^{***}p < 0.001$, $^{****}p < 0.0001$, and $^{\#\#\#\#}P<0.0001$. Scale bars, 1000 μm and 100 μm (A), 20 μm and 5 μm (B). Abbreviation: MCAO, middle cerebral artery occlusion; LDs, lipid droplets; MFI, mean fluorescence intensity.

In our MCAO *in vivo* mice model, we found that compared with the MCAO group, after the treatment of Trc, the number of LDRMs in infarct lesions was significantly reduced and the

infarct lesion size was also significantly diminished due to the inhibition of long-chain fatty acyl-CoA synthase (ACSL) (Figure 9. A). Interestingly, as the size and number of LDs labeled by PLIN2 declined, the number of activated LDRMs also reduced (Figure 9. B-D).

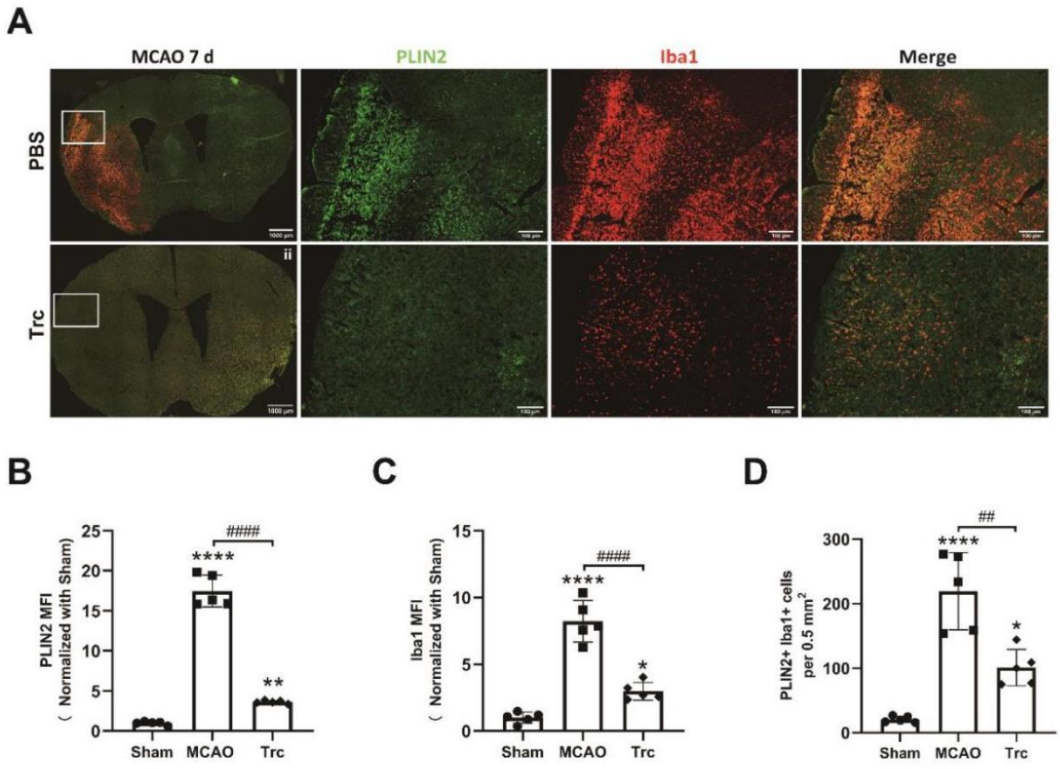

Figure 9. The ACAT inhibitor triacsin C reduces LD formation and actived microglia after MCAO. **A**, Whole brain immunofluorescence staining of one week post-stroke shows that triacsin C (Trc, 1 μM,) reduced PLIN2+ and Iba1+ microglia. **B-D**, Quantification of PLIN2 mean fluorescence intensity (MFI) of cortical infarct core immunofluorescence staining (B), quantification of Iba1 mean fluorescence intensity (MFI) (C), and PLIN2+ Iba1+ cells per 0.5 mm^2 area (D). (n = 5).Statistical tests: Data are expressed as mean ± SD, NS: no significance, *p < 0.05, **p < 0.01, ****p < 0.0001, $^{\#\#}$p < 0.01, and $^{\#\#\#\#}$p < 0.0001. Scale bars, 1000 μm and 100 μm (A). Abbreviation: ACAT, Acyl-CoA cholesterol acyltransferase; MCAO, middle cerebral artery occlusion; LDs, lipid droplets; MFI, mean fluorescence intensity; Trc, triacsin C.

Next, we measured the protein expression levels of PLIN2 and IL-1β in the brains of mice after MCAO under different ischemia-reperfusion time points by Western blotting. We found that the inflammatory factor IL-1β gradually increased after MCAO and peaked on post-ischemia day 7, followed by a gradual decrease (Figure 10. A). Interestingly, the expression level of PLIN2 was also progressively elevated after stroke and peaked on post-ischemia day 7 (Figure 10. B). The difference is that the time point of PLIN2 elevation is earlier than that of IL-1β (a significant increase on post-ischemia day 3). In addition, by immunofluorescence staining, we found that a large number of neurons still remained in the infarct area on post-ischemia day 3, and these

neurons gradually died in the subsequent 4-7 days after ischemia. This time point is also the time period when LDRM formation and inflammation are upregulated. On post-ischemia day 7, we divided the brain into six areas: R1, ipsilateral hemisphere cortex; R2, ipsilateral cortex out of lesion; R3, white matter area of lesion margin; L1, L2, and L3 were the corresponding areas on the contralateral side. The R1 area had only extremely few surviving neurons (labeled by Neun in green) and numerous microglia (labeled by Iba1 in red). In addition, many microglia were also found in R3, but more neurons survived than that in R1. However, both the R2 region and the contralateral side (L1, L2, and L3) showed a considerable amount of neurons and few microglia (Figure 10. C). We also found that most of the microglia in cortical infarct lesion core were M1 phenotype pro-inflammatory microglia labeled by iNOS+PLIN2+, and this pro-inflammatory LDRM was less or none in other regions (Figure 10. D). These results suggest that cellular injury due to energy deficiency after cerebral ischemia causes altered lipid metabolism and consequent upregulation of PLIN2, and thereafter accumulation of LDs in the numerous pro-inflammatory LDRM may subsequently lead to further upregulation of inflammation and aggravate neuronal death.

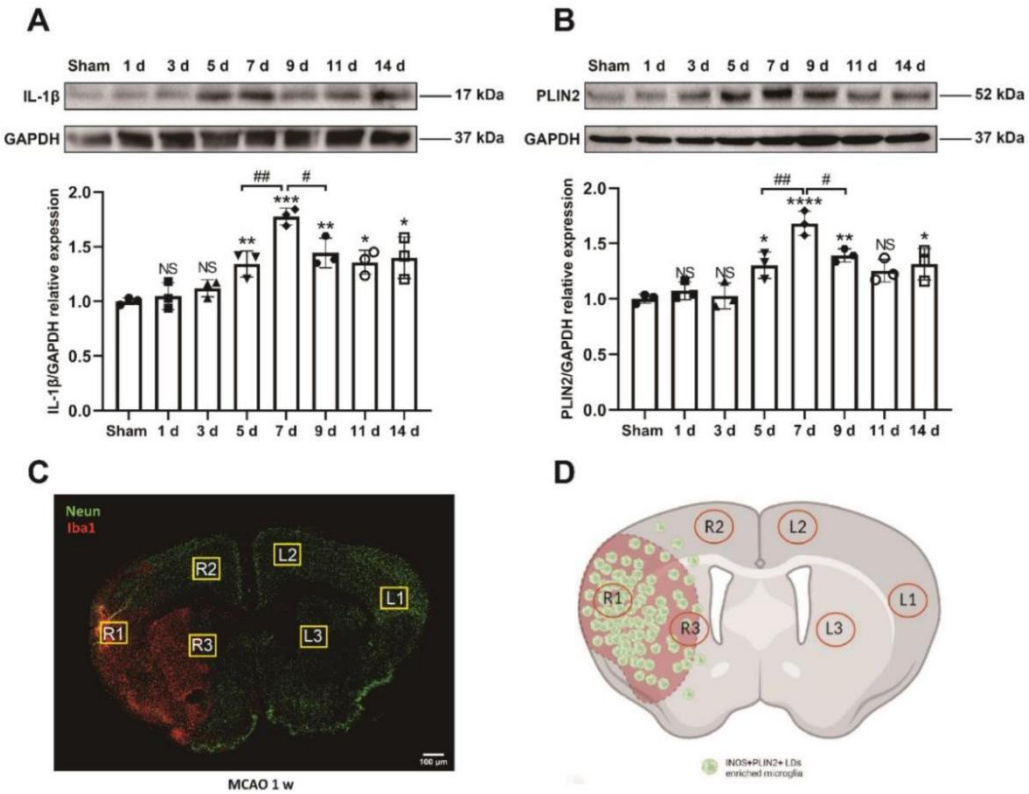

Figure 10. PLIN2 and IL-1β expression were progressively elevated over 7 days in the infarcted hemisphere after middle cerebral artery occlusion (MCAO). A, Quantitative analysis of PLIN2 expression in post-ischemic mice with different reperfusion times (sham, 1, 3, 5, 7, 9, 11, and 14 d) by Western blot analysis of the ischemic hemisphere. Western blot was normalized with the housekeeping protein GAPDH (n = 3). **B**, Quantitative analysis of inflammatory factor IL-1β expression in the same reperfusion time point using Western

blot analysis normalized with the housekeeping protein GAPDH (n = 3). **C**, Distribution of neuron (Neun, green) and microglia (Iba1, red) at day 7 post-ischemia was measured by Immunofluorescence co-staining. Divided the brain hemisphere into different areas: R1 (ipsilateral hemisphere cortex), R2 (ipsilateral cortex out of lesion), R3 (white matter area of lesion margin). L1, L2, and L3 were the corresponding areas on the contralateral side. Most Iba1+ microglia were found in R1; while most Neun+ neurons were located on the contralateral side but very few in R1. **D**, Schematic diagram of the divisions of the post-ischemic LDRM. Majority of iNOS+ PLIN2+ LDRM were found in R1. Statistical tests: Data are expressed as mean ± SD, NS: no significance, *$p < 0.05$, **$p < 0.01$, ***$p < 0.001$, ****$p < 0.0001$, $^{\#}p < 0.05$, and $^{\#\#}p < 0.01$. Scale bars, 100 μm (C). Abbreviation: MCAO, middle cerebral artery occlusion; LDRM, lipid droplet-rich microglia.

3.4 Effect of microglia on post-hypoxia neuronal survival in a co-culture model.

Based on the *in vitro* findings presented above, we further hypothesized that released pro-inflammatory factors from LPS and OGD-CM pretreated microglia might exacerbate neuronal injury. Furthermore, inhibiting fatty acid and cholesterol synthesis and aggregation of LDs in microglia might diminish inflammatory upregulation and attenuate neuronal death after ischemia. First, we divided the isolated and purified primary microglia into seven groups as follows: group 1 (PM treated with drug solvent in normoxic condition); group 2 (OGD/RO treatment with drug solvent); group 3 (1000 ng/ml LPS treatment); group 4 (2 μM Trc inhibitor treatment in group 3); group 5 (incubation with conditioned medium from neurons after OGD/RO), group 6 (2 μM Trc inhibitor treatment in group 5) and group 7 (10 ng/ml recombinant IL-4 treatment) (Figure 11. A). After that, we designed nine groups of neuron-microglia co-culture models in which these preconditioned microglia (seven groups of preconditioned microglia) were co-cultured with neurons after OGD/RO (Figure 11. B). Cell viability and cytotoxicity were analyzed by MTT assay, LIVE/DEAD morphology assay and LDH release assay. *In vitro* experiments were based on a designed timeline that included primary cell extraction, drug treatment, OGD/RO, co-culture and subsequent assays (Figure 11. C).

A

Microglia treatment							
Groups	**1**	**2**	**3**	**4**	**5**	**6**	**7**
OGD	-	+	-	-	-	-	-
LPS	-	-	+	+	-	-	-
OGD-CM	-	-	-	-	+	+	-
Trc	-	-	-	+	-	+	-
IL-4	-	-	-	-	-	-	+

OGD: the cells were exposed to 4 h oxygen-glucose deprivation (OGD) and 24 h reoxygenation (RO).
LPS: 1000 ng/ml LPS preconditioned microglia
OGD-CM: Conditioned medium of neurobasal medium from neurons after OGD/RO.
Trc: 2 μM Triacsin C (Trc) ACAT inhibitor.
IL-4: 10 ng/ml recombinant IL-4.

B

Neuron-Microglia co-culture system									
Groups	**1**	**2**	**3**	**4**	**5**	**6**	**7**	**8**	**9**
OGD	-	+	+	+	+	+	+	+	+
Microglia -1	-	-	+	-	-	-	-	-	-
Microglia -2	-	-	-	+	-	-	-	-	-
Microglia -3	-	-	-	-	+	-	-	-	-
Microglia -4	-	-	-	-	-	+	-	-	-
Microglia -5	-	-	-	-	-	-	+	-	-
Microglia -6	-	-	-	-	-	-	-	+	-
Microglia -7	-	-	-	-	-	-	-	-	+

OGD: the cells were exposed to 4 h oxygen-glucose deprivation (OGD) and 24 h reoxygenation (RO).
Microglia 1-7: preconditioned microglia as previous microglia treatment table.

C

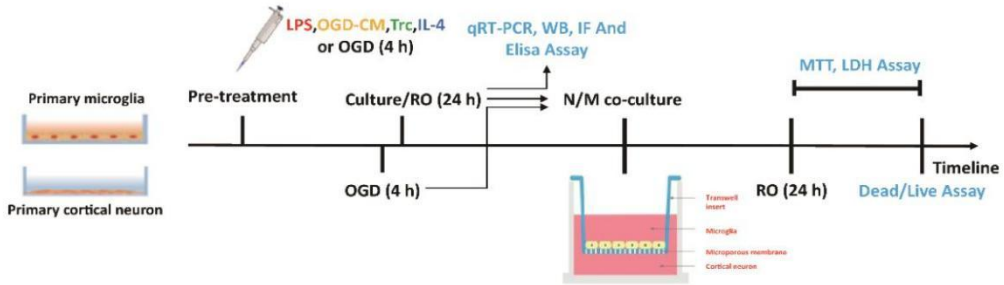

Figure 11. **Grouping of primary microglia (PM) and establishment of microglia-neuron co-culture system. A-B**, To investigate the effect of LDs-enriched PM in primary cortical neurons (PN), seven groups were developed: group 1 (PM treated with drug solvent in normoxic condition); group 2 (OGD/RO treatment with drug solvent); group 3 (1000 ng/ml LPS treatment); group 4 (2 μM Trc inhibitor treatment in group 3); group 5 (incubation with conditioned medium from neurons after OGD/RO), group 6 (2 μM Trc inhibitor treatment in group 5) and group 7 (10 ng/ml recombinant IL-4 treatment) (A). Microglia-neuron co-culture system: Co-culture of differently treated PM with PN after OGD (B). **C**, The timeline of *in vitro* experiments including OGD, RO, co-culture incubations, and post-OGD assays (Sample harvesting, MTT and LDH assay, Dead/Live morphological assay, TUNEL assay in PN). Abbreviations: OGD, oxygen-glucose deprivation; RO, reoxygenation, PM, primary microglia. PN, primary neuron; Trc, triacsin C.

We found that co-culture with preconditioned microglia did not affect the cell survival of neuronal cells in normoxia. In neuron-microglia co-culture experiments with OGD/RO, untreated and IL-4 pretreated microglia (group 3 and group 9) exhibited a protective effect on post-hypoxic neurons. In contrast, the survival of neurons co-cultured with the LDRM groups (LPS preconditioned group 5 and OGD-CM preconditioned group 7) was reduced compared to the control group (neurons without co-culture after hypoxia, group 2). Interestingly, with inhibition of LDs by Trc in groups 6 and 8, LDs-lacked microglia diminished damage to neurons in OGD/RO and even protected neurons. Similarly, elevated cytotoxicity of neurons after hypoxia was found in the LDRM groups and was reversed by Trc treatment of LDs-lacked microglia (Figure 12. A-B). Furthermore, in LIVE/DEAD morphological assay, it was demonstrated that LDRM (group 5 and 7) also significantly caused neuronal damage during co-culture with neuronal RO by quantitatively calculating the ratio of surviving neurons (LIVE, green) to total cell number. Trc precondition transformed LDRM to LDs-lacked microglia reversed this effect (Figure 12. C-D). Hence, these data confirm that microglia play a double-edged role in neuronal ischemic injury: resting and anti-inflammatory phenotypes of microglia can counteract neuronal injury after hypoxia, whereas LDRM loses this protective effect. The lipid metabolism and LD formation are related to functional and phenotypic transformation of microglia.

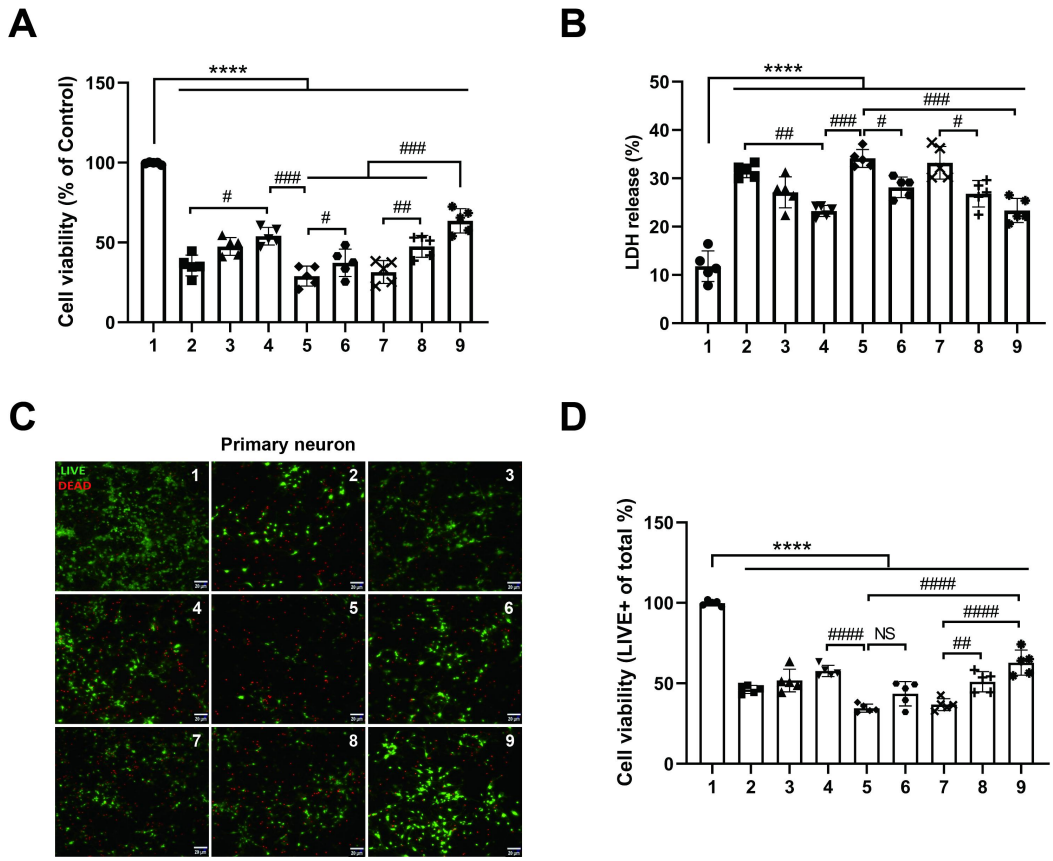

Figure 12. Primary microglia (PM) with different treatments affect the cell viability of primary neurons (PNs) after OGD by a co-cultures system. A, Cell viability was analyzed in PNs exposed to 4 h of OGD followed by 24 h of reoxygenation with co-cultures of pre-treated PM by MTT assay (A) (n = 5). Cells incubated under normoxic conditions were defined as 100% cell survival. **B**, OGD-induced neuronal cell toxicity was further assessed in the lactate dehydrogenase (LDH) release assay (n = 5). **C-D**, The LIVE/DEAD assay of PNs uses the same conditions as mentioned for the MTT assay. The photos display representative immunofluorescence stainings of calcein AM (LIVE cells, green) and ethidium homodimer-1 (DEAD cells, red). (n = 5). Statistical tests: Data are expressed as mean ± SD, NS: no significance, *p < 0.05 **p < 0.01, ***p < 0.001, ****p < 0.0001, $^{\#}$p < 0.05, $^{\#\#}$p < 0.01, $^{\#\#\#}$p < 0.001, and $^{\#\#\#\#}$p < 0.0001. Scale bars, 20 μm (C). Abbreviation: OGD, oxygen-glucose deprivation; PM, primary microglia; PN, primary neuron; Trc, triacsin C, LDH, lactate dehydrogenase.

3.5 Fatty acid synthesis and accumulation of LDs affect inflammation levels in microglia

In our study, we found a dual role of microglia in the survival of neurons after hypoxia. One possible reason is that the high level of inflammatory factors released by this LDRM aggravates neuronal death. Therefore, we used an *in vitro* ELISA assay to detect inflammatory and anti-

inflammatory factors levels in microglia under different conditions. We found that IL-1β and TNF-α levels were significantly higher in LDRM under LPS and OGD-CM treatment than in control group and IL-4 treated groups (Figure 13. A-B). While IL-6, a chronic inflammatory factor and an anti-inflammatory factor in acute inflammation, was elevated in all treatment groups, but more significantly in LDRM (Figure 13. C). On the other hand, the level of the anti-inflammatory factor TGF-β was reduced in LPS group compared to the control group, with a slight increase in OGD-CM group, and showed the highest level in IL-4 group (Figure 13. D).

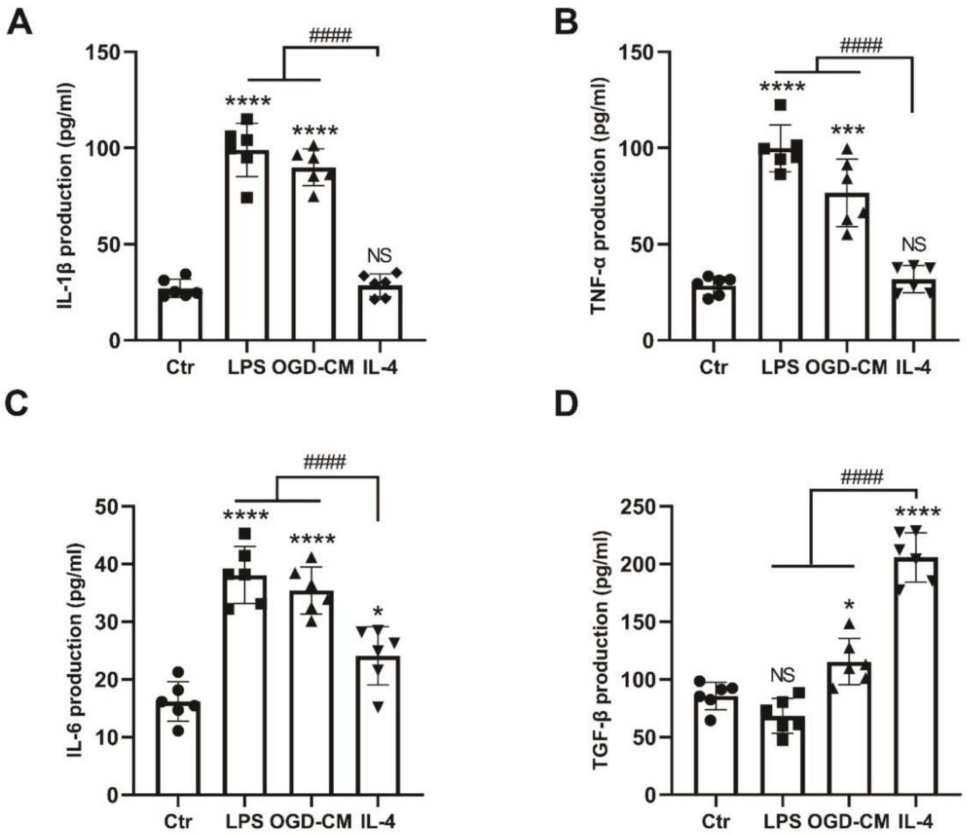

Figure 13. OGD-CM and LPS induce upregulation of inflammatory factor levels in vitro. A-C, ELISA analysis of such LPS and OGD-CM treated lipid droplet-rich microglia (LDRM) revealed higher inflammatory level of IL-1β, IL-6 and TNF-α, while IL-4 did not (n = 6). **D**, The LDRM had lower anti-inflammatory factor TGF-β levels than typical M2 microglia in the IL-4 group. (n = 6). Statistical tests: Data are expressed as mean ± SD, NS: no significance, *p < 0.05, ***p < 0.001, and ****p < 0.0001. Abbreviation: LDRM, lipid droplet-rich microglia; OGD-CM, conditioned medium from primary neuron after OGD.

To verify whether fatty acid synthesis and LD accumulation upregulate the level of inflammation in microglia, we analyzed the levels of inflammatory and anti-inflammatory factors in LDRM and with Trc treatment, respectively. Within 48 h of treatment, IL-1β and TNF-α levels were consistently elevated in LPS and OGD-CM groups and peaked at 24 h, and LPS group exhibited

higher levels of inflammatory factors than OGD-CM group. Reducing LDs aggregation by Trc treatment, a decrease in IL-1β and TNF-α levels was observed in these two groups (Figure 14. A-B). In addition, although a slight increase in IL-6 over time was observed in both LPS and OGD-CM groups, inhibition of LDs did not significantly alter IL-6 levels (Figure 14. C). One can speculate that lipid metabolism is not a key target for regulating IL-6. On the other hand, we observed that TGF-β levels in OGD-CM group tended to increase first and peak at 12 h, then decline after that, and Trc treatment significantly increased TGF-β levels. Interestingly, a similar trend could not be observed in LPS group, where TGF-β remained at a relatively low level and could not be altered by Trc treatment (Figure 14. D).

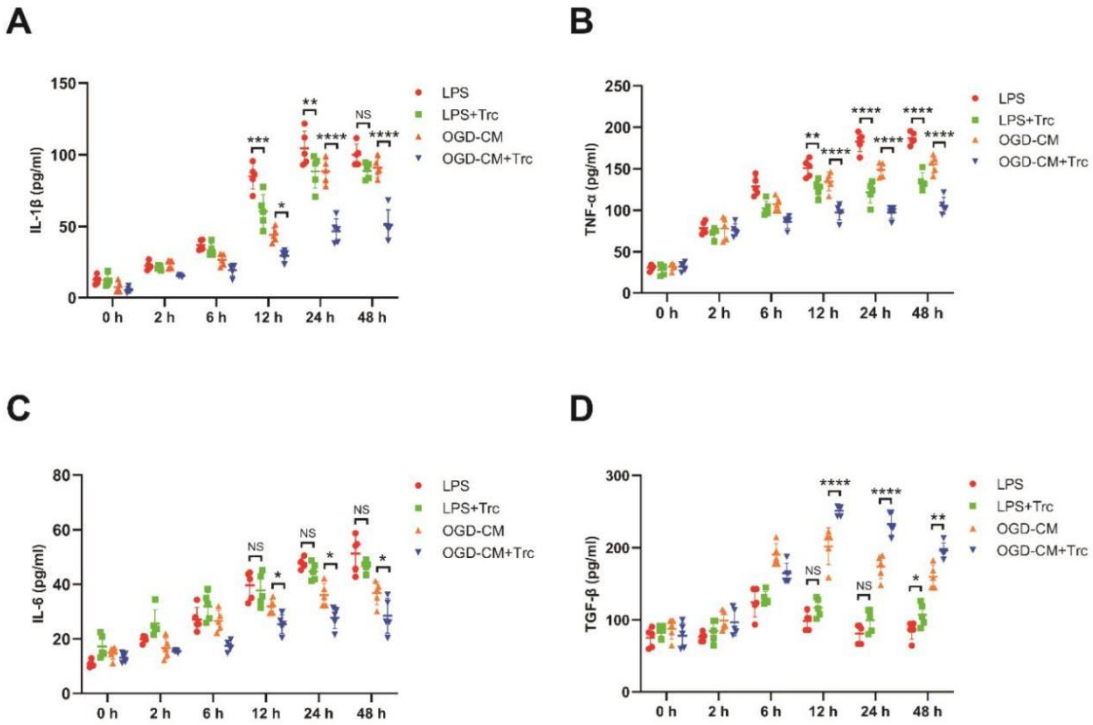

Figure 14. **Triacsin C reduces the upregulation of inflammatory factor levels in OGD-CM and LPS-induced lipid droplet-rich microglia (LDRM) in vitro. A-D**, Quantitative measurement of pro-inflammatory factors (IL-1β, TNF-α, and IL-6) level (A-C) and anti-inflammatory factors (TGF-β) level (D) in lipid droplet rich microglia (LDRM) treated with LPS or OGD-CM followed by different incubation periods (2, 6, 12, 24, and 48 h) using ELISA assay (n = 6). The expression of pro- and anti-inflammatory factors of LDRM co-incubation with Triacsin C was also measured quantitatively. Statistical tests: Data are expressed as mean ± SD, NS: no significance, *$p < 0.05$, **$p < 0.01$, ***$p < 0.001$, and ****$p < 0.0001$. Abbreviation: Trc, triacsin; LDRM, lipid droplet-rich microglia; OGD-CM, conditioned medium from primary neuron after OGD.

3.6 Altered lipid metabolism affect the inflammatory transcriptional characteristics of microglia in vitro.

To analyze if ischemia alters the expression of lipid metabolism-related genes and induces lipid droplet biogenesis in microglia, as well as an accompanying inflammatory response after stroke, we examined ischemia-induced differentially expressed genes (DEGs) encoding typical lipid droplet membrane proteins (PLIN2); fatty acid synthesis and cholesterol esterification (Soat1, SREBP2); fatty acid and cholesterol hydrolysis (Nceh1, LIPA, NPC2); lipid transport (ApoE, ABCA1); Oxidative stress and microglial phenotype (iNOS, CD206); inflammatory factors (TNF-α, IL-1β); and anti-inflammatory factors (IL-10, TGF-β) (Figure 15.).

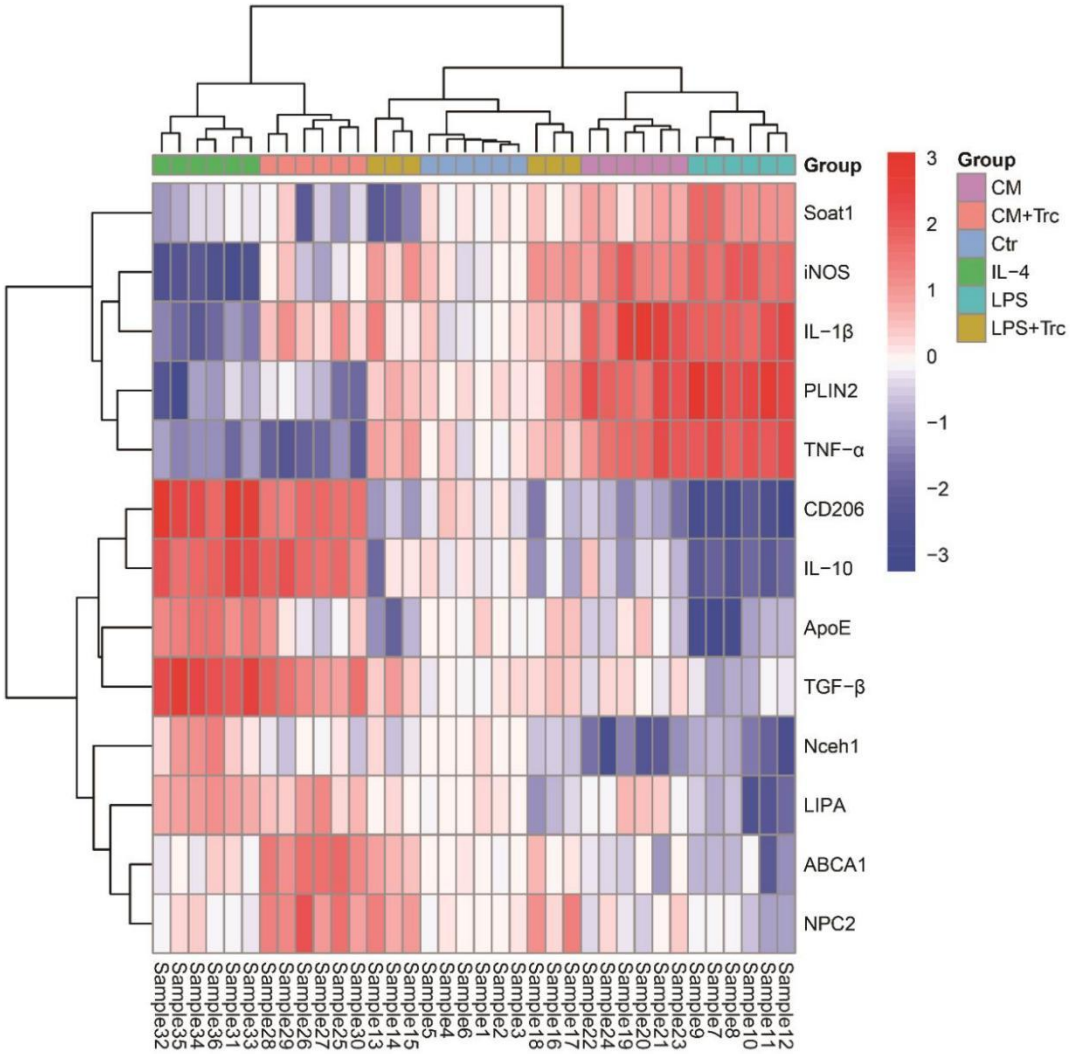

Figure 15. LPS and OGD-conditioned medium (CM) induce the formation of lipid droplet-rich microglia (LDRM), alter lipid metabolism-related gene expression, and regulate the polarization phenotype and inflammatory factor levels in microglia. Heatmap of gene expression comparisons

between 6 groups: control group (primary microglia treated with drug solvent in normoxic condition); LPS group (1000 ng/ml LPS treatment); LPS + Trc group (2 μM Trc inhibitor treatment in LPS group); CM group (incubation with conditioned medium from neurons after OGD/RO), CM + Trc group (2 μM Trc inhibitor treatment in CM group) and IL-4 group (10 ng/ml recombinant IL-4 treatment). Heatmap was produced by pheatmap package in Rstudio. Data were log2 transformed and shown as red to blue: red (up-regulated), blue (down-regulated) and white (no modulation), as shown in the key. Rows and columns are clustered using correlation distances and average associations. Abbreviation: OGD, oxygen-glucose deprivation; CM, conditioned medium from primary neuron after OGD; LDRM, lipid droplet-rich microglia; Trc, triacsin C.

We observed that 12 groups of LDRM (LPS and CM groups) increased microglial mRNA expression of lipophilin protein (PLIN2); cholesterol synthesis esterified protein (Soat1); M1 phenotype-associated enzyme (iNOS); pro-inflammatory factors (IL-1β, TNF-α). Down-regulated expression includes M2 phenotype marker of the mannose receptor (CD206), apolipoprotein (ApoE); lipid transporter protein (ABCA1); Intracellular Cholesterol Transporter 2 (NPC2); Neutral cholesterol ester hydrolase 1 (Nceh1); lysosomal acid lipase (LIPA), and anti-inflammatory factors (TGF-β and IL-10). In contrast, IL-4-treated microglia in the six groups with M2 phenotype showed a distinct transcriptional profile from LDRM: microglial mRNA was significantly upregulated by CD206, TGF-β, and IL-10. ApoE, Nceh1, and LIPA were slightly increased. Down-regulation included iNOS, IL-1β and TNF-α; Soat1 and PLIN2 for fatty acid synthesis and LD formation. ABCA1 and NPC2 were not significantly changed. We further inhibited long-chain fatty acid synthesis and LD formation in LDRM by using Trc and found that it diminished the upregulation of IL-1β, TNF-α, iNOS, PLIN2, and Soat1 in the CM group. However, ApoE and Nceh1 did not change significantly. It was verified that LPS and ischemia-induced lipid metabolism changes could regulate microglia phenotype and inflammation levels. However, the results were different for LPS plus Trc treatment: although we still observed a decrease in PLIN2 and Soat1 compared to LPS group and an increase in CD206, TGF-β, NPC2, ABCA1 and LIPA, this inhibition of fatty acid synthesis did not completely inhibit the LPS-stimulated inflammatory factor upregulation and microglial M1 phenotypic transformation, as evidenced by still relatively high levels of iNOS, IL-1β and TNF-α expression.

We further verified the expression of Plin2, SREBP2 and P65 at the protein level in microglia using Western blotting. We observed that PLIN2 expression levels were significantly higher in LPS and OGD-CM-induced LDRM compared to control group and could be suppressed by Trc, while protein expression levels were lowest in IL-4 group (Figure 16. A). In our study, similar to PLIN2, SREBP2 expression was significantly elevated in LPS and OGD-CM groups,

and this elevation could be suppressed by Trc, and expression was lowest in the IL-4 group (Figure 16. B). Interestingly, P65, a key protein of NF-ϰB, was highly expressed in LDRM in LPS and OGD-CM groups, and Trc could inhibit this high expression only in the OGD-CM group. IL-4 group still keeps the lowest expression level (Figure 16. C).

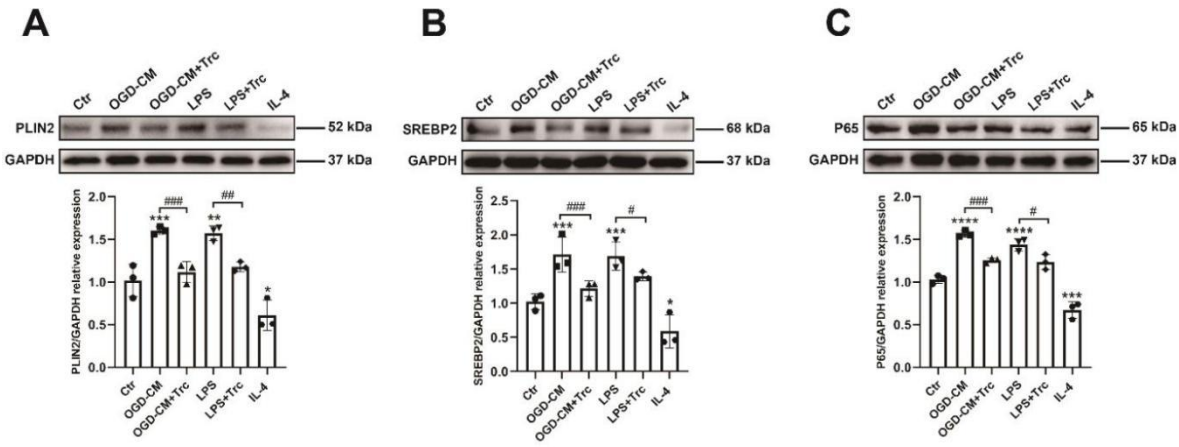

Figure 16. ACAT inhibitor triacsin C (Trc) reverses upregulation of SREBP2 (Sterol regulatory element-binding protein 2) and PLIN2 (Perilipin 2 protein) and activation of NF-ϰB (nuclear factor-ϰB) in lipid droplet-rich microglia (LDRM). A-B, Quantitative analysis of PLIN2 (A) and SREBP2 (B) expression in six group: normoxia as control group, OGD-CM (conditioned medium from primary neurons after OGD), LPS, LPS treated with Trc (1 μM), OGD-CM treated with Trc and IL-4 group using Western blot analysis normalized with the housekeeping protein GAPDH (n = 3). **C**, Quantitative analysis of p65 expression, the NF-ϰB pathway in these six groups using Western blot analysis normalized with the housekeeping protein GAPDH (n = 3). Statistical tests: Data are expressed as mean ± SD, NS: no significance, *p < 0.05, **p < 0.01, ***p < 0.001, ****p < 0.0001, $^{\#}$p < 0.05, $^{\#\#}$p < 0.01, and $^{\#\#\#}$p < 0.001. Abbreviation: Trc triacsin C; SREBP2, sterol regulatory element-binding protein 2; PLIN2, perilipin 2 protein; LDRM, lipid droplet-rich microglia; OGD, oxygen-glucose deprivation; PM, primary microglia; PNs, primary neurons; OGD-CM, conditioned medium from primary neurons after OGD.

3.7 Altered patterns of lipid and energy metabolism play a vital role in microglial polarization in vitro

We further used immunofluorescence staining to determine the microglial phenotype. M1 phenotype microglia were stained by iNOS (Alexa Fluor 488, green), M2 phenotype microglia were stained by CD206 (Cy3, red), and the nuclei were stained by DAPI (Figure 17. A). We observed that the majority of microglia in OGD-CM treated microglia were iNOS+ M1 phenotype microglia, while there were few CD206+ microglia. Furthermore, after the inhibition of fatty acid and cholesterol synthesis by Trc, the number of iNOS+ M1 microglia decreased

significantly, while CD206+ M2 microglia increased. In contrast, in IL-4 group, which served as a positive control for typical M2 microglia, the vast majority exhibited CD206+ M2 phenotype microglia and very few iNOS+ microglia (Figure 17. B-C).

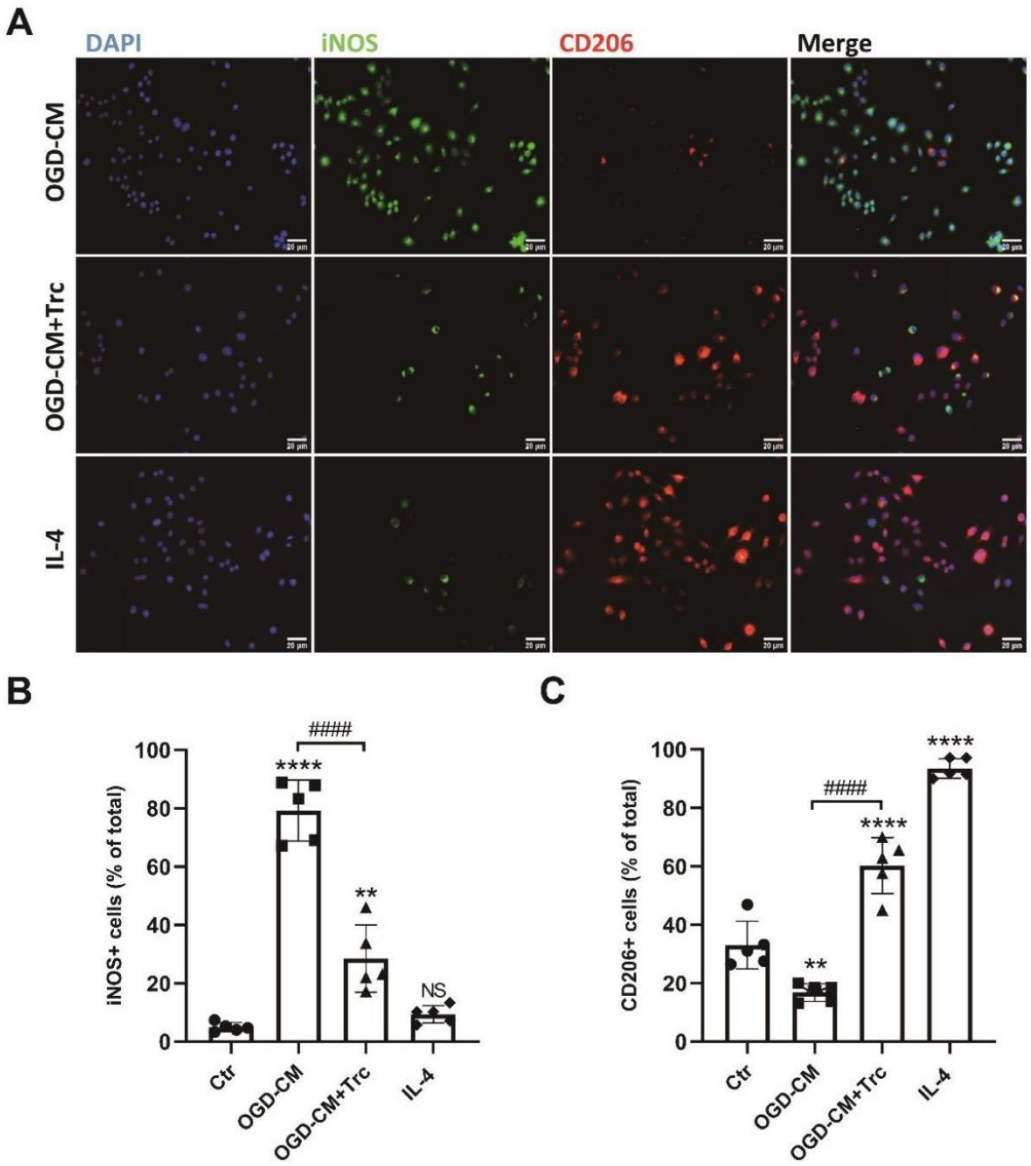

Figure 17. Inflammation induces the formation of lipid droplets (LDs) and stimulates M1 polarization in primary microglia, and this process can be attenuated by inhibition of long-chain fatty acid synthesis and cholesterol esterification by the ACAT inhibitor triacsin C (Trc). A, Immunofluorescence staining of M1 (iNOS, green) and M2 (CD206, red) polarization of primary microglia cells in the four groups: control, conditioned medium (OGD-CM) treatment, OGD-CM with Trc treatment and IL-4 treatment. Trc treatment increases M2 polarization rates of primary microglial cells compared with the OGD-CM group. **B**, Quantitative analysis of M1 polarization of microglia cells by proportion of iNOS+ cells to total cells in the aforementioned four groups (n = 5). **C**, Quantitative analysis of M2 polarization of microglia cells by proportion of CD206+ cells to total cells in the aforementioned four groups (n = 5). Statistical tests: Data are expressed as mean ± SD, NS: no significance, **$p < 0.01$, ****$p < 0.0001$, and

####p < 0.0001. Scale bars, 20 μm (A). Abbreviation: LDs, lipid droplets; OGD, oxygen-glucose deprivation; ACAT, Acyl-coenzyme A: cholesterol acyltransferase; primary microglia; Trc, triacsin C.

Next, we used BODIPY staining to label LDs, and we found that iNOS+BODIPY+ co-localized microglia accounted for the majority of the total cells. Most of the OGD-CM induced iNOS+ M1 microglia, so-called "foam microglia" or LDRM, contained a large amount of LDs, and Trc treatment reduced not only the formation of LDs but also the number of iNOS+M1 phenotype LDRM (Figure 18. A-B). In addition, we found that the number of CD206+ microglia remained relatively few after OGD-CM treatment and that there were almost no BODIPY+ LDs in these CD206+ microglia. After Trc inhibited the biogenesis of LDs, A significant increase of CD206+ M2 phenotype microglia was observed, and relatively few LDs were observed in these microglia (Figure 18. C-D). Thus, we suggest that upregulation of fatty acid and cholesterol synthesis and lipid-overloading formed LDs convert microglia to the M1 phenotype, and this polarization can be reversed by inhibition of ACAT and ACSL.

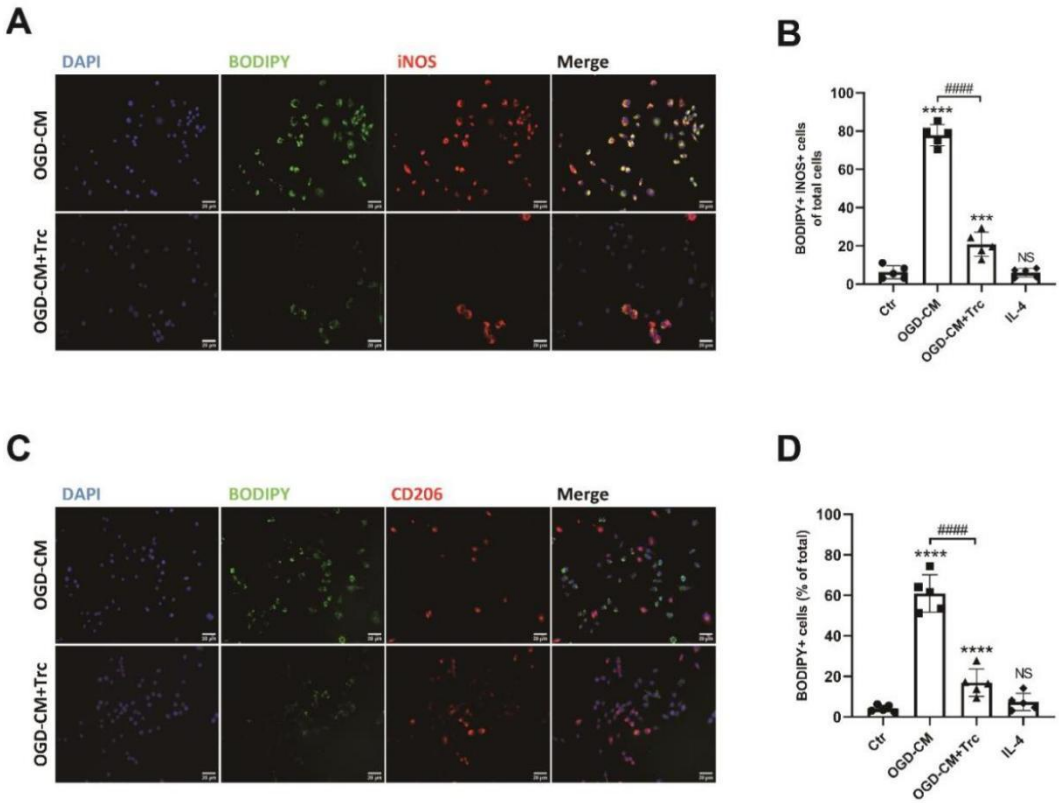

Figure 18. Inhibition of lipid droplets (LDs) formation by triacsin C (Trc) can convert M1 phenotype LDs-rich microglia (LDRM) to M2 phenotype LDs-poor microglia in inflammatory condition. A, Immunofluorescence co-staining of LDs (BODIPY, green) and M1 (iNOS, red) polarization of primary microglia cells in the four groups: control, conditioned medium (OGD-CM) treatment, OGD-CM with Trc

treatment and IL-4 treatment. **B**, Quantitative analysis of BODIPY+iNOS+ microglia of total cells (n = 5). **C**, Immunofluorescence co-staining of LDs (BODIPY, green) and M2 (CD206, red) polarization of primary microglia cells in the aforementioned four groups. **D**, Quantitative analysis of BODIPY+ microglia of total cells (n = 5). Statistical tests: Data are expressed as mean ± SD, NS: no significance, ***$p < 0.001$, ****$p < 0.0001$, and $^{\#\#\#\#}p < 0.0001$. Scale bars, 20 μm (A). Abbreviation: LDs, lipid droplets; LDRM, lipid droplet-rich microglia; OGD, oxygen-glucose deprivation; Trc, triacsin C.

3.8 LDRM in the infarct lesion polarize toward the proinflammatory M1 phenotype over time after MCAO

We partially validated that fatty acid synthesis may stimulate alterations in the microglial phenotype, upregulating neuroinflammation and further causing neural damage. Indeed, our *in vivo* results of post-MCAO mice showed that the polarization of microglia changes dynamically over time and varies in their distribution in different regions (Figure 19. A). In the infarct core (R1) and white matter margin regions (R3) on post-ischemia day 3, activated microglia were observed to be predominantly CD206+ microglia of the M2 phenotype, with some iNOS+ M1 microglia. In contrast, a few CD206+ microglia were observed in the region outside the cortical infarct area (R2), while few iNOS+ microglia were found. In contrast, on post-ischemia day 7, the R1 region was covered with a large number of iNOS+ M1 microglia, while CD206+ M2 microglia were almost absent. Interestingly, the microglia found in the R3 region were predominantly iNOS+M1 microglia on the side close to the infarct lesion and CD206+M2 microglia on the side far from the lesion, while only a few iNOS+ and CD206+ microglia were found in the R2 region. On post-ischemia day 28, there were almost no iNOS+ or CD206+ microglia in the ipsilateral side of the brain except for only limited iNOS+ microglia in the R1 region and CD206+ microglia in the R3 region (Figure 19. B-C).

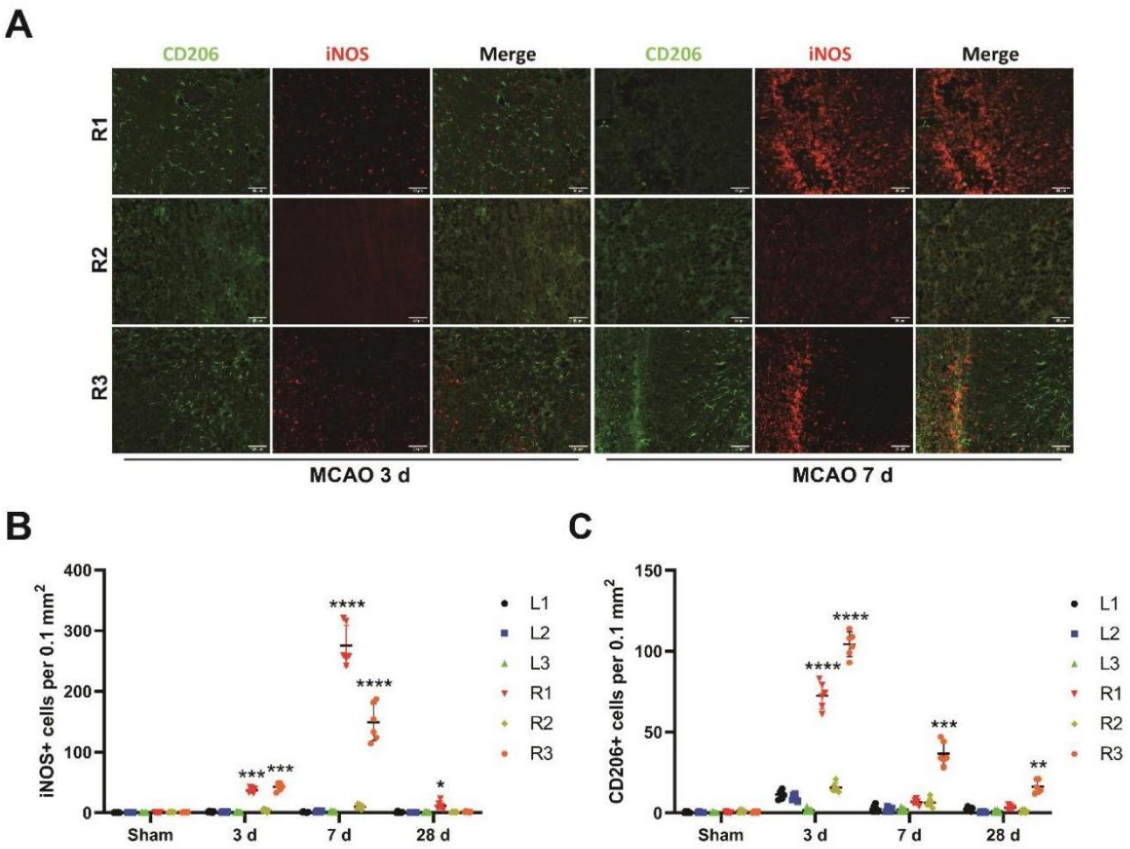

Figure 19. M1/M2 polarization of microglia in different infarct regions of brain in the mouse middle cerebral artery occlusion (MCAO) stroke model. A, Immunofluorescence staining of polarization of M1 phenotype microglia (iNOS, red) and M2 phenotype microglia (CD206, green) at post-MCAO day 3 and 7 in the aforementioned six regions. CD206+ M2 anti-inflammatory microglia were abundant in both the R1 and R3 regions at day 3 post-ischemia; iNOS+ M1 pro-inflammatory microglia peaked in the R1 region at day 7 post-ischemia. **B**, Quantitative analysis of the number of iNOS+ microglia per 0.1 mm^2 area (n = 6). **C**, Quantitative analysis of the number of CD206+ microglia per 0.1 mm^2 area (n = 6). Statistical tests: Data are expressed as mean ± SD, NS: no significance, **p < 0.01, ***p < 0.001, and ****p < 0.0001. Scale bars, 20 μm (A). Abbreviation: MCAO, middle cerebral artery occlusion.

In addition, we used the lipoprotein PLIN2 staining to label LDs and found that PLIN2 expression and LDs biogenesis coincided with microglia polarization from M2 to M1 phenotype (Figure 20. A). The majority of iNOS+ cells could co-localize with PLIN2 and gradually increase in the infarct region (R1, R3) on post-ischemia day 3, whereas only few iNOS+ microglia were found in the R2 region and PLIN2 expression was also relatively rare. Next, PLIN2+iNOS+ microglia peaked in the R1 region on post-ischemia day 7, and both PLIN2 and iNOS expression gradually decreased to pre-infarct levels on post-ischemia day 28 (Figure 20. B-C). These *in vivo* results validate the hypothesis of our *in vitro* section that lipid synthesis and biogenesis of LDs play a vital role in the phenotypic polarization of microglia.

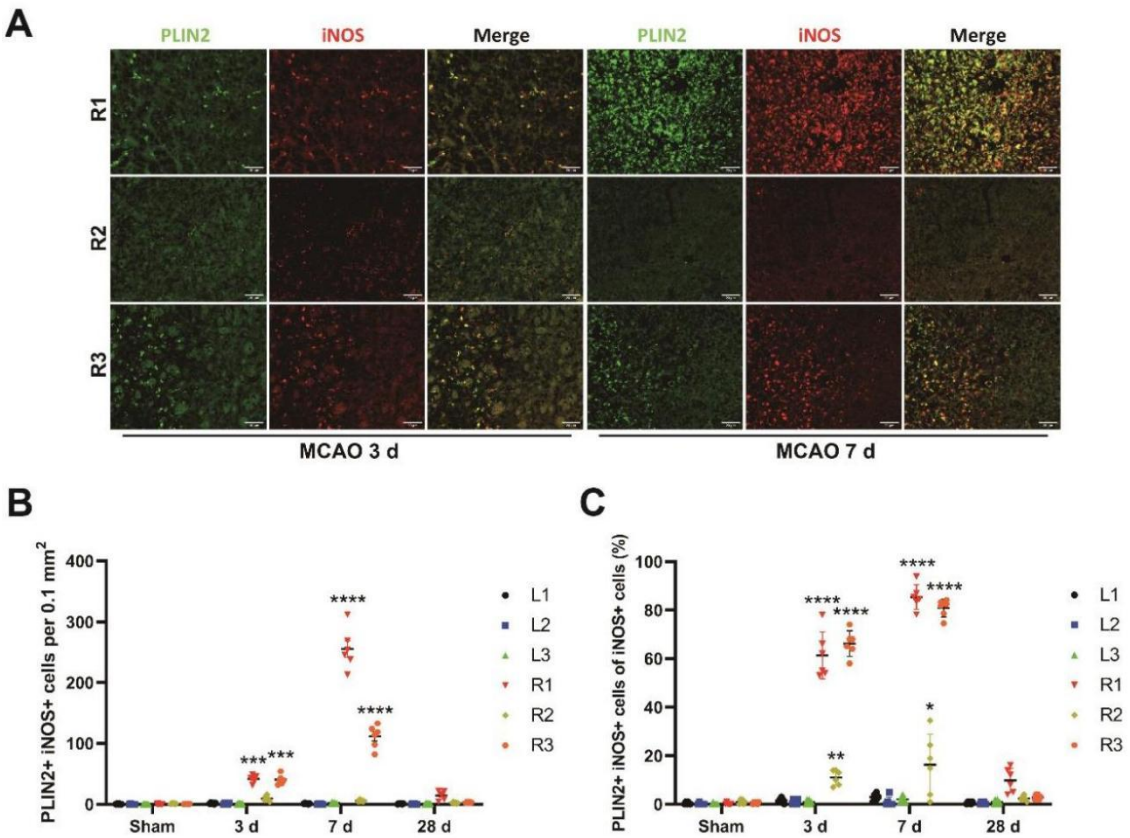

Figure 20. Lipid metabolism and lipid droplets (LDs) accumulating affect the polarization and phenotype of microglia. A, Immunofluorescence staining of M1 microglia (iNOS, red) and lipid droplets surface protein marker (PLIN2, green) at post-ischemia day 3 and 7 in the aforementioned six regions. PLIN2 was highly expressed in iNOS+ M1 phenotype microglia in R1 cortical lesion core after 7 days reperfusion. **B**, Quantitative analysis of PLIN2+iNOS+ microglia per 0.1 mm^2 area (n = 6). **C**, Quantitative analysis of the percentage of PLIN2+iNOS+ cells of total iNOS+ cells (n = 6). Statistical tests: Data are expressed as mean ± SD, NS: no significance, **p < 0.01, ***p < 0.001, and ****p < 0.0001. Scale bars, 20 μm (A). Abbreviation: LDs, lipid droplets.

Meanwhile, we examined the levels of inflammatory factors over time in different regions after stroke using ELISA assay. We found that on post-ischemia day 7, the levels of various inflammatory factors were significantly increased in the ipsilateral side compared with the contralateral side, especially in the R1 region, with the highest expression levels of IL-1β, TNF-α and IL-6. In contrast, TNF-α and IL-6 levels were only slightly increased in the R3 region, while IL-1β levels were not significantly changed. In contrast, the levels of all inflammatory factors in the R2 region were similar to the contralateral side (Figure 21. A-C). On the other hand, the expression levels of the anti-inflammatory factor TGF-β were different from the above, with the highest levels in the R3 region and significantly higher than in the ipsilateral R1 and R2 regions. At the same time, the expression level of TGF-β showed a slight increase in the R2 region, while R1 was not significantly different from the contralateral side (Figure 21. D).

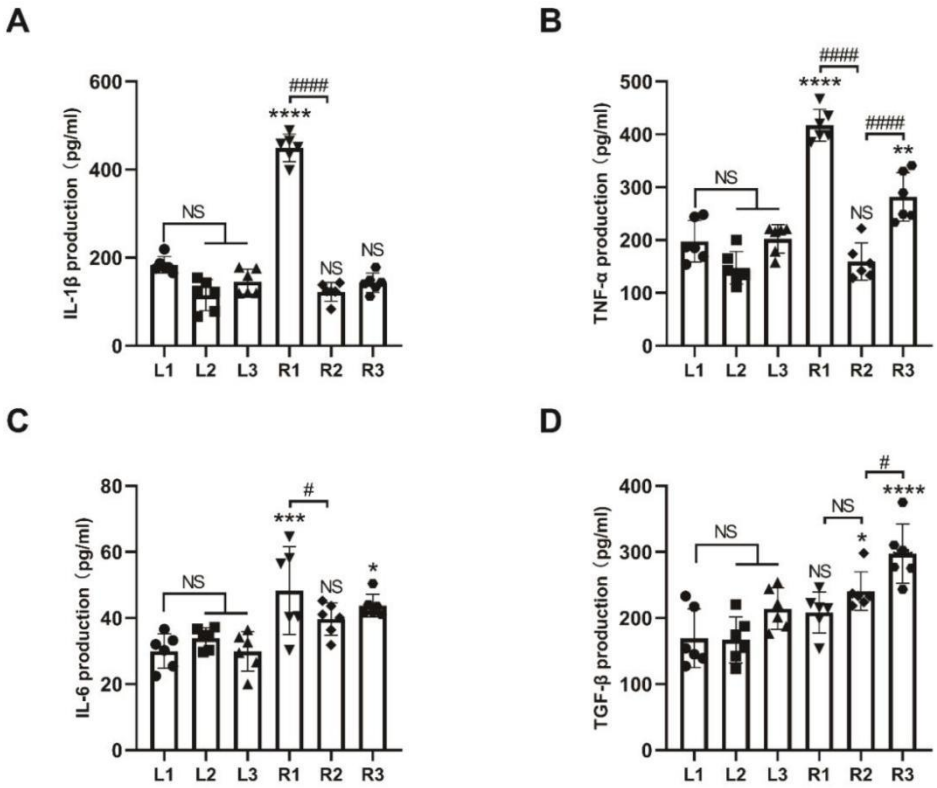

Figure 21. Higher levels of inflammatory factors in lipid droplet-rich microglia (LDRM) enrichment region. A-C, Quantitative measurement of pro-inflammatory factors (IL-1β, TNF-α and IL-6) levels in the aforementioned six regions at day 7 post-ischemia using ELISA assay (n = 6). **D**, Quantitative measurement of anti-inflammatory factor (TGF-β) level in the aforementioned six regions at day 7 post-ischemia using ELISA assay (n = 6). Statistical tests: Data are expressed as mean ± SD, NS: no significance, *$p < 0.05$, **$p < 0.01$, ***$p < 0.001$, ****$p < 0.0001$, $^{\#}p < 0.05$, and $^{\#\#\#\#}p < 0.0001$. Abbreviation: LDRM, lipid droplet-rich microglia**.**

Our results confirm a dynamic transformation in microglial phenotype after stroke. In the early post-ischemia period, microglia dominate the anti-inflammatory phenotype of M2, rescuing the surviving neurons. As more and more cells die, increasing of cellular and myelin debris, and upregulation of fatty acid synthesis, eventually lead to lipids accumulation in microglia and converting microglia from the LDs-poor anti-inflammatory M2 phenotype to the LDs-rich pro-inflammatory M1 phenotype that upregulates chronic inflammation after stroke and may be detrimental to neuronal regeneration.

3.9 MCAO-induced upregulation of SREBP2 and PLIN2 leads to the accumulation of LDs in microglia and the activation of NF-ϰB pathway

The pathophysiology of cerebral ischemia involves a complex series of inflammatory signaling cascades that are regulated by multiple mechanisms and are also deleterious to the surrounding ischemic tissue (Xing et al. 2012). However, their role in post-ischemia induced inflammation still remains unknown. Therefore, we first measured the protein expression levels of SREBP2 and PLIN2 in MCAO mice using Western blotting. On post-ischemia day 7, SREBP2 protein expression levels were significantly upregulated on the ipsilateral side of the infarct compared to the contralateral side. The R1 region of the cortical infarct core showed the highest protein expression levels, followed by the R3 region of the white matter infarct margin and the lowest in the R2 region of the cortex outside the infarct area (Figure 22. A). In addition, the protein expression of PLIN2 showed similar results on post-ischemia day 7, with significantly higher expression levels ipsilateral than contralateral: the R1 region has the highest protein expression level, followed by the R3 region and the lowest in the R2 region (Figure 22. B).

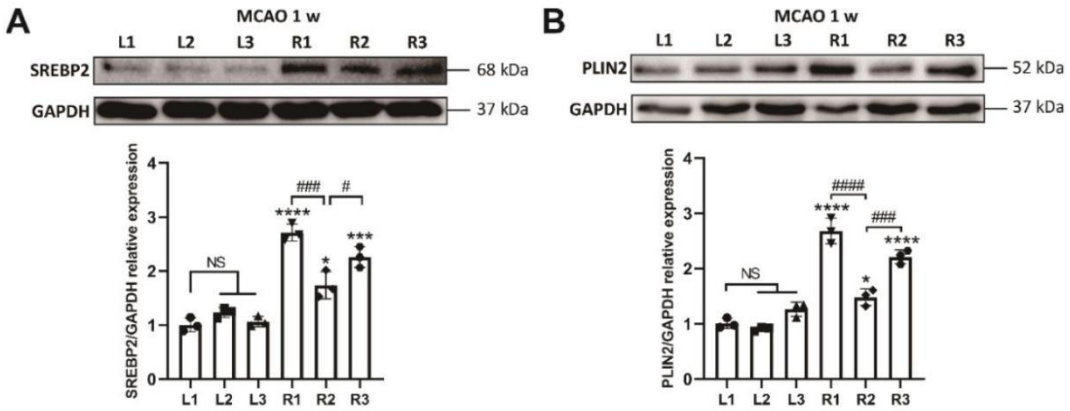

Figure 22. Up-regulation of fatty acid and cholesterol synthesis leads to the accumulation of lipid droplets (LDs) in microglia after stroke. A, Quantitative analysis of SREBP2 expression in the aforementioned six regions with 7 day post-ischemic mice by Western blot analysis normalized with the housekeeping protein GAPDH (n = 3). **B**, Quantitative analysis of PLIN2 expression in the aforementioned six regions with 7 day post-ischemic mice by Western blot analysis normalized with the housekeeping protein GAPDH (n = 3). Statistical tests: Data are expressed as mean ± SD, NS: no significance, *$p < 0.05$, ****$p < 0.0001$, $^{\#}p < 0.05$, $^{\#\#\#}p < 0.001$, and $^{\#\#\#\#}p < 0.0001$. Abbreviation: LDs, lipid droplets.

We subsequently measured the level of NF-ϰB signaling pathway activation in these regions. Interestingly, consistent with the protein expression of SREBP2 and PLIN2, the R1 region with abundant LDRM had the highest p65 and lowest IϰBα protein expression levels (Figure 23. A-

B). Subsequently, we observed that with the activation of NF-ϰB signaling pathway, the R1 region, which possesses the highest expression of p65, also exhibited the highest IL-1β expression level (Figure 23. C). In contrast, TGF-β protein expression levels of R1 region were relatively low compared to other regions (Figure 23. D).

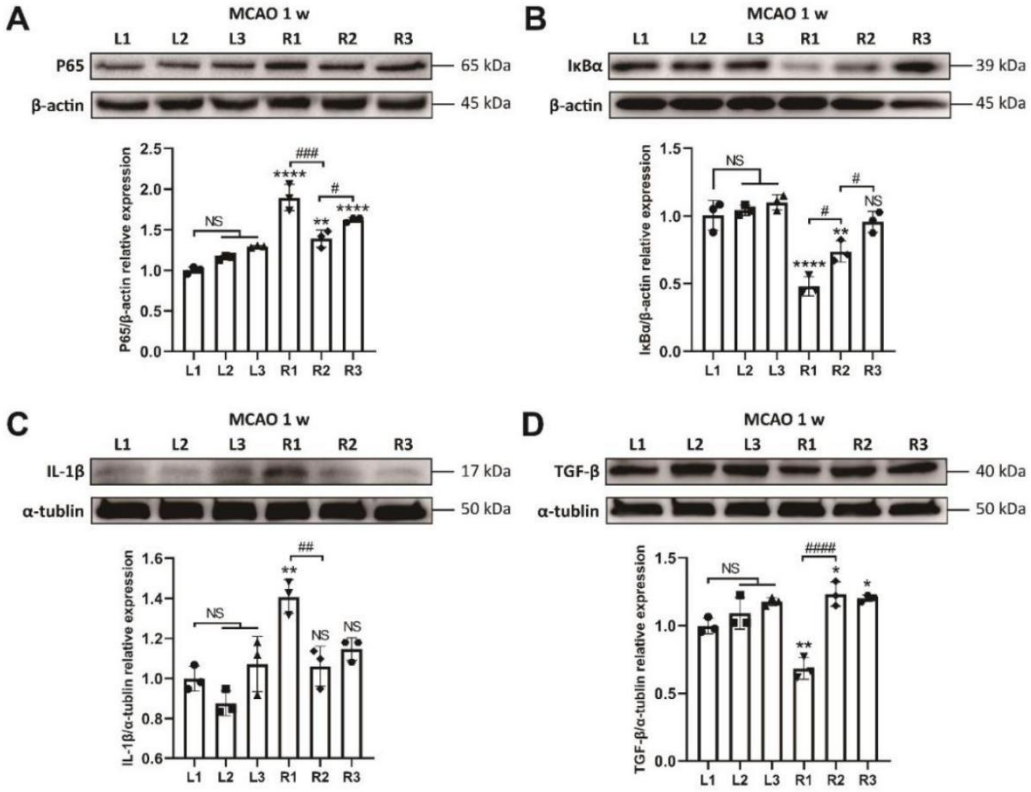

Figure 23. Upregulation of fatty acid and cholesterol synthesis after stroke converts microglia to M1 phenotype proinflammatory lipid droplet-rich microglia (LDRM), leading to activation of NF-ϰB (nuclear factor-ϰB) pathway and inflammation. A-B, Quantitative analysis of p65 (A) and IκBα (B) expression in the aforementioned six regions with 7 day post-ischemic mice by Western blot analysis normalized with the housekeeping protein β-actin (n = 3). **C-D**, Quantitative analysis of IL-1β (C) and TGF-β (D) expression in the aforementioned six regions with 7 day post-ischemic mice by Western blot analysis normalized with the housekeeping protein α-tublin (n = 3). Statistical tests: Data are expressed as mean ± SD, NS: no significance, *$p < 0.05$, **$p < 0.01$, ****$p < 0.0001$, $^{\#}p < 0.05$, $^{\#\#}p < 0.01$, $^{\#\#\#}p < 0.001$, and $^{\#\#\#\#}p < 0.0001$. Abbreviation: LDRM, lipid droplet-rich microglia.

We further hypothesized that upregulated SREBP2 after cerebral ischemia stimulates the synthesis of cholesterol and fatty acids, further forming a large number of LDs in microglia. Moreover, SREBP2 upregulation stimulates NF-ϰB signaling pathway activation and exacerbates neuroinflammation. To confirm this, we detected the transcriptional mRNA expression levels of lipid metabolism-related genes as well as that of microglial polarization and inflammation-related genes using RT-qPCR. Surprisingly, PLIN2, ApoE and ABCA1 were all

highly expressed in the ipsilateral R1 region, in contrast to our *in vitro* results of downregulation of ABCA1 and ApoE in LRDM (Figure 24. A-C). Although the expression was reduced in microglia, the overall expression in brain was still upregulated.

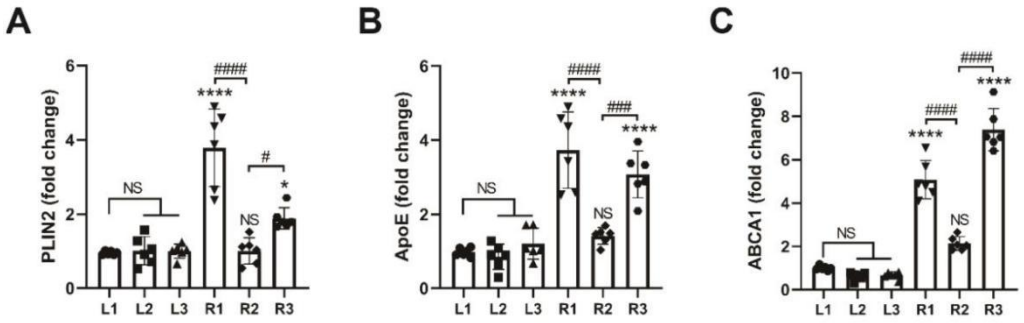

Figure 24. Expression of lipid metabolism related genes in different regions after middle cerebral artery occlusion (MCAO). A-C, Quantitative analysis of PLIN2 (A), ApoE (B), and ABCA1 (C) gene expression in the aforementioned six regions with 7 day post-ischemic mice by RT-qPCR normalized with L1 (as control group) (n = 6). Statistical tests: Data are expressed as mean ± SD, NS: no significance, $^{*}p < 0.05$, $^{****}p < 0.0001$, $^{\#}p < 0.05$, $^{\#\#\#}p < 0.001$, and $^{\#\#\#\#}p < 0.0001$. Abbreviation: LDs, lipid droplets.

Meanwhile, iNOS, TNF-α and IL-1β were highly expressed in the R1 and R3 regions with abundant LDRM, while without significant difference in the R2 region with few LDRM compared with the contralateral side (Figure 25. A-C). On the other hand, although the expression of TGF-β and CD206 remained higher on the ipsilateral side compared to the contralateral side, the expression of the R3 region was higher than that in R1 and R2 (Figure 25. D-E). These findings validate our previous *in vivo* immunofluorescence staining results and are consistent with our RT-qPCR results *in vitro*. In accordance with the aforementioned *in vivo* findings, SREBP2 may be involved in the activation of NF-κB signaling pathway and upregulate the subsequent neuroinflammation. This cross talk of SREBP2 and NF-κB signaling pathways may become a new target for future ischemic stroke therapy.

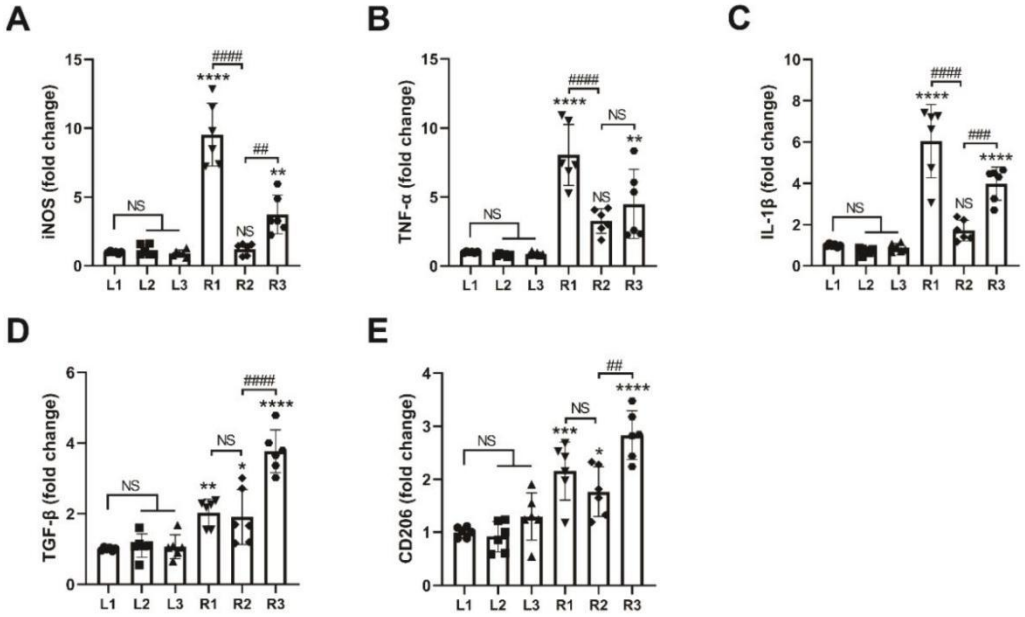

Figure 25. Expression of M1/M2 polarization and inflammation related genes in different regions after middle cerebral artery occlusion (MCAO). A-C, Quantitative analysis of iNOS (A), TNF-α (B), and IL-1β (C) gene expression in the aforementioned six regions with 7 day post-ischemic mice by RT-qPCR normalized with L1 (as control group) (n = 6). **D-E**, Quantitative analysis of TGF-β (D) and CD206 (E) gene expression in the aforementioned six regions with 7 day post-ischemic mice by RT-qPCR normalized with L1 (as control group) (n = 6). Statistical tests: Data are expressed as mean ± SD, NS: no significance, $^{*}p < 0.05$, $^{**}p < 0.01$, $^{***}p < 0.001$, $^{****}p < 0.0001$, $^{\#\#}p < 0.01$, $^{\#\#\#}p < 0.001$, and $^{\#\#\#\#}p < 0.0001$. Abbreviation: MCAO, middle cerebral artery occlusion.

3.10 Lipid profile of LD-rich and LD-poor microglia

Since little is known about the impact of the post-stroke injury on microglial lipid profile, we used colorimetric assays to detect changes in the composition of free fatty acids and cholesterol levels (including total cholesterol, free cholesterol and cholesteryl esters) observed in microglia in six experimental groups. We found that compared to the control group, total cholesterol levels increased in LDRM in LPS and OGD-CM groups while decreasing significantly in groups of co-incubation with Trc. There was no significant difference in the IL-4 group (Figure 26. A). Interestingly, except for the IL-4 group showed a slightly decreasing in free cholesterol levels, there was no statistically significant difference in the other four groups compared to the control group (Figure 26. B). The difference in total cholesterol levels was mainly due to the upregulation of cholesterol esterification in LDRM (Figure 26. C) and could be reversed by inhibition of the ACAT signaling pathway. Meanwhile, glycolytic upregulation in response to LPS and OGD-CM stimulation further leads to an upregulation of fatty acid synthesis, resulting

in a significant increase in free fatty acid levels in both groups compared with the control group; and this increase could be suppressed by Trc inhibition of the fatty acid synthesis mediated by ACSL signaling pathway (Figure 26. D).

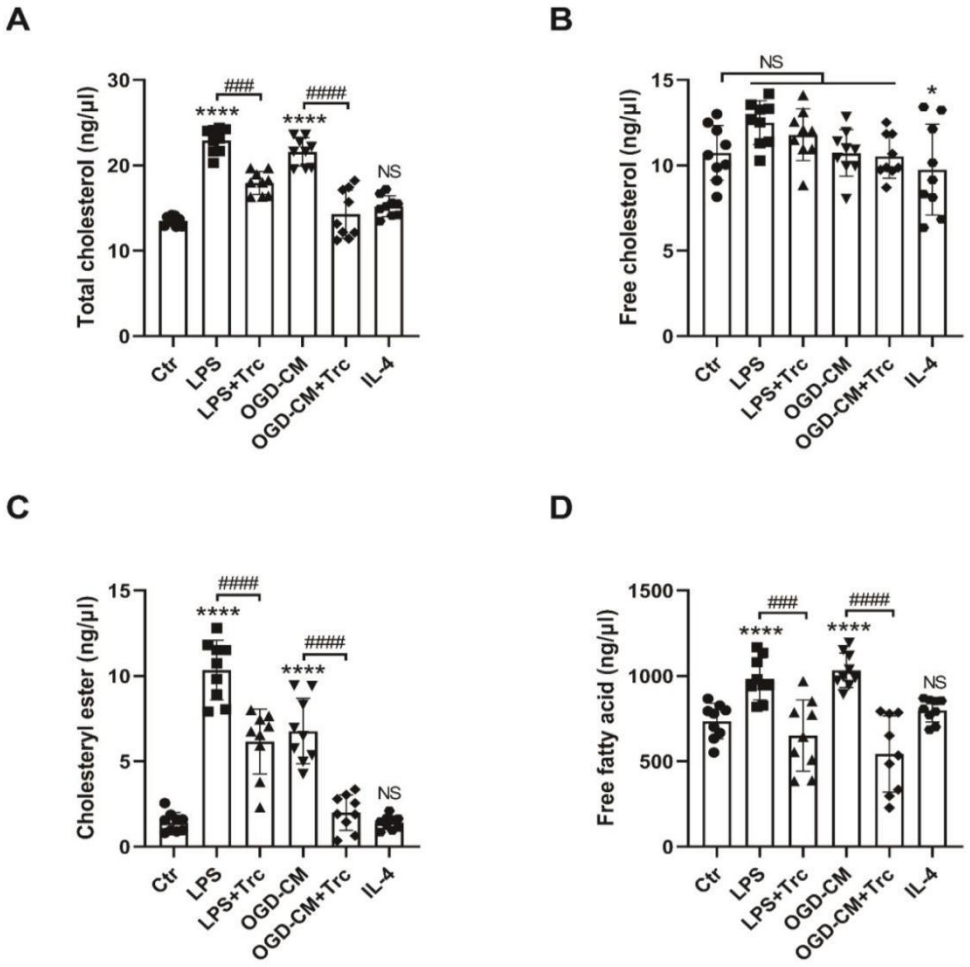

Figure 26. Free fatty acids, free cholesterol and cholesteryl esters in microglia under different conditions. The levels of total cholesterol, free cholesterol, cholesteryl esters and free fatty acids were analyzed in the following 6 groups of microglia (control, LPS, LPS with Trc treatment, OGD-CM, OGD-CM with Trc treatment, and IL-4 groups). Units: ng/μl for all parameters (n = 9). Statistical tests: Data are expressed as mean ± SD, NS: no significance, *$p < 0.05$, **$p < 0.01$, ***$p < 0.001$, ****$p < 0.0001$, $^{\#\#}p < 0.01$, $^{\#\#\#}p < 0.001$, and $^{\#\#\#\#}p < 0.0001$. Abbreviation: OGD, oxygen-glucose deprivation; OGD-CM, conditioned medium from primary neurons after OGD; Trc, triacsin C.

3.11 Higher levels of ROS and impaired phagocytosis in LDRM

In microglia phagocytosis experiments, we determined the phagocytic efficiency of microglia by measuring the fluorescently labeled microsphere. We found that the microsphere within both groups of LDRM was significantly decreased compared to the control group. It indicated that,

similar to LPS-induced LDRM, the phagocytosis of ischemia-induced LDRM was also impaired (Figure 27. A-B).

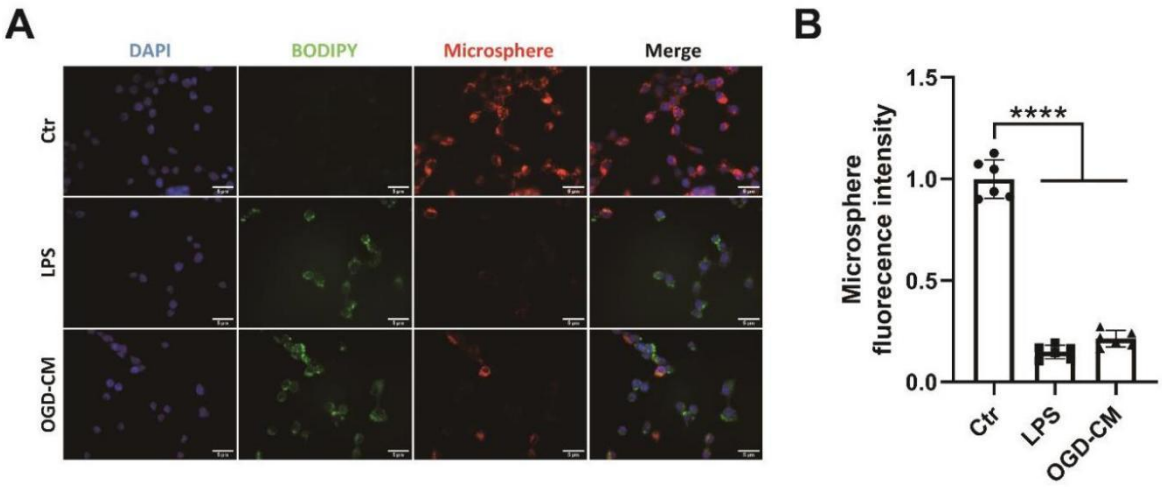

Figure 27. The lipid droplet-rich microglia (LDRM) present impaired phagocytosis. A, immunofluorescence staining of BODIPY and Microsphere in microglia. **B**, Quantification of Microsphere mean fluorescence intensity (MFI) in microglia. (n = 6). Statistical tests: Data are expressed as mean ± SD, NS: no significance, ****p < 0.0001. Scale bars, 5 μm (A). Abbreviation: LDs, lipid droplets; OGD-CM, conditioned medium from primary neurons after OGD; MFI, mean fluorescence intensity.

In addition, we also found that compared to control microglia, LDRM showed higher fluorescence after treatment with CellROX, a dye that shows bright fluorescence only after oxidation by ROS (Marschallinger et al. 2020). The inhibition of LDs biogenesis by triacsin C reduced ROS levels compared to LDRM (Figure 28. A-B). Furthermore, microglia with high CellROX fluorescence tended to be loaded with abundant lipid droplets. This suggests that LPS and hypoxia treatment can cause LDRM generation and have higher ROS concentrations. Thus, lipid droplet biogenesis may be associated with ROS generation.

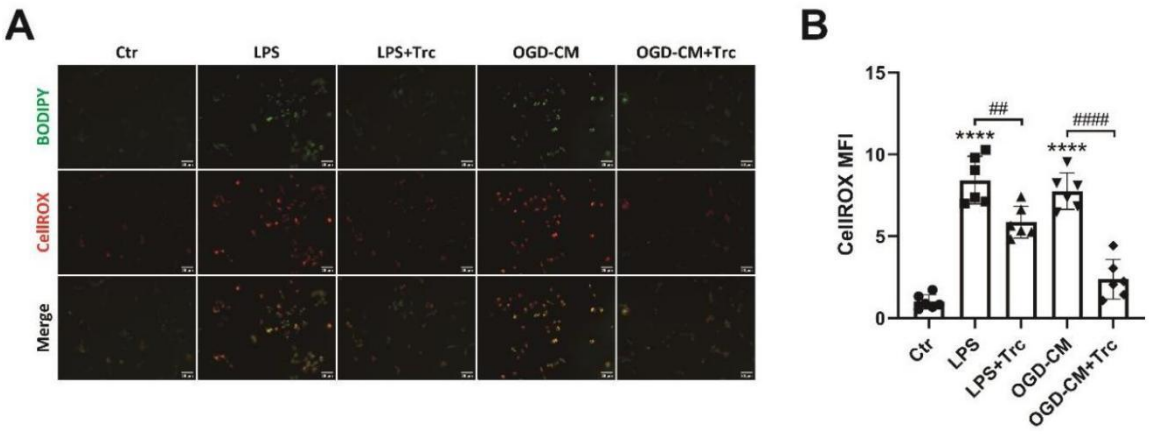

Figure 28. Higher levels of reactive oxygen species (ROS) in the lipid droplet-rich microglia (LDRM). **A**, Representative micrographs of BODIPY and CellROX staining in LPS treated or OGD-CM treated cells. **B**, Quantification of CellROX MFI in microglia. Statistical tests: Data are expressed as mean ± SD, NS: no significance, $^{****}p < 0.0001$, $^{\#\#}p < 0.01$, and $^{\#\#\#\#}p < 0.0001$. Scale bars, 20 μm (A). Abbreviation: ROS, reactive oxygen species; LDRM, lipid droplet-rich microglia; LDs, lipid droplets; OGD-CM, conditioned medium from primary neurons after OGD; MFI, mean fluorescence intensity.

4 Discussion

Stroke is one of the leading causes of death and disability worldwide (Guilbert 2003). For decades, many therapeutic tools for ischemic stroke have been developed, such as neuroprotective drugs, endovascular treatment, and stem cell transplantation (George and Steinberg 2015). Although the neuroprotective drugs showed neuroprotective effects in animal stroke models, most of them have failed in clinical trials (Xu and Pan 2013). Hence, new treatments for ischemic stroke are urgently needed, and microglia, the resident immune cells in the brain, have become a new research hotspot attracting widespread attention. In our study, we used in vitro and in vivo stroke models to analyze the role of post-ischemic lipid metabolism and LDs biogenesis on the regulation of microglial function, including neuroinflammation, phenotypic polarization and immune regulation. Our results here validate the previous hypothesis that LDs are not only organelles for fatty acid storage but are also involved in the management of microglial cell functions. In post-stroke microglia, pro-inflammatory signals enhanced the content, number and size of LDs, upregulated the synthesis of multiple lipids and ultimately polarized microglia to a pro-inflammatory phenotype. These results suggest that lipid composition and distribution in LD are critical for controlling the phenotype and function of microglia. We found that stress stimulates the formation and accumulation of microglia, and that disruption of microglia lipid metabolism in turn drives the biogenesis of LDs. LDs and lipid metabolism play important roles in multiple functions of microglia and serve as markers of microglial cell reactivity and pathogenicity.

Microglia maintain the homeostasis of the internal environment under physiological condition and are rapidly activated when imbalances are perceived, with dynamic changes in morphology and function (Chew et al. 2006; Hanisch and Kettenmann 2007; Kettenmann et al. 2011; Ransohoff and Perry 2009; Yenari et al. 2010). Traditionally, activated microglia are thought to play a deleterious role during ischemic stroke, as inhibition of microglia activation attenuates ischemia-induced brain damage. Such activated microglia that induce neuronal cell death by releasing various pro-inflammatory cytokines and toxic substances are known as M1-like pro-inflammatory microglia. However, previous study of our group has demonstrated that microglia activation can also provide benefits by attenuating neuronal apoptosis, enhancing neurogenesis and promoting functional recovery after cerebral ischemia, and such microglia are referred to as M2-like anti-inflammatory microglia (Zhang et al. 2021a). The different polarization of microglia may explain the dual role of microglia in various pathological conditions. Many substances and mechanisms are involved in regulating microglia polarization, among which lipid

droplets (LDs) and lipid metabolism have shown potential for microglia-targeted therapy (Claes et al. 2021; Hu et al. 2017; Marschallinger et al. 2020).

LDs are organelles that store lipids and are present in the vast majority of cells, consisting mainly of a core of neutral lipids such as triglycerides (TG) and cholesteryl esters, and measuring 0.1-2 μm (Guo et al. 2009; Martin and Parton 2006; Murphy and Vance 1999; Thiele and Spandl 2008). Recent studies have revealed that LDs are not only involved in lipid storage but also in regulating lipid metabolism, inflammation, and various cell signaling (Beller et al. 2010; Melo et al. 2011), which have a diverse protein and lipid composition and can act as hubs of energy metabolism, participating in a variety of metabolic and inflammation-related disease pathologies cooperated with other organelles such as lysosomes, endoplasmic reticulum (ER), plasma membrane and mitochondria (Farmer et al. 2020; Jarc and Petan 2020; Marschallinger et al. 2020; Sunami et al. 2017; Wang et al. 2020). Based on the results of our study, we found that exposure to both hypoxia and the inflammatory condition of LPS can trigger the aggregation of LDs in microglia, but the underlying mechanisms are different. LPS operates as a toxin macromolecule of bacteria composed of a lipid and a polysaccharide, can intensely activated the c-Jun N-terminal kinase (JNK) and p38 MAPK stress signaling pathways and increased the expression of the LD-associated protein PLIN2. Inhibition of p38 α/β and PI3K/Akt pathways reduced LPS-induced LD accumulation and abolished the activation of PLIN2 by LPS (Khatchadourian et al. 2012). In addition, LPS operate directly to activate Toll-like receptor 4 (TLR4), CD14 and CD11b, induce dimerization of the TLR4 complex, further activate downstream molecules such as PI3K and MyD88, and signal the activation of transcription factor NF-κB and various other cellular pathways of immune and inflammatory responses (Zusso et al. 2019). On the other hand, neurological injury due to hypoxia is a complex process involving multiple mechanisms. LD formation occur not only from adequate exogenous lipids (high-fat diet and media treated with lipids), but also from nutrient deprivation and cellular stress (Ralhan et al. 2021). In reperfusion-induced post-ischemic injury, hypoxia leads to a severe shortage of ATP supply, which in turn induces mitochondrial dysfunction, ER stress, ROS releasing and inflammation, and a large number of myelin debris, lipoprotein particles and lipids from dead cells are phagocytosed or endocytosed by activated microglia. In addition, elevated lipid synthesis and decreased lipid oxidation contribute to the accumulation of free fatty acids .(Madison 2016; Prior et al. 2014) These multiple sources of lipids ultimately lead to the accumulation of LDs. Our findings imply that the formation of LD may be a possible consequence of post-ischemic inflammation.

We further investigated the role of lipid metabolism and LD accumulation of microglia in neuronal survival, as well as neuron-microglia interactions in neuronal regeneration. We found that microglia exhibited a double-edged effect in a co-culture model with neurons: resting untreated microglia and IL-4 pretreated microglia showed a protective effect on neurons after hypoxia. On the other hand, LDs-rich microglia (LDRM) pretreated with LPS and conditioned medium lost this protective effect and even exacerbated neuronal damage. Interestingly, inhibition of LDs biogenesis in microglia using the ACAT/ACSL inhibitor Trc reversed the damage to neurons in OGD/RO by LDRM and even protected neurons. One possibility is that in hypoxia-induced excitotoxic conditions, oxidative stress results in increased cell necrosis and apoptosis as well as autophagy. The disintegrated organelles and cellular debris further elevate ROS, impairing mitochondrial function and excess free fatty acid production in microglia (Liu et al. 2015; Madison 2016). The increase of ROS also activates sterol regulatory element binding proteins (SREBPs) that drive the de novo synthesis of fatty acids and cholesterol. This excess of fatty acids not only leads to lipotoxicity, but also induces a new type of programmed cell death-ferroptosis due to ROS peroxidation (Bai et al. 2019; Wang et al. 2020). Ferroptosis is not an isolated pathological process, but is intimately related to a multitude of other pathological processes, including lipid metabolism, autophagy, inflammation, and oxidative stress (Bai et al. 2019; Cui et al. 2021; Gao et al. 2016; Hou et al. 2016; Sun et al. 2020; Zhou et al. 2020). Current studies have identified that lipid metabolism plays an important role in regulating ferroptosis, which has unique morphological and bioactive features, mainly iron accumulation and lipid peroxidation (Latunde-Dada 2017; Yang et al. 2016), involved in the pathological process and neuronal cell death after stroke (Weiland et al. 2019; Xu et al. 2022), and ferroptosis inhibition has been shown to effectively reduce ischemic injury (Alim et al. 2019; Cui et al. 2021; Li et al. 2017). After ischemic stroke, neurons of infarct lesions undergo mitochondrial lipid peroxidation, which results in iron toxicity and cell death (Bai et al. 2019; Wang et al. 2020; Yang et al. 2016). Recent research indicates that inhibiting lipid peroxidation can treat ischemic stroke and that the usage of some small-molecule antioxidants (e.g., vitamin E, CoQ10) can protect against ischemic injury (Belousova et al. 2016; Nasoohi et al. 2019; Rodrigo et al. 2013). In addition, in our study, lipotoxicity in microglia was alleviated by regulating lipid metabolism genes or using ACAT/ACSL inhibitors (e.g., Trc, Beauveriolide) to inhibit the synthesis of free fatty acids and cholesterol, which also attenuated neuronal injury. Hence, microglia transfer fatty acids from neighboring neuronal cells for uptake and storage in glial droplets. By taking up lipids produced by neurons, glial cells may act as a protective role for neurons from lipid-mediated toxicity.

We further investigated the potential link between lipid metabolism and inflammation in microglia. As mentioned above, following hypoxic or inflammatory stimuli, we have observed large numbers of LDs attached around lysosomes in microglia. Similar observations have been reported in studies of age-related neurodegenerative diseases (Hu et al. 2017; Marschallinger et al. 2020; Zhao et al. 2021). We observed that such lipid droplet-rich "foam microglia" is in an activated state and show increased production of pro-inflammatory cytokines such as TNF-α, IL-1β and IL-6 and exacerbate post-ischemic neuronal damage. In addition, their phagocytic activity is impaired and high levels of ROS are produced, suggesting that LDRM may be a pro-inflammatory harmful microglia state. Hence, our results indicated that microglia have a unique metabolic pattern involved in various functions, including inflammatory regulation. Compared to normal homeostatic microglia, microglia will have distinct metabolic patterns and altered morphology and function under multiple pathological conditions such as immune stress, elevated extracellular lipid concentrations, inflammatory events, increased ROS levels, and energy deficiency, which all contribute to lipid droplet biogenesis. This particular lipid metabolism-inflammation connection has also been demonstrated in previous studies of other diseases, including atherosclerosis, cancer, ischemic heart disease, and respiratory and digestive diseases, that lipid droplet-rich macrophages or microglia have higher levels of inflammatory factors and upregulate multiple inflammation-related signaling pathways (Bosch et al. 2020; Cheng et al. 2018; Heller et al. 2016; Larigauderie et al. 2006; Li et al. 2022; Mardani et al. 2019; Son et al. 2016).

Furthermore, we also found that SREBPs, which are mainly responsible for the activation of genes involved in cholesterol synthesis, could regulate fatty acid metabolism and inflammation as well. In our study, upregulation of SREBPs mediated by activation of mTOR results in increased fatty acid synthesis and cholesterol esterification after ischemia, ultimately may lead to dramatic changes in the lipid profile of the brain, which we will confirm in the ongoing lipidomics analysis. Our in vivo results also indicate that lipid droplets accumulate in microglia within days of stroke onset, possibly due to increased expression of SREBPs in microglia, impaired lipid transport and cholesterol clearance (ApoE, ABCA1, TREM2), phagocytosis of dead cell debris and myelin, and expression of specific lipid droplet-associated proteins (e.g. Plin2, Plin3). In addition, cerebral ischemia leads to tissue necrosis and inflammation, a large number of dead cells and tissues, myelin debris, and short-term accumulation of fatty acids and cholesterol in phagocytes leading to "lipid overload", which further impairs lipid transport and cholesterol clearance, and likewise phagocytosis efficiency. In addition, we have shown that SREBP2 has a cross-talk with TLR4/NF-κB signaling pathways, which further regulating inflammation via upregulation of the NF-κB pathway. Various other signaling pathways, such

as PI3K/AKT/mTOR and SIRT1/AMPK, were also found to be regulated by SREBPs, involved in downstream inflammation, proliferation, and polarization of microglia and macrophages (Eid et al. 2017; He et al. 2017; Li et al. 2013; Li et al. 2013; Zhang et al. 2020).

Next, we confirmed the role of lipid metabolism and LD formation on the polarization phenotype of microglia after ischemia-induced neuroinflammation. The upregulated pathways in LDRM include "glycolysis", "long-chain fatty acid synthesis", "lipid transport", "oxidative stress and Reactive oxygen species (ROS)", "autophagy", and "inflammasome complex" (Arbaizar-Rovirosa et al. 2022; Cheon and Cho 2021; Jarc and Petan 2020; Marschallinger et al. 2020). Down-regulated pathways include "beta-oxidation of long-chain fatty acid", "phagocytosis", and "cholesterol clearance" (Cantuti-Castelvetri et al. 2018; Nugent et al. 2020; Raas et al. 2019). However, the mechanisms regulating dynamic changes in microglia phenotype and function remain largely unclear. We found that changes in lipid metabolism and lipid profile are regulated by shifts in energy metabolism patterns, and play a key role in the regulation of the microglia phenotype. Microglia transcriptome profiling under ischemic or inflammatory conditions showed that pathways related to lipid synthesis were upregulated in LDRM (PLIN2, Soat1, and SREBP2), while pathways involving peroxisomal β-oxidation and hydrolysis of fatty acids and cholesterol were downregulated (Nceh1, LIPA, NPC2). Lipid transporters were also impaired (ABCA1, TREM2, and ApoE). Interestingly, these elevated lipid synthesis and impaired degradation produced LDRM with higher expression of M1 phenotype and inflammation, thus suggesting altered polarization of LD-rich microglia. In turn, we found that microglia with less lipid droplet accumulation after inhibition of long-chain fatty acid synthesis and cholesterol esterification in microglia showed decreased lipid synthesis and a phenotypic shift toward an M2 anti-inflammatory phenotype. This result is consistent with previous studies that microglia stimulated by LPS and OGD-CM inflammation are polarized toward the pro-inflammatory M1 phenotype and IL-4 treatment toward the anti-inflammatory M2 phenotype (Hu et al. 2012; Zhang et al. 2021a). Similar results were shown by the studies of other neuroinflammation-related diseases that LDRM exhibit a distinct transcriptional profile than the homeostatic microglia, and that multiple microglial functions are affected (Gao et al. 2017; Nadjar et al. 2017; Rambold et al. 2015; Ransohoff 2016). Meanwhile, the results of our *in vivo* studies suggest that microglia phenotypes change dynamically over time in the post-ischemia brain, playing multiple roles and interfering with neuronal regeneration. As mentioned before, the microglial phenotype can be mainly divided into M0 microglia, which are in a resting state under physiological conditions; pro-inflammatory M1 phenotype microglia induced by activation of pro-inflammatory stimuli (e.g., LPS), characterized by high expression of nitric

oxide synthase (iNOS), tumor necrosis factor-α (TNF-α) and IL-1β; and IL-4 stimulation that transforms microglia into an anti-inflammatory M2 phenotype with high expression of arginase-1 (Arg-1), mannose receptor (CD206) and transforming growth factor β (TGF-β). Normally, pro-inflammatory microglia are associated with an inflammatory response with high levels of inflammatory factors, nitric oxide (NO) and ROS, while anti-inflammatory microglia attenuate the inflammatory response and promote tissue repair. Our finding confirms the involvement of lipid metabolism-related genes and lipid profiles in microglial polarization and inflammation. Other research of the pathogenesis of macrophage polarization on inflammatory diseases found that SREBP2 activation upregulates cholesterol biosynthesis and is involved in the binding and activation of multiple genes, including inflammatory and interferon response, independent of its function in sterol metabolism (Kusnadi et al. 2019). Moreover, the silence of the gene SREBP2 function shifts the balance of macrophages, from an inflammatory phenotype to an anti-inflammatory phenotype that promotes regeneration and healing (Hu et al. 2017; Khatchadourian et al. 2012; Loving and Bruce 2020; Marschallinger et al. 2020). Therefore, lipid metabolism may play an important role in microglial phenotype and function.

Hence, we suggest that lipid droplet biogenesis induced by hypoxia or LPS leads to acute inflammatory responses, with upregulation of SREBP2 which activates the NF-κB signaling pathway and further upregulates downstream inflammatory factors, including TNF-α, IL-1β, and IL-6. Upregulation of SREBP2 also promotes ACSL-mediated fatty acid synthesis, as well as HMG-CoA reductase (HMGCR)-mediated cholesterol synthesis and ACAT-mediated cholesterol esterification, producing large amounts of unsaturated fatty acids and cholesterol esters (Chen et al. 2018). This "lipid overload" further activates TLRs and exacerbates neuroinflammation. Furthermore, in addition to inflammation, metabolic changes leading to increased lipid synthesis are also involved in the formation of microglial lipid droplets. We found that ischemia caused a rapid "polarization" of microglia from anti-inflammatory microglia in the first few days to pro-inflammatory LD-rich microglia, as also confirmed by the accumulation of cholesterol in phagocytes observed in a model of experimental autoimmune encephalomyelitis (Chen et al. 2018). These results are consistent with that in our previous transcriptional profile analysis section. Other recent studies have also reported that ischemia-induced lipid droplet aggregation of microglia in aged mice impairs stroke recovery and that this impairment can be mitigated by the renewal of young microglia lacking LDs (Arbaizar-Rovirosa et al. 2022). This evidence demonstrates that fatty acid and cholesterol synthesis may mediate inflammatory upregulation after ischemic injury in stroke.

Interestingly, our study indicated that intervention in lipid metabolism and LD formation can enhance neuroregeneration, neurological recovery and modulate neuroinflammation. Inhibition of free fatty acid and cholesterol synthesis by modulating lipid metabolism genes in microglia or by using ACAT inhibitors (such as Trc, Beauveriolide, etc.) can attenuate inflammation mediated by NF-*κ*B signaling pathways. These results reveal a complex connection between lipid droplets and inflammatory signaling. Moreover, previous studies by our group have shown that in a model of demyelination, aged mice fail to resolve the inflammatory response initiated after myelin injury (Cantuti-Castelvetri et al. 2018). Aged phagocytes accumulate excess myelin debris and cholesterol accumulates in cells, leading to impairment of cellular cholesterol efflux capacity and upregulating chronic inflammation, inducing a poor immune response and impeding tissue regeneration. In another study on age-related and Alzheimer's disease models, quantitative shotgun lipidomic studies was performed on specific regions of the mouse brain, identifying cell types and brain region-specific lipid profiles in adult mice, which were analyzed in conjunction with protein expression profiles (Fitzner et al. 2020). It was shown that the expression and metabolism of fatty acids, such as fatty acid oxidation in astrocytes and sphingolipid metabolism in microglia, mediate brain function. Thus, one can suggest that component changes in lipids may directly regulate the characteristics and functions of various cells, including microglia, which may be relevant to inflammation-related CNS disorders, including neurodegenerative diseases and strokes. After stroke, energy deficiency leads to neuronal cell damage, microglia aggregation in infarct lesions, a consequent inflammatory response, and changes in genes involved in regulating lipid metabolism.

In our study, both in vitro experiments of inflammation-induced LDRM and in vivo experiments of MCAO-induced LDRM in the infarct core region exhibited distinct lipid profiles. The levels of free fatty acids and cholesterol esters were significantly elevated compared to the normal condition. Interestingly, however, the levels of free cholesterol were only slightly elevated. This evidence confirms our previous transcriptional and protein levels results that multiple lipid synthesis pathways are upregulated upon exposure to inflammatory and hypoxic environments mediated by ACSL, ACLY, ACAT and HMGCR, leading to "lipid overload" lipotoxicity and subsequent inflammatory and immune responses. Although how lipid metabolism regulates microglia phenotype and expression of pro-inflammatory genes after stroke is unclear, one possibility is that the energy pattern of hypoxic microglia is altered after cerebral infarction. Neutral lipids in microglia under pathological conditions accumulate through cytolytic action of impaired cells, increased fatty acid synthesis and glycolysis, and eventually lead to the formation of LDs (Bozza et al. 2010; Cheon and Cho 2021; Jarc and Petan 2020). Importantly, this altered lipid accumulation state deviates microglia from

homeostatic monitoring, making microglia more vulnerable and causing damage to neurons. Current studies have found that LDs are critical for various cellular stress response mechanisms, including inflammation and immune response over the years (Jarc and Petan 2020; Jung and Mook-Jung 2020). Fatty acid synthesis and metabolism mediates the formation of LDs in multiple types of cells (including macrophages, microglia, astrocytes, endothelial cells, etc.) and activates multiple signaling pathways in research of cancer and other inflammation-related diseases (Bozza et al. 2010; Chaves-Filho et al. 2019; Fanning et al. 2019; Farmer et al. 2020; Haidar et al. 2022; Ogawa et al. 2009). Normally, energy support of cells is generated through glucose metabolism, glycolysis, tricarboxylic acid cycle (TCA) and ATP from oxidative phosphorylation, and oxygen consumption and glucose utilization are in balance (Chen et al. 2018; Li et al. 2021; Liu et al. 2021; Meng et al. 2020). After cerebral ischemia, under the condition of hypoxia, the metabolic profile of activated microglia changes from ATP supply to glycolytic supply mode due to the tremendous energy demand of activated microglial functions such as phagocytosis, the release of inflammatory cytokines and immune response (Hu et al. 2020), accompanied by a large amount of NADPH oxidase-mediated generation of reactive oxygen species (ROS) (Liu et al. 2015; Park et al. 2015). ROS play an important role in regulating microglia phagocytosis and activate various signaling pathways and transcription factors, including PI3K/AKT and NF-κB, which in turn upregulate the expression of pro-inflammatory genes (Simpson and Oliver 2020; Yao et al. 2020). In our study, lipid signaling pathway-related such as SREBPs, TREM2, ApoE and ABCA1, mainly expressed by microglia and astrocytes, are upregulated after ischemia were involved not only in energy metabolism and lipid synthesis/transport, but more importantly in regulating inflammatory processes associated with lipid signaling pathways.

Current research has found that fatty acids can also be used as a therapeutic target. The brain is highly enriched in long-chain polyunsaturated fatty acids (LC-PUFAs), which are esterified to phospholipids and are the main components of cell membranes (Bazinet and Layé 2014). The possibility of a regulated microglial lipid profile in the brain and its subsequent impact on brain in physiological and pathological activities have also been identified (Blank et al. 2022; Bruce et al. 2018; Claes et al. 2021; Rey et al. 2018). Physiologically, cholesterol and fatty acids are essential components of cell membranes and maintain a dynamic balance of multiple cellular functions in the brain (Hąc-Wydro et al. 2007), such as neuronal plasticity and microglia phagocytosis (Bogie et al. 2020; Hasegawa et al. 2012). Saturated fatty acids have been reported to increase the pro-inflammatory phenotype of microglia, while unsaturated fatty acids affect the anti-inflammatory phenotype of microglia, that saturated fatty acids produce inflammation in both peripheral tissues and the brain (Carey et al. 2020; Chen et al. 2018; Howe et al. 2022;

Little et al. 2012; Tracy et al. 2013). Meanwhile, more and more evidence indicates that microglia treated with large amounts of saturated fatty acids exhibit a pro-inflammatory phenotype similar to that of the LPS-induced inflammation model (Leyrolle et al. 2019; Tracy et al. 2013). Saturated fatty acids upregulate several inflammatory factors such as interferon-γ (IFN-γ), IL-1β, and TNF-α through the activation of TLR-4 receptor-mediated mTOR and NF-κB pathways by LPS-like ligands (Li et al. 2022; Oh et al. 2009; Wang et al. 2012). Moreover, phosphorylation and translocation of p65 into the nucleus also confirmed the activation of the NF-κB pathway by unsaturated fatty acids (Wang Z et al. 2012). On the other hand, it has also been demonstrated that polyunsaturated fatty acid-treated microglia express more anti-inflammatory cytokines (TGF-β, IL 10) and M2 phenotypic markers (CD206, Arg-1, and Ym-1) and reduce neuroinflammation (Carey et al. 2020; Kurtys et al. 2016; Lu et al. 2010). Our result is consistent with previous studies on ischemic disease and atherosclerosis that inhibition of ACSL and ACAT attenuates the vascular inflammatory component associated with ischemia-reperfusion injury and reduces cellular damage (Blakeman et al. 2012; Matsuda et al. 2008; Prior et al. 2014). Furthermore, the reduced phagocytosis of LDRM found in our study suggests that deleterious lipid accumulation and LDs aggregation due to altered lipid metabolism may occur earlier than the pro-inflammatory phenotypic transformation of microglia and contribute to the upregulation of inflammation. The occurrence of lipid droplets regulates the phagocytosis of microglia, and there may be a feedback system whereby excessive lipid droplet accumulation in these cells impedes the phagocytosis of microglia.

Our results here validate the previous hypothesis that LDs are not only organelles for fatty acid storage but also involved in the management of microglial functions. In microglia, pro-inflammatory signaling enhances LDs content, quantity, and size, upregulating multiple lipid syntheses, such as triglycerides and promotes cholesterol biosynthesis, ultimately polarizing microglia to a pro-inflammatory phenotype. These results illustrate that lipid composition and distribution in LDs are critical for controlling microglia phenotype and function. In our study, we found that stress stimulates the formation and accumulation of LDs in microglia, and disturbances in microglial lipid metabolism in turn drive the biogenesis of LDs. LDs and lipid metabolism play an important role in multiple microglial functions and serve as markers of microglial cell reactivity and pathogenicity. A variety of biological functions of microglia, including phagocytosis, are regulated by intracellular lipid metabolism. For example, the phagocytic efficiency of microglia is disrupted by the incorporation of unbalanced lipids into the plasma membrane (Calder et al. 1990). Moreover, microglia phagocytosis is particularly important in synaptic regeneration and clearance of cellular debris and myelin, and is regulated by the involvement of several lipid metabolism-related genes such as TREM2, ApoE, and

ABCA1. In addition, the abnormal mitochondrial function accompanied by the lysosomal dysfunction impaired phagocytic efficiency and product abundant reactive oxygen species (ROS) in activated microglia in pathological conditions. ROS have been found to be involved in various signaling pathways regulated by lipid metabolism, including autophagy, ferroptosis, and inflammation, and are also associated with the phenotypic polarization of microglia (Wu et al. 2020; Yao et al. 2020; Ye et al. 2017).

In conclusion, our findings on the regulation of lipid metabolism on the microglia phenotype and its involvement in the subsequent response to neuroinflammation. Fatty acid synthesis and lipid droplet biogenesis direct microglia toward proinflammatory LDRM after stroke, while inhibition of lipid droplets improves microglial function, suppresses inflammation, and attenuates post-ischemic brain injury. Because microglia have complex functions, the underlying mechanisms are variable and complicated, and elucidation of these mechanisms still requires additional studies. Despite these limitations, our study demonstrates that regulation of lipid metabolism in microglia has attractive potential in the treatment of cerebral ischemic stroke, providing a new perspective on inflammation-related central nervous system diseases including stroke.

5 Summary

Ischemic stroke is one of the leading causes of death and disability in adults worldwide. In developed countries, approximately 15 million people experience an ischemic or hemorrhagic stroke each year. Resident microglia are the main immune cells of the brain and have an important role in the pathophysiology of ischemic stroke. For many decades, microglia activation was thought to be detrimental in ischemic stroke; however, accumulating evidence indicated that microglia exacerbate tissue damage by producing inflammatory cytokines and cytotoxic substances following ischemic injury, while also promoting tissue repair and remodeling by clearing debris and producing anti-inflammatory cytokines and growth factors. Microglia activation is also essential for neurogenesis, angiogenesis, and synaptic remodeling, facilitating functional recovery after cerebral ischemia. This dual role of microglia is related to their functional status in different cellular contexts and pathological stages after ischemia. In recent years, it has been found that oxidative metabolism and fatty acid synthesis/oxidation may regulate the phenotypic polarization of microglia, which in turn regulates inflammation may serve as a potential new target for the treatment of ischemic stroke. Here, to investigate whether lipid metabolism and biogenesis of LDs in microglia can affect neurological outcomes and neurogenesis after ischemia, we investigated the effect of microglia under different conditions on hypoxic neurons with an OGD model and the effect of microglia in different post-ischemic stages in a mouse MCAO stroke model, as well as the role of lipid metabolism and LDs biogenesis in microglia on the post-ischemic inflammation.

First, we compared the biogenesis of LDs in microglia under hypoxia or under LPS treatment which is considered typical proinflammatory M1 phenotype microglia. We used Western blot (WB), immunofluorescence staining (IF) and fluorescence-activated cell sorting analysis (FACS) to identify LDs in microglia. WB results indicated that the surface protein PLIN2 of LDs was highly expressed in microglia under LPS or hypoxia conditions. IF and FACS results revealed that most of these microglia had abundant LDs stained by BODIPY. These results suggest that both hypoxia and inflammation can induce the accumulation of LDs in microglia and that ACAT/ACSL inhibitors can block this effect (Figure 29. A).

In the second part of our study, we determined the effect of LDRM on neurons with hypoxic injury. After establishing a neuron-microglia co-culture model, we found that LDRM exacerbated neuronal injury in OGD/RO, whereas IL-4 conditioned and Trc (ACAT/ACSL inhibitor) suppressed LDs-poor microglia could play a neuronal protective role. We further used RT-qPCR and ELISA to find that LDRM exhibited higher levels of inflammatory factors and

upregulated levels of fatty acid and cholesterol synthesis. In addition, we also validated the shift in the phenotypic polarization pattern of microglia by IF.

The third part of this study was an *in vivo* experiment with a mouse MCAO model. We found that LDs accumulate in microglia over time after ischemia and convert from an initial (3 days post-ischemia) dominant anti-inflammatory M2 phenotype to a pro-inflammatory M1 phenotype (7 days post-ischemia). Furthermore, we found that SREBP2, a master regulator of sterol and fatty acid synthesis, not only altered the lipid profile of post-ischemic microglia, but also upregulated inflammation levels by activating the NF-κB signaling pathway (Figure 29. B). Thus, our study provides the first *in vivo* and *in vitro* evidence of the role of lipid metabolism in regulating microglia function, especially in microglial inflammation, providing a new perspective on ischemic stroke treatment.

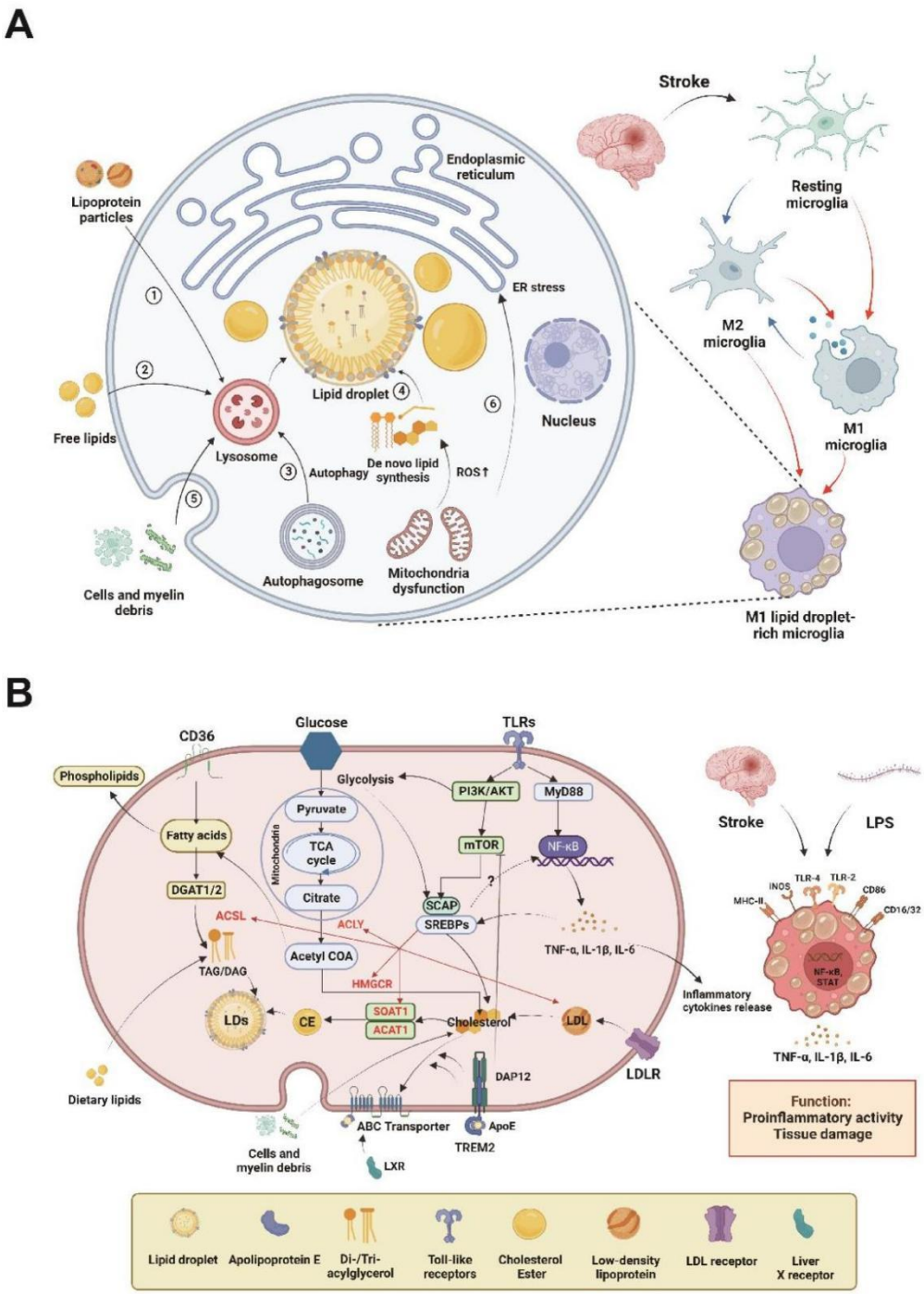

Figure 29. Graphical abstract of the present thesis. A, Lipid droplet biogenesis in microglia. **B**, Pathway map of genes related to lipid metabolism and inflammation that are differentially expressed in LDRM. LDRM tend to have a metabolic profile with a pro-inflammatory phenotype, including increased glycolysis and fatty acid synthesis. Abbreviations: LDRM, lipid droplet-rich microglia; ApoE, apolipoprotein E; TREM2, triggering receptor expressed on myeloid cells 2; TLRs, toll-like receptors; mTOR, mammalian target of rapamycin; PI3K, phosphatidylinositol 3-kinase; NF-*κ*B, nuclear factor-kappa B; CE, cholesterol ester; ABC: ATP-binding cassette; ACAT, Acyl-CoA: cholesterol acyltransferase; ACSL, long-chain acyl-CoA synthetase; ACLY, ATP citrate lyase; HMGCR, HMG-CoA reductase; SREBPs, Sterol regulatory element-binding proteins; SCAP, SREBP cleavage-activating protein; DGAT, Diglyceride acyltransferase.

6 References

Alim I, Caulfield JT, Chen Y, Swarup V, Geschwind DH, Ivanova E, Seravalli J, Ai Y, Sansing LH, Ste Marie EJ, et al. (2019): Selenium Drives a Transcriptional Adaptive Program to Block Ferroptosis and Treat Stroke. Cell 177, 1262-1279.e1225

Amantea D, Nappi G, Bernardi G, Bagetta G, Corasaniti MT (2009): Post-ischemic brain damage: pathophysiology and role of inflammatory mediators. FEBS J 276(1), 13-26

Anrather J, Iadecola C (2016): Inflammation and Stroke: An Overview. Inflammation and Stroke: An Overview. Neurotherapeutics 13(4):661-670.

Arbaizar-Rovirosa M, Pedragosa J, Lozano JJ, Casal C, Pol A, Gallizioli M, Planas AM (2022): Aged lipid-laden microglia display impaired responses to stroke. EMBO Mol Med 15(2):e17175.

Bai Y, Meng L, Han L, Jia Y, Zhao Y, Gao H, Kang R, Wang X, Tang D, Dai E (2019): Lipid storage and lipophagy regulates ferroptosis. Biochem Biophys Res Commun 508(4):997-1003.

Bano D, Nicotera P (2007): Ca2+ signals and neuronal death in brain ischemia. Stroke 38, 674-676

Bazinet RP, Layé S (2014): Polyunsaturated fatty acids and their metabolites in brain function and disease. Nat Rev Neurosci 15, 771-785

Beckman M (2006): Cell biology - Great balls of fat. Science 311, 1232-1234

Beller M, Thiel K, Thul PJ, Jäckle H (2010): Lipid droplets: a dynamic organelle moves into focus. FEBS Lett 584(11):2176-82.

Belousova M, Tokareva OG, Gorodetskaya E, Kalenikova EI, Medvedev OS (2016): Intravenous Treatment With Coenzyme Q10 Improves Neurological Outcome and Reduces Infarct Volume After Transient Focal Brain Ischemia in Rats. J Cardiovasc Pharmacol 67(2):103-9.

Bernier LP, York EM, MacVicar BA (2020): Immunometabolism in the Brain: How Metabolism Shapes Microglial Function. Trends Neurosci 43(11):854-869.

Bersuker K, Olzmann JA (2017): Establishing the lipid droplet proteome: Mechanisms of lipid droplet protein targeting and degradation. Biochim Biophys Acta Mol Cell Biol Lipids 862(10):1166-1177.

Bickel PE, Tansey JT, Welte MA (2009): PAT proteins, an ancient family of lipid droplet proteins that regulate cellular lipid stores. Biochim Biophys Acta 1791(6):419-40.

Blakeman N, Chen Q, Tolson J, Rueter B, Diaz B, Casey B, Young LH, Weis MT (2012): Triacsin C, a Fatty Acyl CoA Synthetase Inhibitor, Improves Cardiac Performance Following Global Ischemia. Am. J. Biomed. Sci 4(3):1136-18.

Blank M, Enzlein T, Hopf C (2022): LPS-induced lipid alterations in microglia revealed by MALDI mass spectrometry-based cell fingerprinting in neuroinflammation studies. Sci Rep 12, 2908

Bogie JFJ, Grajchen E, Wouters E, Corrales AG, Dierckx T, Vanherle S, Mailleux J, Gervois P, Wolfs E, Dehairs J, et al. (2020): Stearoyl-CoA desaturase-1 impairs the reparative properties of macrophages and microglia in the brain. J Exp Med. 12(1):2908.

Bosch M, Sánchez-Álvarez M, Fajardo A, Kapetanovic R, Steiner B, Dutra F, Moreira L, López JA, Campo R, Marí M, et al. (2020): Mammalian lipid droplets are innate immune hubs integrating cell metabolism and host defense. Science 370

Bozza PT, Viola JP (2010): Lipid droplets in inflammation and cancer. Prostaglandins, leukotrienes, and essential fatty acids 82, 243-250

Bozza PT, Melo RC, Bandeira-Melo C (2007): Leukocyte lipid bodies regulation and function: contribution to allergy and host defense. Pharmacol Ther 113(1), 30-49

Breil C, Abert Vian M, Zemb T, Kunz W, Chemat F (2017): "Bligh and Dyer" and Folch Methods for Solid-Liquid-Liquid Extraction of Lipids from Microorganisms. Comprehension of Solvatation Mechanisms and towards Substitution with Alternative Solvents. Int J Mol Sci 18(4):708.

Broughton BR, Reutens DC, Sobey CG (2009): Apoptotic mechanisms after cerebral ischemia. Stroke 40, e331-339

Brown GC, Neher JJ (2014): Microglial phagocytosis of live neurons. Nat Rev Neurosci 15(4):209-16.

Bruce KD, Gorkhali S, Given K, Coates AM, Boyle KE, Macklin WB, Eckel RH (2018): Lipoprotein Lipase Is a Feature of Alternatively-Activated Microglia and May Facilitate Lipid Uptake in the CNS During Demyelination. Front Mol Neurosci 11, 57

Brustovetsky T, Bolshakov A, Brustovetsky N (2010): Calpain activation and Na+/Ca2+ exchanger degradation occur downstream of calcium deregulation in hippocampal neurons exposed to excitotoxic glutamate. J Neurosci Res 88(6):1317-28.

Calder PC, Bond JA, Harvey DJ, Gordon S, Newsholme EA (1990): Uptake and incorporation of saturated and unsaturated fatty acids into macrophage lipids and their effect upon macrophage adhesion and phagocytosis. Biochem J 269(3):807-14.

Cantley JL, Yoshimura T, Camporez JP, Zhang D, Jornayvaz FR, Kumashiro N, Guebre-Egziabher F, Jurczak MJ, Kahn M, Guigni BA, et al. (2013): CGI-58 knockdown sequesters diacylglycerols in lipid droplets/ER-preventing diacylglycerol-mediated hepatic insulin resistance. Proc Natl Acad Sci U S A 110(5):1869-74.

Cantuti-Castelvetri L, Fitzner D, Bosch-Queralt M, Weil MT, Su M, Sen P, Ruhwedel T, Mitkovski M, Trendelenburg G, Lütjohann D, et al. (2018): Defective cholesterol clearance limits remyelination in the aged central nervous system. Science 359, 684-688

Caplan LR, Biller J (2000): Nonatherosclerotic vasculopathies. Caplan's Stroke. A Clinical Approach, 295-342

Carey AN, Fisher DR, Bielinski DF, Cahoon DS, Shukitt-Hale B (2020): Walnut-Associated Fatty Acids Inhibit LPS-Induced Activation of BV-2 Microglia. Inflammation 43, 241-250

Catanese L, Tarsia J, Fisher M (2017): Acute Ischemic Stroke Therapy Overview. Circulation research 120, 541-558

Chamorro A, Hallenbeck J (2006): The harms and benefits of inflammatory and immune responses in vascular disease. Stroke 37, 291-293

Chausse B, Kakimoto PA, Kann O (2021): Microglia and lipids: how metabolism controls brain innate immunity. Semin Cell Dev Biol 112:137-144.

Chaves-Filho AB, Pinto IFD, Dantas LS, Xavier AM, Inague A, Faria RL, Medeiros MHG, Glezer I, Yoshinaga MY, Miyamoto S (2019): Alterations in lipid metabolism of spinal cord linked to amyotrophic lateral sclerosis. Sci Rep 9(1):11642.

Chen X, Chen C, Fan S, Wu S, Yang F, Fang Z, Fu H, Li Y (2018): Omega-3 polyunsaturated fatty acid attenuates the inflammatory response by modulating microglia polarization through SIRT1-mediated deacetylation of the HMGB1/NF-κB pathway following experimental traumatic brain injury. J Neuroinflammation 15(1):116.

Chen Z, Yang D, Peng X, Lin J, Su Z, Li J, Zhang X, Weng Y (2018): Beneficial effect of atorvastatin-modified dendritic cells pulsed with myelin oligodendrocyte glycoprotein autoantigen on experimental autoimmune encephalomyelitis. Neuroreport 29, 317-327

Cheng C, Geng F, Cheng X, Guo D (2018): Lipid metabolism reprogramming and its potential targets in cancer. Cancer Commun (Lond) 38(1):27.

Cheon SY, Cho K (2021): Lipid metabolism, inflammation, and foam cell formation in health and metabolic disorders: targeting mTORC1. J Mol Med (Berl) 99(11):1497-1509.

Cherry JD, Olschowka JA, O'Banion MK (2014): Neuroinflammation and M2 microglia: the good, the bad, and the inflamed. J Neuroinflammation 11:98.

Chew LJ, Takanohashi A, Bell M (2006): Microglia and inflammation: impact on developmental brain injuries. Ment Retard Dev Disabil Res Rev 12(2):105-12.

Chhor V, Le Charpentier T, Lebon S, Oré MV, Celador IL, Josserand J, Degos V, Jacotot E, Hagberg H, Sävman K, et al. (2013): Characterization of phenotype markers and neuronotoxic potential of polarised primary microglia in vitro. Brain Behav Immun 32:70-85.

Choi SR, Lim JH, Kim MY, Kim EN, Kim Y, Choi BS, Kim YS, Kim HW, Lim KM, Kim MJ, et al. (2018): Adiponectin receptor agonist AdipoRon decreased ceramide, and lipotoxicity, and ameliorated diabetic nephropathy. Metabolism 85:348-360.

Ciccone A, Valvassori L, Nichelatti M, Sgoifo A, Ponzio M, Sterzi R, Boccardi E (2013): Endovascular treatment for acute ischemic stroke. N Engl J Med 368, 904-913

Claes C, Danhash EP, Hasselmann J, Chadarevian JP, Shabestari SK, England WE, Lim TE, Hidalgo JLS, Spitale RC, Davtyan H, et al. (2021): Plaque-associated human microglia accumulate lipid droplets in a chimeric model of Alzheimer's disease. Mol Neurodegener 16(1):50.

Coleman RA, Mashek DG (2011): Mammalian triacylglycerol metabolism: synthesis, lipolysis, and signaling. Chem Rev 111(10):6359-86.

Colton CA (2009): Heterogeneity of microglial activation in the innate immune response in the brain. J Neuroimmune Pharmacol 4(4):399-418.

Cui Y, Zhang Y, Zhao X, Shao L, Liu G, Sun C, Xu R, Zhang Z (2021): ACSL4 exacerbates ischemic stroke by promoting ferroptosis-induced brain injury and neuroinflammation. Brain Behav Immun 93:312-321.

Datta A, Sarmah D, Mounica L, Kaur H, Kesharwani R, Verma G, Veeresh P, Kotian V, Kalia K, Borah A, et al. (2020): Cell Death Pathways in Ischemic Stroke and Targeted Pharmacotherapy. Transl Stroke Res 11(6):1185-1202.

Dechandt CRP, Zuccolotto-Dos-Reis FH, Teodoro BG, Fernandes A, Eberlin MN, Kettelhut IC, Curti C, Alberici LC (2017): Triacsin C reduces lipid droplet formation and induces mitochondrial biogenesis in primary rat hepatocytes. J Bioenerg Biomembr 49(5):399-411.

Desale SE, Chinnathambi S (2020): Role of dietary fatty acids in microglial polarization in Alzheimer's disease. J Neuroinflammation 17(1):93.

Dirnagl U, Iadecola C, Moskowitz MA (1999): Pathobiology of ischaemic stroke: an integrated view. Trends Neurosci 22(9):391-7.

Doens D, Fernández PL (2014): Microglia receptors and their implications in the response to amyloid β for Alzheimer's disease pathogenesis. J Neuroinflammation 11:48.

Doeppner TR, Traut V, Heidenreich A, Kaltwasser B, Bosche B, Bähr M, Hermann DM (2017): Conditioned Medium Derived from Neural Progenitor Cells Induces Long-term Post-ischemic Neuroprotection, Sustained Neurological Recovery, Neurogenesis, and Angiogenesis. Mol Neurobiol 54(2):1531-1540.

Doeppner TR, Herz J, Görgens A, Schlechter J, Ludwig AK, Radtke S, de Miroschedji K, Horn PA, Giebel B, Hermann DM (2015): Extracellular Vesicles Improve Post-Stroke Neuroregeneration and Prevent Postischemic Immunosuppression. Stem Cells Transl Med 4(10):1131-43.

Doll DN, Hu H, Sun J, Lewis SE, Simpkins JW, Ren X (2015): Mitochondrial crisis in cerebrovascular endothelial cells opens the blood-brain barrier. Stroke 46, 1681-1689

Dong H, Cui B, Hao X (2019): MicroRNA-22 alleviates inflammation in ischemic stroke via p38 MAPK pathways. Mol Med Rep 20(1):735-744.

Edinger AL, Thompson CB (2004): Death by design: apoptosis, necrosis and autophagy. Curr Opin Cell Biol 16(6):663-9.

Ehehalt R, Füllekrug J, Pohl J, Ring A, Herrmann T, Stremmel W (2006): Translocation of long chain fatty acids across the plasma membrane--lipid rafts and fatty acid transport proteins. Mol Cell Biochem 284(1-2):135-40.

Eichmann TO, Lass A (2015): DAG tales: the multiple faces of diacylglycerol--stereochemistry, metabolism, and signaling. Cell Mol Life Sci 72(20):3931-52.

Eid W, Dauner K, Courtney KC, Gagnon A, Parks RJ, Sorisky A, Zha X (2017): mTORC1 activates SREBP-2 by suppressing cholesterol trafficking to lysosomes in mammalian cells. Proc Natl Acad Sci U S A 114(30):7999-8004.

Fanning S, Haque A, Imberdis T, Baru V, Barrasa MI, Nuber S, Termine D, Ramalingam N, Ho GPH, Noble T, et al. (2019): Lipidomic Analysis of α-Synuclein Neurotoxicity Identifies Stearoyl CoA Desaturase as a Target for Parkinson Treatment. Mol Cell 73(5):1001-1014.e8.

Farese RV, Jr., Walther TC (2009): Lipid droplets finally get a little R-E-S-P-E-C-T. Cell 139, 855-860

Farmer BC, Walsh AE, Kluemper JC, Johnson LA (2020): Lipid Droplets in Neurodegenerative Disorders. Front Neurosci 14:742.

Fath T, Ke YD, Gunning P, Götz J, Ittner LM (2009): Primary support cultures of hippocampal and substantia nigra neurons. Nat Protoc 4(1):78-85.

Fazolini NP, Cruz AL, Werneck MB, Viola JP, Maya-Monteiro CM, Bozza PT (2015): Leptin activation of mTOR pathway in intestinal epithelial cell triggers lipid droplet formation, cytokine production and increased cell proliferation. Cell Cycle 14(16):2667-76.

Feigin VL, Roth GA, Naghavi M, Parmar P, Krishnamurthi R, Chugh S, Mensah GA, Norrving B, Shiue I, Ng M, et al. (2016): Global burden of stroke and risk factors in 188 countries, during 1990-2013: a systematic analysis for the Global Burden of Disease Study 2013. Lancet Neurol 15(9):913-924.

Feigin VL, Stark BA, Johnson CO, Roth GA, Bisignano C, Abady GG, Abbasifard M, Abbasi-Kangevari M, Abd-Allah F, Abedi V, et al. (2021): Global, regional, and national burden of stroke and its risk factors, 1990-2019: a systematic analysis for the Global Burden of Disease Study 2019. Lancet Neurol 20(10):795-820.

Fernandes A, Miller-Fleming L, Pais TF (2014): Microglia and inflammation: conspiracy, controversy or control? Cell Mol Life Sci 71(20):3969-85.

Fink SL, Cookson BT (2005): Apoptosis, pyroptosis, and necrosis: mechanistic description of dead and dying eukaryotic cells. Infect Immun 73(4):1907-16.

Fitzner D, Bader JM, Penkert H, Bergner CG, Su M, Weil MT, Surma MA, Mann M, Klose C, Simons M (2020): Cell-Type- and Brain-Region-Resolved Mouse Brain Lipidome. Cell Rep 32(11):108132.

Forrester SJ, Kikuchi DS, Hernandes MS, Xu Q, Griendling KK (2018): Reactive Oxygen Species in Metabolic and Inflammatory Signaling. Circ Res 122(6):877-902.

Fricker M, Tolkovsky AM, Borutaite V, Coleman M, Brown GC (2018): NEURONAL CELL DEATH. Physiol Rev 98(2):813-880.

Furie KL, Kasner SE, Adams RJ, Albers GW, Bush RL, Fagan SC, Halperin JL, Johnston SC, Katzan I, Kernan WN, et al. (2011): Guidelines for the Prevention of Stroke in Patients With Stroke or Transient Ischemic Attack A Guideline for Healthcare Professionals From the American Heart Association/American Stroke Association. Stroke 42, 227-276

Gaber T, Strehl C, Buttgereit F (2017): Metabolic regulation of inflammation. Nat Rev Rheumatol 13(5):267-279.

Gao M, Monian P, Pan Q, Zhang W, Xiang J, Jiang X (2016): Ferroptosis is an autophagic cell death process. Cell Res 26(9):1021-32.

Gao Y, Vidal-Itriago A, Kalsbeek MJ, Layritz C, García-Cáceres C, Tom RZ, Eichmann TO, Vaz FM, Houtkooper RH, van der Wel N, et al. (2017): Lipoprotein Lipase Maintains Microglial Innate Immunity in Obesity. Cell Rep 20(13):3034-3042.

Gasparovic C, Rosenberg GA, Wallace JA, Estrada EY, Roberts K, Pastuszyn A, Ahmed W, Graham GD (2001): Magnetic resonance lipid signals in rat brain after experimental stroke correlate with neutral lipid accumulation. Neurosci Lett 301(2):87-90.

George PM, Steinberg GK (2015): Novel Stroke Therapeutics: Unraveling Stroke Pathophysiology and Its Impact on Clinical Treatments. Neuron 87, 297-309

Golstein P, Kroemer G (2007): Cell death by necrosis: towards a molecular definition. Trends Biochem Sci 32(1):37-43.

Guilbert JJ (2003): The world health report 2002 - reducing risks, promoting healthy life. Educ Health (Abingdon) 16(2):230.

Guo Y, Cordes KR, Farese RV, Jr., Walther TC (2009): Lipid droplets at a glance. J Cell Sci 122(Pt 6):749-52.

Hac-Wydro K, Wydro P (2007): The influence of fatty acids on model cholesterol/phospholipid membranes. Chem Phys Lipids 150(1):66-81.

Haidar M, Loix M, Vanherle S, Dierckx T, Vangansewinkel T, Gervois P, Wolfs E, Lambrichts I, Bogie JFJ, Hendriks JJA (2022): Targeting lipophagy in macrophages improves repair in multiple sclerosis. Autophagy 18, 2697-2710

Hanisch UK, Kettenmann H (2007): Microglia: active sensor and versatile effector cells in the normal and pathologic brain. Nat Neurosci 10(11):1387-94.

Hasegawa S, Kume H, Iinuma S, Yamasaki M, Takahashi N, Fukui T (2012): Acetoacetyl-CoA synthetase is essential for normal neuronal development. Biochem Biophys Res Commun 427(2):398-403.

He M, Zhang W, Dong Y, Wang L, Fang T, Tang W, Lv B, Chen G, Yang B, Huang P, et al. (2017): Pro-inflammation NF-κB signaling triggers a positive feedback via enhancing cholesterol accumulation in liver cancer cells. J Exp Clin Cancer Res 36(1):15.

He Z, Du L, Ke Y, Wen C, Zhang Y (2019): PP2ACα of Alveolar Macrophages Is a Novel Protective Factor for LPS-Induced Acute Respiratory Distress Syndrome. Inflammation 42, 1004-1014

Hellemans K, Kerckhofs K, Hannaert JC, Martens G, Van Veldhoven P, Pipeleers D (2007): Peroxisome proliferator-activated receptor alpha-retinoid X receptor agonists induce beta-cell protection against palmitate toxicity. The FEBS journal 274, 6094-6105

Heller S, Cable C, Penrose H, Makboul R, Biswas D, Cabe M, Crawford SE, Savkovic SD (2016): Intestinal inflammation requires FOXO3 and prostaglandin E2-dependent lipogenesis and elevated lipid droplets. Am J Physiol Gastrointest Liver Physiol 310(10):G844-54.

Herpich F, Rincon F (2020): Management of acute ischemic stroke. Crit. Care Med 48, 1654

Hickman SE, Kingery ND, Ohsumi TK, Borowsky ML, Wang LC, Means TK, El Khoury J (2013): The microglial sensome revealed by direct RNA sequencing. Nat Neurosci 16(12):1896-905.

Hisham NF, Bayraktutan U (2013): Epidemiology, pathophysiology, and treatment of hypertension in ischaemic stroke patients. J Stroke Cerebrovasc Dis 22(7):e4-14.

Hoehn BD, Palmer TD, Steinberg GK (2005): Neurogenesis in rats after focal cerebral ischemia is enhanced by indomethacin. Stroke 36, 2718-2724

Holland R, McIntosh AL, Finucane OM, Mela V, Rubio-Araiz A, Timmons G, McCarthy SA, Gun'ko YK, Lynch MA (2018): Inflammatory microglia are glycolytic and iron retentive and typify the microglia in APP/PS1 mice. Brain Behav Immun 68:183-196.

Hou W, Xie Y, Song X, Sun X, Lotze MT, Zeh HJ, 3rd, Kang R, Tang D (2016): Autophagy promotes ferroptosis by degradation of ferritin. Autophagy 12, 1425-1428

Howe AM, Burke S, O'Reilly ME, McGillicuddy FC, Costello DA (2022): Palmitic Acid and Oleic Acid Differently Modulate TLR2-Mediated Inflammatory Responses in Microglia and Macrophages. Mol Neurobiol 59(4):2348-2362.

Hu X, Xu B, Ge W (2017): The Role of Lipid Bodies in the Microglial Aging Process and Related Diseases. Neurochem Res 42(11):3140-3148.

Hu X, Li P, Guo Y, Wang H, Leak RK, Chen S, Gao Y, Chen J (2012): Microglia/macrophage polarization dynamics reveal novel mechanism of injury expansion after focal cerebral ischemia. Stroke 43, 3063-3070

Hu X, Liou AK, Leak RK, Xu M, An C, Suenaga J, Shi Y, Gao Y, Zheng P, Chen J (2014): Neurobiology of microglial action in CNS injuries: receptor-mediated signaling mechanisms and functional roles. Prog Neurobiol 119-120:60-84.

Hu Y, Mai W, Chen L, Cao K, Zhang B, Zhang Z, Liu Y, Lou H, Duan S, Gao Z (2020): mTOR-mediated metabolic reprogramming shapes distinct microglia functions in response to lipopolysaccharide and ATP. Glia 68, 1031-1045

Huang M, Wan Y, Mao L, He QW, Xia YP, Li M, Li YN, Jin HJ, Hu B (2017): Inhibiting the Migration of M1 Microglia at Hyperacute Period Could Improve Outcome of tMCAO Rats. CNS Neurosci Ther 23(3):222-232.

Huang YL, Morales-Rosado J, Ray J, Myers TG, Kho T, Lu M, Munford RS (2014): Toll-like receptor agonists promote prolonged triglyceride storage in macrophages. J Biol Chem 289(5):3001-12.

Iadecola C, Anrather J (2011): The immunology of stroke: from mechanisms to translation. Nat Med 17(7):796-808.

Ide K, Secher NH (2000): Cerebral blood flow and metabolism during exercise. Prog Neurobiol 61(4):397-414.

Incalza MA, D'Oria R, Natalicchio A, Perrini S, Laviola L, Giorgino F (2018): Oxidative stress and reactive oxygen species in endothelial dysfunction associated with cardiovascular and metabolic diseases. Vascul Pharmacol 100:1-19.

Infantino V, Convertini P, Cucci L, Panaro MA, Di Noia MA, Calvello R, Palmieri F, Iacobazzi V (2011): The mitochondrial citrate carrier: a new player in inflammation. Biochem J 438(3):433-6.

Ioannou MS, Jackson J, Sheu SH, Chang CL, Weigel AV, Liu H, Pasolli HA, Xu CS, Pang S, Matthies D, et al. (2019): Neuron-Astrocyte Metabolic Coupling Protects against Activity-Induced Fatty Acid Toxicity. Cell 177, 1522-1535.e1514

Jackman K, Kahles T, Lane D, Garcia-Bonilla L, Abe T, Capone C, Hochrainer K, Voss H, Zhou P, Ding A, et al. (2013): Progranulin deficiency promotes post-ischemic blood-brain barrier disruption. J Neurosci 33(50):19579-89.

Jarc E, Petan T (2020): A twist of FATe: Lipid droplets and inflammatory lipid mediators. Biochimie 169, 69-87

Jayaraj RL, Azimullah S, Beiram R, Jalal FY, Rosenberg GA (2019): Neuroinflammation: friend and foe for ischemic stroke. J Neuroinflammation 16(1):142.

Jia J, Yang L, Chen Y, Zheng L, Chen Y, Xu Y, Zhang M (2021): The Role of Microglial Phagocytosis in Ischemic Stroke. Front Immunol 12:790201.

Jiang CT, Wu WF, Deng YH, Ge JW (2020): Modulators of microglia activation and polarization in ischemic stroke (Review). Mol Med Rep 21(5):2006-2018.

Jin R, Yang G, Li G (2010): Inflammatory mechanisms in ischemic stroke: role of inflammatory cells. J Leukoc Biol 87(5):779-89.

Jin R, Liu L, Zhang S, Nanda A, Li G (2013): Role of inflammation and its mediators in acute ischemic stroke. J Cardiovasc Transl Res 6(5):834-51.

Jump DB (2004): Fatty acid regulation of gene transcription. Crit Rev Clin Lab Sci 41(1):41-78.

Jun-Long H, Yi L, Bao-Lian Z, Jia-Si L, Ning Z, Zhou-Heng Y, Xue-Jun S, Wen-Wu L (2018): Necroptosis Signaling Pathways in Stroke: From Mechanisms to Therapies. Curr Neuropharmacol 16(9):1327-1339.

Jung ES, Mook-Jung I (2020): New Microglia on the Block. Cell Metab 31(4):664-666.

Kanazawa M, Ninomiya I, Hatakeyama M, Takahashi T, Shimohata T (2017): Microglia and Monocytes/Macrophages Polarization Reveal Novel Therapeutic Mechanism against Stroke. Int J Mol Sci 18(10):2135.

Katan M, Luft A (2018): Global Burden of Stroke. Semin Neurol 38(2):208-211.

Kettenmann H, Hanisch U-K, Noda M, Verkhratsky A (2011): Physiology of microglia. Physiol. Rev 91, 461-553

Khatchadourian A, Bourque SD, Richard VR, Titorenko VI, Maysinger D (2012): Dynamics and regulation of lipid droplet formation in lipopolysaccharide (LPS)-stimulated microglia. Biochim Biophys Acta 1821(4):607-17.

Khoshnam SE, Winlow W, Farzaneh M, Farbood Y, Moghaddam HF (2017): Pathogenic mechanisms following ischemic stroke. Neurol Sci 38(7):1167-1186.

Kim HJ, Miyazaki M, Ntambi JM (2002): Dietary cholesterol opposes PUFA-mediated repression of the stearoyl-CoA desaturase-1 gene by SREBP-1 independent mechanism. J Lipid Res 43(10):1750-7.

Kim J, Thayabaranathan T, Donnan GA, Howard G, Howard VJ, Rothwell PM, Feigin V, Norrving B, Owolabi M, Pandian J (2020): Global stroke statistics 2019. Int J Stroke 15(8):819-838.

Kroemer G, Galluzzi L, Vandenabeele P, Abrams J, Alnemri ES, Baehrecke EH, Blagosklonny MV, El-Deiry WS, Golstein P, Green DR, et al. (2009): Classification of cell death: recommendations of the Nomenclature Committee on Cell Death 2009. Cell Death Differ 16(1):3-11.

Kuang Y, Zheng X, Zhang L, Ai X, Venkataramani V, Kilic E, Hermann DM, Majid A, Bähr M, Doeppner TR (2020): Adipose-derived mesenchymal stem cells reduce autophagy in stroke mice by extracellular vesicle transfer of miR-25. J Extracell Vesicles 10(1):e12024.

Kuerschner L, Moessinger C, Thiele C (2008): Imaging of lipid biosynthesis: how a neutral lipid enters lipid droplets. Traffic 9(3):338-52.

Kurtys E, Eisel ULM, Verkuyl JM, Broersen LM, Dierckx R, de Vries EFJ (2016): The combination of vitamins and omega-3 fatty acids has an enhanced anti-inflammatory effect on microglia. Neurochem Int 99:206-214.

Kusnadi A, Park SH, Yuan R, Pannellini T, Giannopoulou E, Oliver D, Lu T, Park-Min KH, Ivashkiv LB (2019): The Cytokine TNF Promotes Transcription Factor SREBP Activity and Binding to Inflammatory Genes to Activate Macrophages and Limit Tissue Repair. Immunity 51(2):241-257.e9.

Larigauderie G, Furman C, Jaye M, Lasselin C, Copin C, Fruchart JC, Castro G, Rouis M (2004): Adipophilin enhances lipid accumulation and prevents lipid efflux from THP-1 macrophages: potential role in atherogenesis. Arterioscler Thromb Vasc Biol 24(3):504-10.

Larigauderie G, Cuaz-Pérolin C, Younes AB, Furman C, Lasselin C, Copin C, Jaye M, Fruchart JC, Rouis M (2006): Adipophilin increases triglyceride storage in human macrophages by stimulation of biosynthesis and inhibition of beta-oxidation. FEBS J 273(15):3498-510.

Latunde-Dada GO (2017): Ferroptosis: Role of lipid peroxidation, iron and ferritinophagy. Biochim Biophys Acta Gen Subj 1861(8):1893-1900.

Lauro C, Chece G, Monaco L, Antonangeli F, Peruzzi G, Rinaldo S, Paone A, Cutruzzolà F, Limatola C (2019): Fractalkine Modulates Microglia Metabolism in Brain Ischemia. Front Cell Neurosci 13:414.

Lee SJ, Zhang J, Choi AM, Kim HP (2013): Mitochondrial dysfunction induces formation of lipid droplets as a generalized response to stress. Oxid Med Cell Longev 2013:327167.

Lemke G (2019): How macrophages deal with death. Nat Rev Immunol 19(9):539-549.

Levard D, Buendia I, Lanquetin A, Glavan M, Vivien D, Rubio M (2021): Filling the gaps on stroke research: Focus on inflammation and immunity. Brain Behav Immun 91:649-667.

Leyrolle Q, Layé S, Nadjar A (2019): Direct and indirect effects of lipids on microglia function. Neurosci Lett 708:134348.

Li B, Concepcion K, Meng X, Zhang L (2017): Brain-immune interactions in perinatal hypoxic-ischemic brain injury. Prog Neurobiol 159:50-68.

Li J, Cao F, Yin HL, Huang ZJ, Lin ZT, Mao N, Sun B, Wang G (2020): Ferroptosis: past, present and future. Cell Death Dis 11(2):88.

Li L, Liu Y, Liu X, Zheng N, Gu Y, Song Y, Wang X (2022): Regulatory roles of external cholesterol in human airway epithelial mitochondrial function through STARD3 signalling. Clin Transl Med 12(6):e902.

Li L, Gan H, Jin H, Fang Y, Yang Y, Zhang J, Hu X, Chu L (2021): Astragaloside IV promotes microglia/macrophages M2 polarization and enhances neurogenesis and angiogenesis through PPARγ pathway after cerebral ischemia/reperfusion injury in rats. Int Immunopharmacol 92:107335.

Li LC, Varghese Z, Moorhead JF, Lee CT, Chen JB, Ruan XZ (2013): Cross-talk between TLR4-MyD88-NF-κB and SCAP-SREBP2 pathways mediates macrophage foam cell formation. Am J Physiol Heart Circ Physiol 304(6):H874-84.

Li M, Lu H, Wang X, Duan C, Zhu X, Zhang Y, Ge X, Ji F, Wang X, Su J, et al. (2021): Pyruvate kinase M2 (PKM2) interacts with activating transcription factor 2 (ATF2) to bridge glycolysis and pyroptosis in microglia. Mol Immunol 140:250-266.

Li Q, Han X, Lan X, Gao Y, Wan J, Durham F, Cheng T, Yang J, Wang Z, Jiang C, et al. (2017): Inhibition of neuronal ferroptosis protects hemorrhagic brain. JCI insight 2, e90777

Li Y, Xu S, Jiang B, Cohen RA, Zang M (2013): Activation of sterol regulatory element binding protein and NLRP3 inflammasome in atherosclerotic lesion development in diabetic pigs. PLoS One 8(6):e67532.

Li Y, Cheng Y, Zhou Y, Du H, Zhang C, Zhao Z, Chen Y, Zhou Z, Mei J, Wu W, et al. (2022): High fat diet-induced obesity leads to depressive and anxiety-like behaviors in mice via AMPK/mTOR-mediated autophagy. Exp Neurol 348:113949.

Li Y, Lu B, Sheng L, Zhu Z, Sun H, Zhou Y, Yang Y, Xue D, Chen W, Tian X, et al. (2018): Hexokinase 2-dependent hyperglycolysis driving microglial activation contributes to ischemic brain injury. J Neurochem 144(2):186-200.

Lian H, Roy E, Zheng H (2016): Protocol for Primary Microglial Culture Preparation. Bio Protoc 6(21):e1989.

Liao B, Geng L, Zhang F, Shu L, Wei L, Yeung PKK, Lam KSL, Chung SK, Chang J, Vanhoutte PM, et al. (2020): Adipocyte fatty acid-binding protein exacerbates cerebral ischaemia injury by disrupting the blood-brain barrier. Eur Heart J 41(33):3169-3180.

Liao M, Hu F, Qiu Z, Li J, Huang C, Xu Y, Cheng X (2021): Pim-2 kinase inhibits inflammation by suppressing the mTORC1 pathway in atherosclerosis. Aging 13, 22412-22431

Lin CH, Liao LY, Yang TY, Chang YJ, Tung CW, Hsu SL, Hsueh CM (2019): Microglia-Derived Adiposomes are Potential Targets for the Treatment of Ischemic Stroke. Cell Mol Neurobiol 39(5):591-604.

Lipton P (1999): Ischemic cell death in brain neurons. Physiol Rev 79, 1431-1568

Little JP, Madeira JM, Klegeris A (2012): The saturated fatty acid palmitate induces human monocytic cell toxicity toward neuronal cells: exploring a possible link between obesity-related metabolic impairments and neuroinflammation. J Alzheimers Dis 30 Suppl 2:S179-83.

Liu C, Zhang K, Shen H, Yao X, Sun Q, Chen G (2018): Necroptosis: A novel manner of cell death, associated with stroke (Review). Int J Mol Med 41(2):624-630.

Liu J, Feng R, Wang D, Huo T, Jiang H (2021): Triclosan-induced glycolysis drives inflammatory activation in microglia via the Akt/mTOR/HIF 1α signaling pathway. Ecotoxicol Environ Saf 224:112664.

Liu L, Zhang K, Sandoval H, Yamamoto S, Jaiswal M, Sanz E, Li Z, Hui J, Graham BH, Quintana A, et al. (2015): Glial lipid droplets and ROS induced by mitochondrial defects promote neurodegeneration. Cell 160, 177-190

Loving BA, Bruce KD (2020): Lipid and Lipoprotein Metabolism in Microglia. Front Physiol 11:393.

Lu DY, Tsao YY, Leung YM, Su KP (2010): Docosahexaenoic acid suppresses neuroinflammatory responses and induces heme oxygenase-1 expression in BV-2 microglia: implications of antidepressant effects for ω-3 fatty acids. Neuropsychopharmacology 35(11):2238-48.

Lu H, Lei X, Zhang Q (2015): Moderate activation of IKK2-NF-kB in unstressed adult mouse liver induces cytoprotective genes and lipogenesis without apparent signs of inflammation or fibrosis. BMC Gastroenterol 15:94

Luis G, Godfroid A, Nishiumi S, Cimino J, Blacher S, Maquoi E, Wery C, Collignon A, Longuespée R, Montero-Ruiz L, et al. (2021): Tumor resistance to ferroptosis driven by Stearoyl-CoA Desaturase-1 (SCD1) in cancer cells and Fatty Acid Biding Protein-4 (FABP4) in tumor microenvironment promote tumor recurrence. Redox Biol 43:102006.

Ma Y, Wang J, Wang Y, Yang GY (2017): The biphasic function of microglia in ischemic stroke. Prog Neurobiol 157:247-272.

Madison BB (2016): Srebp2: A master regulator of sterol and fatty acid synthesis. J Lipid Res 57(3):333-5.

Maida CD, Norrito RL, Daidone M, Tuttolomondo A, Pinto A (2020): Neuroinflammatory Mechanisms in Ischemic Stroke: Focus on Cardioembolic Stroke, Background, and Therapeutic Approaches. Int J Mol Sci 21(18):6454.

Mardani I, Tomas Dalen K, Drevinge C, Miljanovic A, Ståhlman M, Klevstig M, Scharin Täng M, Fogelstrand P, Levin M, Ekstrand M, et al. (2019): Plin2-deficiency reduces lipophagy and results in increased lipid accumulation in the heart. Sci Rep 9(1):6909.

Marschallinger J, Iram T, Zardeneta M, Lee SE, Lehallier B, Haney MS, Pluvinage JV, Mathur V, Hahn O, Morgens DW, et al. (2020): Lipid-droplet-accumulating microglia represent a dysfunctional and proinflammatory state in the aging brain. Nat Neurosci 23(2):194-208.

Martin S, Parton RG (2006): Lipid droplets: a unified view of a dynamic organelle. Nat Rev Mol Cell Biol 7(5):373-8.

Matsuda D, Namatame I, Ohshiro T, Ishibashi S, Omura S, Tomoda H (2008): Anti-atherosclerotic activity of triacsin C, an acyl-CoA synthetase inhibitor. J Antibiot (Tokyo) 61(5):318-21.

Maya-Monteiro CM, Bozza PT (2008): Leptin and mTOR: partners in metabolism and inflammation. Cell Cycle 7(12):1713-7.

Maya-Monteiro CM, Almeida PE, D'Avila H, Martins AS, Rezende AP, Castro-Faria-Neto H, Bozza PT (2008): Leptin induces macrophage lipid body formation by a phosphatidylinositol 3-kinase- and mammalian target of rapamycin-dependent mechanism. J Biol Chem 283(4):2203-10.

McColl BW, Allan SM, Rothwell NJ (2009): Systemic infection, inflammation and acute ischemic stroke. Neuroscience 158(3):1049-61.

Mecha M, Feliú A, Carrillo-Salinas FJ, Rueda-Zubiaurre A, Ortega-Gutiérrez S, de Sola RG, Guaza C (2015): Endocannabinoids drive the acquisition of an alternative phenotype in microglia. Brain Behav Immun 49:233-45.

Mehla K, Singh PK (2019): Metabolic Regulation of Macrophage Polarization in Cancer. Trends Cancer 5(12):822-834.

Melo RC, D'Avila H, Wan HC, Bozza PT, Dvorak AM, Weller PF (2011): Lipid bodies in inflammatory cells: structure, function, and current imaging techniques. J Histochem Cytochem 59(5):540-56.

Meng F, Yu W, Duan W, Wang T, Liu Y (2020): Dexmedetomidine attenuates LPS-mediated BV2 microglia cells inflammation via inhibition of glycolysis. Fundam Clin Pharmacol 34(3):313-320.

Michiels C (2004): Physiological and pathological responses to hypoxia. Am J Pathol 164(6):1875-82.

Mrak RE, Griffin WS (2005): Glia and their cytokines in progression of neurodegeneration. Neurobiol Aging 26(3):349-54.

Murphy DJ, Vance J (1999): Mechanisms of lipid-body formation. Trends Biochem Sci 24, 109-115

Nadjar A, Leyrolle Q, Joffre C, Laye S (2017): Bioactive lipids as new class of microglial modulators: When nutrition meets neuroimunology. Prog Neuropsychopharmacol Biol Psychiatry 79(Pt A):19-26.

Nagy L, Tontonoz P, Alvarez JG, Chen H, Evans RM (1998): Oxidized LDL regulates macrophage gene expression through ligand activation of PPARgamma. Cell 93, 229-240

Namatame I, Tomoda H, Arai H, Inoue K, Omura S (1999): Complete inhibition of mouse macrophage-derived foam cell formation by triacsin C. J Biochem 125(2):319-27.

Nasoohi S, Simani L, Khodagholi F, Nikseresht S, Faizi M, Naderi N (2019): Coenzyme Q10 supplementation improves acute outcomes of stroke in rats pretreated with atorvastatin. Nutr Neurosci 22(4):264-272.

Nazarinia D, Dolatshahi M, Faezi M, Nasseri Maleki S, Aboutaleb N (2021): TLR4 /NF-κB and JAK2/STAT3 signaling pathways: Cellular signaling pathways targeted by cell-conditioned medium therapy in protection against ischemic stroke. J Chem Neuroanat 113:101938.

Newcomer JW, Farber NB, Olney JW (2000): NMDA receptor function, memory, and brain aging. Dialogues Clin Neurosci 2(3):219-32.

Nielsen MM, Lambertsen KL, Clausen BH, Meyer M, Bhandari DR, Larsen ST, Poulsen SS, Spengler B, Janfelt C, Hansen HS (2016): Mass spectrometry imaging of biomarker lipids for phagocytosis and signalling during focal cerebral ischaemia. Sci Rep 6:39571.

Nugent AA, Lin K, van Lengerich B, Lianoglou S, Przybyla L, Davis SS, Llapashtica C, Wang J, Kim DJ, Xia D, et al. (2020): TREM2 Regulates Microglial Cholesterol Metabolism upon Chronic Phagocytic Challenge. Neuron 105, 837-854.e839

Ogawa K, Hishiki T, Shimizu Y, Funami K, Sugiyama K, Miyanari Y, Shimotohno K (2009): Hepatitis C virus utilizes lipid droplet for production of infectious virus. Proc Jpn Acad Ser B Phys Biol Sci 85(7):217-28.

Oh YT, Lee JY, Lee J, Kim H, Yoon KS, Choe W, Kang I (2009): Oleic acid reduces lipopolysaccharide-induced expression of iNOS and COX-2 in BV2 murine microglial cells: possible involvement of reactive oxygen species, p38 MAPK, and IKK/NF-kappaB signaling pathways. Neurosci Lett 464(2):93-7.

Ohsaki Y, Cheng J, Suzuki M, Shinohara Y, Fujita A, Fujimoto T (2009): Biogenesis of cytoplasmic lipid droplets: from the lipid ester globule in the membrane to the visible structure. Biochim Biophys Acta 1791(6):399-407.

Oishi Y, Spann NJ, Link VM, Muse ED, Strid T, Edillor C, Kolar MJ, Matsuzaka T, Hayakawa S, Tao J, et al. (2017): SREBP1 Contributes to Resolution of Pro-inflammatory TLR4 Signaling by Reprogramming Fatty Acid Metabolism. Cell Metab 25(2):412-427.

Olofsson SO, Boström P, Andersson L, Rutberg M, Perman J, Borén J (2009): Lipid droplets as dynamic organelles connecting storage and efflux of lipids. Biochim Biophys Acta 1791(6):448-58.

Owolabi MO, Thrift AG, Martins S, Johnson W, Pandian J, Abd-Allah F, Varghese C, Mahal A, Yaria J, Phan HT, et al. (2021): The state of stroke services across the globe: Report of World Stroke Organization-World Health Organization surveys. Int J Stroke 16(8):889-901.

Paolicelli RC, Sierra A, Stevens B, Tremblay ME, Aguzzi A, Ajami B, Amit I, Audinat E, Bechmann I, Bennett M, et al. (2022): Microglia states and nomenclature: A field at its crossroads. Neuron 110, 3458-3483

Papackova Z, Cahova M (2015): Fatty acid signaling: the new function of intracellular lipases. Int J Mol Sci 16(2):3831-55.

Park J, Min JS, Kim B, Chae UB, Yun JW, Choi MS, Kong IK, Chang KT, Lee DS (2015): Mitochondrial ROS govern the LPS-induced pro-inflammatory response in microglia cells by regulating MAPK and NF-κB pathways. Neurosci Lett 584:191-6.

Peruzzotti-Jametti L, Pluchino S (2018): Targeting Mitochondrial Metabolism in Neuroinflammation: Towards a Therapy for Progressive Multiple Sclerosis. Trends Mol Med 24(10):838-855.

Petan T, Jarc E, Jusović M (2018): Lipid Droplets in Cancer: Guardians of Fat in a Stressful World. Molecules 23(8):1941.

Ponomarev ED, Veremeyko T, Weiner HL (2013): MicroRNAs are universal regulators of differentiation, activation, and polarization of microglia and macrophages in normal and diseased CNS. Glia 61, 91-103

Prior AM, Zhang M, Blakeman N, Datta P, Pham H, Chen Q, Young LH, Weis MT, Hua DH (2014): Inhibition of long chain fatty acyl-CoA synthetase (ACSL) and ischemia reperfusion injury. Bioorg Med Chem Lett 24(4):1057-61.

Puig B, Brenna S, Magnus T (2018): Molecular Communication of a Dying Neuron in Stroke. Int J Mol Sci 19(9):2834.

Qin C, Zhou LQ, Ma XT, Hu ZW, Yang S, Chen M, Bosco DB, Wu LJ, Tian DS (2019): Dual Functions of Microglia in Ischemic Stroke. Neurosci Bull 35(5):921-933.

Raas Q, Saih FE, Gondcaille C, Trompier D, Hamon Y, Leoni V, Caccia C, Nasser B, Jadot M, Ménétrier F, et al. (2019): A microglial cell model for acyl-CoA oxidase 1 deficiency. Biochim Biophys Acta Mol Cell Biol Lipids 1864(4):567-576.

Radak D, Katsiki N, Resanovic I, Jovanovic A, Sudar-Milovanovic E, Zafirovic S, Mousad SA, Isenovic ER (2017): Apoptosis and Acute Brain Ischemia in Ischemic Stroke. Curr Vasc Pharmacol 15(2):115-122.

Ralhan I, Chang CL, Lippincott-Schwartz J, Ioannou MS (2021): Lipid droplets in the nervous system. J Cell Biol 220(7):e202102136.

Rambold AS, Cohen S, Lippincott-Schwartz J (2015): Fatty acid trafficking in starved cells: regulation by lipid droplet lipolysis, autophagy, and mitochondrial fusion dynamics. Dev Cell 32(6):678-92.

Ransohoff RM (2016): A polarizing question: do M1 and M2 microglia exist? Nat Neurosci 19(8):987-91.

Ransohoff RM, Perry VH (2009): Microglial physiology: unique stimuli, specialized responses. Annu Rev Immunol 27:119-45.

Rey C, Nadjar A, Joffre F, Amadieu C, Aubert A, Vaysse C, Pallet V, Layé S, Joffre C (2018): Maternal n-3 polyunsaturated fatty acid dietary supply modulates microglia lipid content in the offspring. Prostaglandins Leukot Essent Fatty Acids 133:1-7.

Riss TL, Moravec RA, Niles AL, Duellman S, Benink HA, Worzella TJ, Minor L (2016): Cell viability assays. Assay Guidance Manual

Robenek H, Buers I, Hofnagel O, Robenek MJ, Troyer D, Severs NJ (2009): Compartmentalization of proteins in lipid droplet biogenesis. Biochim Biophys Acta 1791(6):408-18.

Rodrigo R, Fernández-Gajardo R, Gutiérrez R, Matamala JM, Carrasco R, Miranda-Merchak A, Feuerhake W (2013): Oxidative stress and pathophysiology of ischemic stroke: novel therapeutic opportunities. CNS Neurol Disord Drug Targets 12(5):698-714.

Sarmah D, Kaur H, Saraf J, Vats K, Pravalika K, Wanve M, Kalia K, Borah A, Kumar A, Wang X, et al. (2018): Mitochondrial Dysfunction in Stroke: Implications of Stem Cell Therapy. Transl Stroke Res 10:121-36.

Satriotomo I, Bowen KK, Vemuganti R (2006): JAK2 and STAT3 activation contributes to neuronal damage following transient focal cerebral ischemia. J Neurochem 98(5):1353-68.

Sekerdag E, Solaroglu I, Gursoy-Ozdemir Y (2018): Cell Death Mechanisms in Stroke and Novel Molecular and Cellular Treatment Options. Curr Neuropharmacol 16(9):1396-1415.

Shang K, He J, Zou J, Qin C, Lin L, Zhou LQ, Yang LL, Wu LJ, Wang W, Zhan KB, et al. (2020): Fingolimod promotes angiogenesis and attenuates ischemic brain damage via modulating microglial polarization. Brain Res 1726:146509.

Shi K, Tian DC, Li ZG, Ducruet AF, Lawton MT, Shi FD (2019): Global brain inflammation in stroke. Lancet Neurol 18(11):1058-1066.

Shmarakov IO, Jiang H, Liu J, Fernandez EJ, Blaner WS (2019): Hepatic stellate cell activation: A source for bioactive lipids. Biochim Biophys Acta Mol Cell Biol Lipids 1864(5):629-642.

Siesjö BK, Bengtsson F (1989): Calcium fluxes, calcium antagonists, and calcium-related pathology in brain ischemia, hypoglycemia, and spreading depression: a unifying hypothesis. J Cereb Blood Flow Metab 9(2):127-40.

Simpson DSA, Oliver PL (2020): ROS Generation in Microglia: Understanding Oxidative Stress and Inflammation in Neurodegenerative Disease. Antioxidants (Basel) 9(8):743.

Skaper SD, Facci L (2018): Central Nervous System Neuron-Glia co-Culture Models and Application to Neuroprotective Agents. Methods Mol Biol 1727:63-80.

Son SH, Goo YH, Choi M, Saha PK, Oka K, Chan LC, Paul A (2016): Enhanced atheroprotection and lesion remodelling by targeting the foam cell and increasing plasma cholesterol acceptors. Cardiovasc Res 109(2):294-304.

Starke RM, Turk A, Ding D, Crowley RW, Liu KC, Chalouhi N, Hasan DM, Dumont AS, Jabbour P, Durst CR, et al. (2016): Technology developments in endovascular treatment of intracranial aneurysms. J Neurointerv Surg 8(2):135-44.

Stith JL, Velazquez FN, Obeid LM (2019): Advances in determining signaling mechanisms of ceramide and role in disease. J Lipid Res 60(5):913-918.

Struijs JN, van Genugten ML, Evers SM, Ament AJ, Baan CA, van den Bos GA (2006): Future costs of stroke in the Netherlands: the impact of stroke services. Int J Technol Assess Health Care 22(4):518-24.

Sun B, Jia Y, Hong J, Sun Q, Gao S, Hu Y, Zhao N, Zhao R (2018): Sodium Butyrate Ameliorates High-Fat-Diet-Induced Non-alcoholic Fatty Liver Disease through Peroxisome Proliferator-Activated Receptor α-Mediated Activation of β Oxidation and Suppression of Inflammation. J Agric Food Chem 66(29):7633-7642.

Sun Y, Chen P, Zhai B, Zhang M, Xiang Y, Fang J, Xu S, Gao Y, Chen X, Sui X, et al. (2020): The emerging role of ferroptosis in inflammation. Biomed Pharmacother 127:110108.

Sunami Y, Rebelo A, Kleeff J (2017): Lipid Metabolism and Lipid Droplets in Pancreatic Cancer and Stellate Cells. Cancers 10(1):3.

Suzuki K, Takahashi K, Nishimaki-Mogami T, Kagechika H, Yamamoto M, Itabe H (2009): Docosahexaenoic acid induces adipose differentiation-related protein through activation of retinoid x receptor in human choriocarcinoma BeWo cells. Biol Pharm Bull 32(7):1177-82.

Szigeti A, Minik O, Hocsak E, Pozsgai E, Boronkai A, Farkas R, Balint A, Bodis J, Sumegi B, Bellyei S (2009): Preliminary study of TIP47 as a possible new biomarker of cervical dysplasia and invasive carcinoma. Anticancer Res 29(2):717-24.

Tai CC, Ding ST (2010): N-3 polyunsaturated fatty acids regulate lipid metabolism through several inflammation mediators: mechanisms and implications for obesity prevention. J Nutr Biochem 21(5):357-63.

Thiele C, Spandl J (2008): Cell biology of lipid droplets. Curr Opin Cell Biol 20(4):378-85.

Tracy LM, Bergqvist F, Ivanova EV, Jacobsen KT, Iverfeldt K (2013): Exposure to the saturated free fatty acid palmitate alters BV-2 microglia inflammatory response. J Mol Neurosci 51(3):805-12.

Vandenabeele P, Galluzzi L, Vanden Berghe T, Kroemer G (2010): Molecular mechanisms of necroptosis: an ordered cellular explosion. Nat Rev Mol Cell Biol 11(10):700-14.

Volobоueva LA, Emery JF, Sun X, Giffard RG (2013): Inflammatory response of microglial BV-2 cells includes a glycolytic shift and is modulated by mitochondrial glucose-regulated protein 75/mortalin. FEBS Lett 587(6):756-62.

Walther TC, Farese RV, Jr. (2009): The life of lipid droplets. Biochim Biophys Acta 1791(6):459-66.

Wang H, Liu C, Zhao Y, Gao G (2020): Mitochondria regulation in ferroptosis. Eur J Cell Biol 99(1):151058.

Wang Y, Qiu Y, Sun A, Xiong Y, Tan H, Shi Y, Yu P, Roy G, Zhang L, Yan J (2020): Dual-functional AIE fluorescent probes for imaging β-amyloid plaques and lipid droplets. Anal Chim Acta 1133:109-118.

Wang Z, Liu D, Wang F, Liu S, Zhao S, Ling EA, Hao A (2012): Saturated fatty acids activate microglia via Toll-like receptor 4/NF-κB signalling. Br J Nutr 107(2):229-41.

Weiland A, Wang Y, Wu W, Lan X, Han X, Li Q, Wang J (2019): Ferroptosis and Its Role in Diverse Brain Diseases. Mol Neurobiol 56(7):4880-4893.

Wendt A, Thompson VF, Goll DE (2004): Interaction of calpastatin with calpain: a review. Biol Chem 385(6):465-72.

Wu L, Xiong X, Wu X, Ye Y, Jian Z, Zhi Z, Gu L (2020): Targeting Oxidative Stress and Inflammation to Prevent Ischemia-Reperfusion Injury. Front Mol Neurosci 13:28.

Wu T, Liang X, Liu X, Li Y, Wang Y, Kong L, Tang M (2020): Induction of ferroptosis in response to graphene quantum dots through mitochondrial oxidative stress in microglia. Part Fibre Toxicol 17(1):30.

Xing C, Arai K, Lo EH, Hommel M (2012): Pathophysiologic cascades in ischemic stroke. Int J Stroke 7(5):378-85.

Xiong XY, Liu L, Yang QW (2016): Functions and mechanisms of microglia/macrophages in neuroinflammation and neurogenesis after stroke. Prog Neurobiol 142:23-44.

Xu SY, Pan SY (2013): The failure of animal models of neuroprotection in acute ischemic stroke to translate to clinical efficacy. Med Sci Monit Basic Res 19:37-45.

Xu Y, Li K, Zhao Y, Zhou L, Liu Y, Zhao J (2023): Role of Ferroptosis in Stroke. Cell Mol Neurobiol 43(1):205-222.

Yang L, Tucker D, Dong Y, Wu C, Lu Y, Li Y, Zhang J, Liu TC, Zhang Q (2018): Photobiomodulation therapy promotes neurogenesis by improving post-stroke local microenvironment and stimulating neuroprogenitor cells. Exp Neurol 299(Pt A):86-96.

Yang S, Qin C, Hu ZW, Zhou LQ, Yu HH, Chen M, Bosco DB, Wang W, Wu LJ, Tian DS (2021): Microglia reprogram metabolic profiles for phenotype and function changes in central nervous system. Neurobiol Dis 152:105290.

Yang WS, Kim KJ, Gaschler MM, Patel M, Shchepinov MS, Stockwell BR (2016): Peroxidation of polyunsaturated fatty acids by lipoxygenases drives ferroptosis. Proc Natl Acad Sci U S A 113(34):E4966-75.

Yao Z, Liu N, Zhu X, Wang L, Zhao Y, Liu Q, Gao C, Li J (2020): Subanesthetic isoflurane abates ROS-activated MAPK/NF-κB signaling to repress ischemia-induced microglia inflammation and brain injury. Aging 12, 26121-26139

Ye J, Jiang Z, Chen X, Liu M, Li J, Liu N (2017): The role of autophagy in pro-inflammatory responses of microglia activation via mitochondrial reactive oxygen species in vitro. J Neurochem 142(2):215-230.

Yenari MA, Kauppinen TM, Swanson RA (2010): Microglial activation in stroke: therapeutic targets. Neurotherapeutics 7(4):378-91.

Yi JH, Park SW, Kapadia R, Vemuganti R (2007): Role of transcription factors in mediating post-ischemic cerebral inflammation and brain damage. Neurochem Int 50(7-8):1014-27.

Zechner R, Zimmermann R, Eichmann TO, Kohlwein SD, Haemmerle G, Lass A, Madeo F (2012): FAT SIGNALS--lipases and lipolysis in lipid metabolism and signaling. Cell Metab 15(3):279-91.

Zhang-Gandhi CX, Drew PD (2007): Liver X receptor and retinoid X receptor agonists inhibit inflammatory responses of microglia and astrocytes. J Neuroimmunol 183(1-2):50-9.

Zhang B, Wu J, Guo P, Wang Y, Fang Z, Tian J, Yu Y, Teng W, Luo Y, Li Y (2020): Down-Regulation of SREBP via PI3K/AKT/mTOR Pathway Inhibits the Proliferation and Invasion of Non-Small-Cell Lung Cancer Cells. Onco Targets Ther 15:1039-1040.

Zhang L, Wei W, Ai X, Kilic E, Hermann DM, Venkataramani V, Bähr M, Doeppner TR (2021a): Extracellular vesicles from hypoxia-preconditioned microglia promote angiogenesis and repress apoptosis in stroke mice via the TGF-β/Smad2/3 pathway. Cell Death Dis 12(11):1068.

Zhang L, Graf I, Kuang Y, Zheng X, Haupt M, Majid A, Kilic E, Hermann DM, Psychogios MN, Weber MS, et al. (2021b): Neural Progenitor Cell-Derived Extracellular Vesicles Enhance Blood-Brain Barrier Integrity by NF-κB (Nuclear Factor-κB)-Dependent Regulation of ABCB1 (ATP-Binding Cassette Transporter B1) in Stroke Mice. Arterioscler Thromb Vasc Biol 41(3):1127-1145.

Zhang W, Tian T, Gong SX, Huang WQ, Zhou QY, Wang AP, Tian Y (2021): Microglia-associated neuroinflammation is a potential therapeutic target for ischemic stroke. Neural Regen Res 16(1):6-11.

Zhang Y, Chen K, Sloan SA, Bennett ML, Scholze AR, O'Keeffe S, Phatnani HP, Guarnieri P, Caneda C, Ruderisch N, et al. (2014): An RNA-sequencing transcriptome and splicing database of glia, neurons, and vascular cells of the cerebral cortex. J Neurosci 34(36):11929-47.

Zhao J, Lu W, Ren Y, Fu Y, Martens YA, Shue F, Davis MD, Wang X, Chen K, Li F, et al. (2021): Apolipoprotein E regulates lipid metabolism and α-synuclein pathology in human iPSC-derived cerebral organoids. Acta Neuropathol 142(5):807-825.

Zheng P, Xie Z, Yuan Y, Sui W, Wang C, Gao X, Zhao Y, Zhang F, Gu Y, Hu P, et al. (2017): Plin5 alleviates myocardial ischaemia/reperfusion injury by reducing oxidative stress through inhibiting the lipolysis of lipid droplets. Sci Rep 7:42574.

Zhou B, Liu J, Kang R, Klionsky DJ, Kroemer G, Tang D (2020): Ferroptosis is a type of autophagy-dependent cell death. Semin Cancer Biol 66:89-100.

Zhu J, Cao D, Guo C, Liu M, Tao Y, Zhou J, Wang F, Zhao Y, Wei J, Zhang Y, et al. (2019): Berberine Facilitates Angiogenesis Against Ischemic Stroke Through Modulating Microglial Polarization via AMPK Signaling. Cell Mol Neurobiol 39(6):751-768.

Zong X, Dong Y, Li Y, Yang L, Li Y, Yang B, Tucker L, Zhao N, Brann DW, Yan X, et al. (2020): Beneficial Effects of Theta-Burst Transcranial Magnetic Stimulation on Stroke Injury via Improving Neuronal Microenvironment and Mitochondrial Integrity. Transl Stroke Res 11(3):450-467.

Zusso M, Lunardi V, Franceschini D, Pagetta A, Lo R, Stifani S, Frigo AC, Giusti P, Moro S (2019): Ciprofloxacin and levofloxacin attenuate microglia inflammatory response via TLR4/NF-kB pathway. J Neuroinflammation 16(1):148.

Acknowledgements

This thesis has been written at the Department of Neurology, University Medical Center Göttingen (UMG), Georg-August-University Göttingen, Germany (director: Prof. Dr. med. Mathias Bähr). I would like to thank everyone who provided me with support and encouragement through the process of researching and writing this thesis. Especially, I would like to express my gratidtude to my advisor Prof. Dr. Thorsten R. Döppner and PD. Dr. Dirk Fitzner for the continuous support. Finally, I would like to express my gratitude to Prof. Dr. Mathias Bähr for giving me the opportunity to study and work in the Department of Neurology in UMG.